Roberto Mecca

A PDE approach to Shape from Shading via photometric stereo techniques

Dottorato in Matematica, Roma «La Sapienza» (2011).

<http://www.bdim.eu/item?id=tesi_2011_MeccaRoberto_1>

SAPIENZA
UNIVERSITÀ DI ROMA

A PDE approach to *Shape from Shading* via photometric stereo techniques

Scuola di Dottorato "Vito Volterra" in Scienze Astronomiche, Chimiche, Fisiche, Matematiche e della Terra

Dottorato di Ricerca in Matematica – XXIII Ciclo

Candidate

Roberto Mecca

ID number 11123419

Thesis Advisor

Prof. Maurizio Falcone

A thesis submitted in partial fulfillment of the requirements for the degree of Doctor of Philosophy in Math

June 2011

Thesis defended on 2011
in front of a Board of Examiners composed by:

Prof. (chairman)

Dr.

Roberto Mecca. *A PDE approach to Shape from Shading via photometric stereo techniques.*
Ph.D. thesis. Sapienza – University of Rome
 ISBN: 000000000-0

VERSION: 30 June 2011

WEBSITE: www.mat.uniroma1.it/people/mecca

EMAIL: mecca@mat.uniroma1.it

Dedicated to Giulia

Acknowledgments

A special thank goes to all the people who have had the patience to work and believe in me starting with my advisor Prof. Maurizio Falcone for all the support he succeeded to give me during our collaboration period, including the thesis writing. I want to thank Elisabetta Carlini for all the time she has dedicated to me and to this thesis and also for her suggestions in the academic life. I'm very grateful to Jean-Denis Durou for his human and professional help especially during my stay in Toulouse at the Université Paul Sabatier and at the ENSEEIHT.

Let me express my personal and professional gratitude to Viorica whose importance has never been underestimated.

Finally, the greatest thank goes to Giulia whose artistic talent and culture permit me to find myself every time I need.

Contents

Introduction

The problems that involve the image processing field concern a large quantity of areas very wide. This openness to the applications reflects for first the easiness of the phenomenon through the human vision and, as a second step, the enormous capacity of data processing that today the computers provide for this kind of problems.

In the image processing field, the tridimensional reconstruction of an object has gained a growing importance since expensive instruments (like laser scanner) can solve the problem only for objects whose dimensions do not prevent a correct working of the detector. So, beyond the costly limit of these instruments, this they are unable to reconstruct those objects whose dimensions are not compatible, and it must be considered also that the distance from the object may represent a problem. Therefore, in order to overcome these inconveniences, a new research direction has appeared, which uses an object's digital pictures as basic data for the 3D reconstruction, that is the SfS problem [1, 2, 3]. Even if the firsts to take an interest of the problem were some optics [4, 5, 6], the coming of the computer has marked a true out-and-out change of the scientific brach interested opening to the computer science. Afterwards, on the impulse of Horn [1, 7] and of his collaborators of MIT, another change of scientific interests is arrived. It regards the mathematics field where, starting from the first work of Lions [8, 9], it has introduced the SfS problem of image processing in a much more theoretical area.

The Shape from Shading one, that in the next parts of the thesis will be abbreviated as SfS, is a classical problem of image processing that bring into play some concepts not only relative to the human vision and computer science, but it uses widely elements of mathematics (analysis, geometry, probability) and optics. The model of the SfS problem that we will consider is related to the 3D reconstruction of surfaces which represent objects photographed by simple digital cameras. That is, given a gray scale digital image $I(x, y)$ the target is to reconstruct the surface $z = u(x, y)$ that corresponds to the object photographed. The first equation that bring us to consider the variation of the gray values of the image with respect to the surface is the following brightness equation:

$$R(n(x, y)) = I(x, y)$$

where the reflectance function R depends on the unitary normal vector n outgoing from the surface u. This function R indicate the way the light is reflected from the surface. In a simplified model where a Lambertian surface and a light source at infinity are considered, this equation can be expressed as:

$$I(x, y) = \gamma n(x, y) \cdot \omega \quad \forall (x, y) \in \overline{\Omega}$$

where γ is a parameter that represents the albedo (i.e. the percentage of the light that can be reflected by the surface). In our case we consider $\gamma = 1$ that is all the points of the surface reflect completely the light that hits them. The unitary vector $\omega = (\tilde{\omega}, \omega_3) \in \mathbb{R}^3$ represents the light source direction that hits the surface and it is considered constant for all the image domain $\overline{\Omega}$.

Once we express the surface normal vector $n(x, y)$ in terms of u is possible to obtain the formulation of our problem:

$$I(x, y) = \frac{-\nabla u(x, y) \cdot \tilde{\omega} + \omega_3}{\sqrt{1 + ||\nabla u(x, y)||^2}} \quad \forall (x, y) \in \overline{\Omega}$$

that is a nonlinear equation that represents a first model of the orthographic SfS. It results to be an ill posed inverse problem, this means that it has not a unique solution and small perturbations of the data can produce big variation of the solution. Just in this field, respecting the base hypotheses for the model (that we will see in the next), some results on impossibility to solve univocally this problem using only one digital image are well known.

Many articles have been written about the impossibility to solve the problem considering only one picture [2]; this impossibility, from the PDEs point of view, comes out from the difficulty we meet in differentiating the concave surfaces from the convex ones. However, they represent solutions of non-linear problem which are provided, as further starting data, even with the boundary condition (that is the surface's height on the image's boundary which retracts it). As described in the survey of Durou-Falcone-Sagona [2] the methods that permit to solve this inverse problem can be collect in two big types: methods of resolution of PDEs (in particular the characteristics method and the approximation of viscosity solutions) and optimization methods based on the variational approach.

However this methods do not permit to obtain the unique solution and from this new start were born several ways to solve the problem, which use more than one picture. An interesting result was obtained by Chambolle [10] considering the stereo vision technique: he proved that if we have two images of the same object taken from two different point of view (but considering the same light source) then the solution of the problem is unique. The technique that will be take into consideration in this thesis is the photometric stereo one (SfS-PS) that allows us to study the problem when we have, as initial data, only the images which portray the object (photographed always from the same point of view) and the relative luminous source position for each image [11]. It brings us to consider the following nonlinear system of PDEs:

$$\begin{cases} \dfrac{-\nabla u(x, y) \cdot \tilde{\omega}' + \omega_3'}{\sqrt{1 + ||\nabla u(x, y)||^2}} = I_1(x, y), & \forall (x, y) \in \Omega; \\ \dfrac{-\nabla u(x, y) \cdot \tilde{\omega}'' + \omega_3''}{\sqrt{1 + ||\nabla u(x, y)||^2}} = I_2(x, y), & \forall (x, y) \in \Omega. \end{cases}$$

with the Dirichlet boundary condition $u(x, y) = g(x, y)$ known for all $(x, y) \in \partial\Omega$.

The work of the thesis has began with the aim to find, coherently with the starting SfS model, a formulation of the problem that permits to obtain the uniqueness of solution. The study of the presented new differential approach, beyond a well posed definition, has permitted to arrive also to other conclusion regarding some problem strictly connected to the SfS-PS one. In fact we have studied some satellite problems

around the main one with the purpose to give a better collocation inside a very big set of techniques related to the SfS-PS problem.

The Chapter (1) describes in detail the SfS orthographic problem using only one image giving the formulation of the model and of the hypotheses (Lambertian surface, without black shadows and self-reflection and light source placed at infinity in order to avoid prospectives deformations). It summarizes the classes of methods used to solve this problem showing how it is impossible to obtain a unique solution (even if the surface is supposed C^1) caused by the concave/convex ambiguity.

In Chapter (2) we introduce the new differential model that permits to obtain the uniqueness. In particular, assuming the absence of black shadows, the initial results permit to illustrate the stoutness of this model for which it is possible to prove the uniqueness of the solution in a very weak function space. In fact the solution is found in $W^{1,\infty}$ (Lipschitz functions) and it is possible also to prove that this is the weakest kind of solution that this problem permits to obtain. An exhaustive study, which concerns the surface reconstruction of the object using two images, made the problem evolve from the initial study of a non-linear PDE system to the analysis of an hyperbolic partial differential equation whose solution is exactly the searched surface. But this approximation doesn't satisfy wholly the applications demands. In fact we can't obtain the uniqueness of the solution without taking into account the Dirichlet type boundary condition, even though switching from a system of non-linear PDEs to a single partial differential equation makes the study extremely simpler.

In this part we introduce the numerical schemes we use for the tests. We compare some finite difference schemes with two semi-lagrangians schemes. In particular this last method permits to obtain the best result on term of approximation of the solution. With the aim to prove the efficiency of the semi-lagrangians schemes we consider synthetic image for the approximation of the consistence order on several type of surfaces, especially on Lipschitz one.

The Dirichlet boundary condition (that we need to know just to make the problem well-posed) in the real applications consists to know a priori the height of the surface on the boundary of the image. This is a supplementary data that in the Chapter (3) we want to approximate using the classical (not differential) approach of photometric stereo, following the seminal paper by Woodham [12], aims at reconstructing the surface through its normal field approximation and integration. The use of only two digital images, for this local method, brings an ambiguity of the solution which involves, for each pixel, the determination of two possible normals. In this Chapter the main goal is to merge the two approaches in order to solve the problem using only two images. Then we use the normal field approximation to determine a boundary condition, while we use the PDE numerical techniques for the surface approximation in all other internal points.

In the last part, Chapter (4), we obtain the uniqueness of the SfS-PS problem using only the information relatives to three images (and then also considering the light source vectors). The increase of one image (passing from two to three images) in fact permits us to solve the differential problem explained in Chapter (2) without considering the boundary condition. In order to emphasize the possibility to apply this approach also to the real applications we test the semi-lagrangians schemes also on real images.

In this part we introduce the definition of linear independent images with the aim

to focus our attention on the possibility to take advantage of symmetry properties of the object pictured. In particular we prove that it is possible so solve the SfS-PS problem (without boundary condition) using two images if the surface has only one axis of symmetry and using only one image if the axis of symmetry are (at least) four. This means that we arrive to solve the SfS classic problem (passing from the photometric stereo) if the surface has a particular geometrical structure (i.e. if it has four axis of symmetry).

Chapter 1

Shape from shading problem introduction

Shape from Shading (SfS) has been a central problem in the field of computer vision since the early days. The problem is to compute the three-dimensional shape of a surface from the brightness variation in a gray scale image Fig. 1.1.

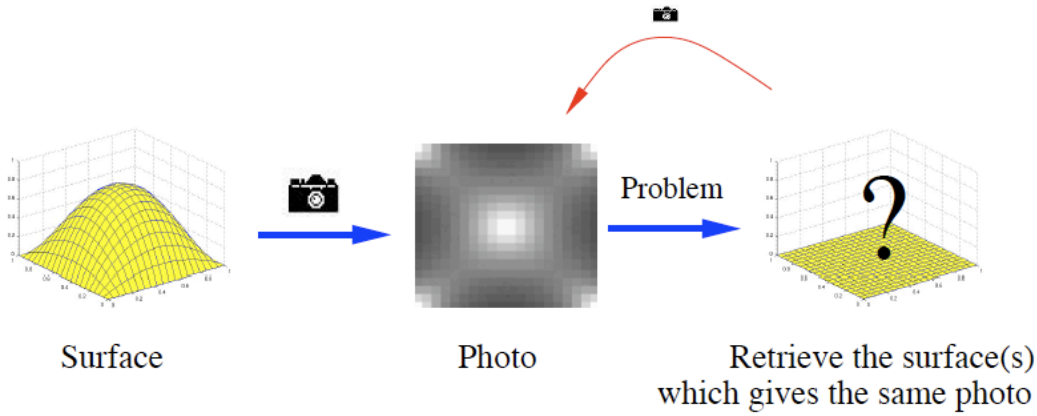

Figure 1.1. The Shape-from-Shading problem.

The work in our field was pioneered by Horn who was the first to pose the problem as that of finding the solution of a nonlinear first order partial differential equation called the brightness equation [3]. This initial idea was limited by the particular numerical method that was used (the method of characteristics) and was enriched by posing the problem as a variational problem [13] within which additional constrains such as those provides by occluding contours [14] can be taken into account. The book [1] contains a very nice panorama of the research in this area up to 1989. Questions about the existence and the uniqueness of solutions to the problem were simply not even posed at that time with the important exception of the work of Bruss [15]. These questions as well as those related to the convergence of numerical schemes for computing the solutions became central in the last decade of the 20th century. Brightness equations that do not admit continuously differentiable solution were produced [16, 17], Durou and his co-workers showed that some well-known numerical schemes were in fact almost never convergent [18] and exhibited a continuous family of ambiguous solutions [19] A breakthrough was achieved by people who realized

that control theory could be bought to bear on this problem. Dupuis and Oliensis showed that this theory provided a way of constructing numerical schemes with provable convergence properties in the case where a continuously differentiable solution existed [20]. More significantly papers, Lions, Rouy and Tourin used the theory of viscosity solution of Hamilton-Jacobi equation and to characterize the existence and uniqueness of weak solutions to the brightness equation and to come up with provably convergent numerical schemes to compute them [9, 21]. In doing so, they considerably generalized the applicability of SfS since solutions could be only continuous and they opened the way to the mathematically well-posed use of such constrains as occluding edges and shadows as well as general light sources.

1.1 Mathematical formulation

We start by giving an outline of the SfS problem and introducing the basic assumptions. In this thesis we have worked on the simplest version of SfS problem where we attach the camera a three-dimensional coordinate system $(Oxyz)$, such that Oxy coincides with the image plane and Oz coincides with the optical axis. Under the assumption of orthographic projection, the visible part of the scene is, up to a scale factor, a graph $z = u(x, y)$, where (x, y) is an image point. As is well know [1] the SfS problem can be modeled by the "image irradiance equation":

$$R(n(x, y)) = I(x, y) \tag{1.1}$$

where $I(x, y)$ is the grey level measured in the image at point (x, y) (in fact $I(x, y)$ is the irradiance at point (x, y), but both quantity are proportional) and $R(n(x, y))$ is the reflectance function, giving the value of the light re-emitted by the surface as a function of its orientation (i.e. of the unit normal $n(x, y)$ to the surface at point $(x, y, u(x, y))$. This normal can easily be expressed as:

$$n(x, y) = \frac{1}{\sqrt{1 + ||\nabla u(x, y)||^2}}(-\nabla u(x, y), 1), \tag{1.2}$$

where $\nabla u(x, y) = (\frac{\partial u}{\partial x}(x, y), \frac{\partial u}{\partial y}(x, y))$. Irradiance function I is the datum in the model since it is measured at each pixel of the image, for example in terms of a grey level (from 0 to 255). To construct a continuous model, we will assume that I takes real values in the interval $[0, 1]$. Height function $u : \overline{\Omega} \to \mathbb{R}$, which is the unknown of the problem, has to be reconstructed on a compact domain $\overline{\Omega} \subset \mathbb{R}^2$ (where $\overline{\Omega} = \Omega \cup \partial\Omega$), called the reconstruction domain. Assume that there is a unique light source at infinity whose direction is indicated by the unit vector $\omega = (\omega_1, \omega_2, \omega_3) = (\widetilde{\omega}, \omega_3) \in \mathbb{R}^3$ where $(\omega_3 > 0)$. Also assume for simplicity that ω is given (in some works, ω as well is considered as unknown, see [22, 23], even if this problem is sometimes ill-posed [24]). Recalling that for a Lambertian surface of uniform albedo equal to 1, $R(n(x, y)) = \omega \cdot n(x, y)$, equation (1.1) can be written using (1.2):

$$I(x, y)\sqrt{1 + ||\nabla u(x, y)||^2} + \widetilde{\omega} \cdot \nabla u(x, y) - \omega_3 = 0 \quad \forall (x, y) \in \Omega \tag{1.3}$$

that is a first order nonlinear partial differential equation (PDE) of the Hamilton-Jacobi type. In order to complete the formulation of the SfS problem we add the

Dirichlet boundary condition $u(x,y) = g(x,y)\ \forall (x,y) \in \partial\Omega$ that must be known. The complete problem can be written as follow:

$$\begin{cases} H(x,y,\nabla u(x,y)) = 0, & \text{on } \Omega; \\ u(x,y) = g(x,y) & \text{on } \partial\Omega; \end{cases} \tag{1.4}$$

where H is the Hamiltonian of the problem.

Points $(x,y) \in \Omega$ such that $I(x,y)$ is maximal correspond to the particular situation where ω and $n(x,y)$ point in the same direction: these points are usually called "singular points".

Let us mention that that (1.3) is not the most general equation of SfS [25]: since real material are not purely Lambertian, some publications are concerned with non-Lambertian SfS problems [26, 27, 28]; moreover, the situation is more complex in the presence of other lighting models [29, 30] or when the inter-reflection are taken into account [31, 32]. We will also consider the equation which appears in most of the papers and corresponds to frontal light source at infinity (i.e. $\omega = (0,0,1)$). Then (1.3) becomes the "eikonal equation":

$$||\nabla u(x,y)|| = f(x,y) \quad \forall (x,y) \in \Omega, \tag{1.5}$$

where

$$f(x,y) = \sqrt{\frac{1}{I(x,y)^2} - 1}. \tag{1.6}$$

In the last few years, new model have appeared. The main goal of those models is to modify the classical assumptions, in order to deal with real-life applications. In fact, if we suppose the surface Lambertian this means that the intensity reflected by a point of the surface is proportional only to the cosine of the angle between the direction of the illumination and the normal vector to the surface.

Although the classical SfS problem has attracted many researcher for years, its impact on applications has been rather limited. The major modification that has been considered is to replace the usual assumption that the projection of scene points during a photographic process is orthographic, with the more realistic assumption of perspective projection [33, 34, 35, 36, 37], and none of them had established the equation of this more realistic model.

Equations (1.3) and (1.5) have attracted much attention in the research community in PDEs for their wide range of applications. In the framework of the SfS problem, several methods of resolution have been tested: characteristic strips expansion, approximation of viscosity solutions, etc.

1.2 Viscosity solution

In this section we present a brief introduction to the notion of continuous viscosity solutions of first order Hemilton-Jacobi equations. Its aim is first to present the fundamental definitions and theorems which are used to try to solve the SfS problem (i.e. the differential problem (1.4)). In a more general sense, we will only consider thorems dealing with Dirichlet problems.

The notion of viscosity solution of Hamilton-Jacobi equations ha been introduced by Crandall and Lions [38, 39, 40, 41] in the 80s. It is a very nice way of making

quantitative and operational the intuitive idea of weak solutions of first-order (and for that matter, second-order) PDEs. In the context of the SfS problem we are only concerned with first-order PDEs.

The following definitions and results can be found in Barles's, Bardi and Capuzzo Dolcetta's or Lions' book [42, 43, 41].

1.2.1 A notion of weak solutions

Let $u : \Omega \subset \mathbb{R}^2 \to \mathbb{R}$ be a C^1 function (Ω is an open set of $\mathbb{R}^2$) and consider a Hemilton-Jacobi equation of the form:

$$H(x, y, u(x, y), \nabla u(x, y)) = 0 \quad \text{on } (x, y) \in \Omega, \tag{1.7}$$

where H is a continuous scalar function on $\Omega \times \mathbb{R} \times \mathbb{R}^n$ and it is called Hamiltonian.

Definition 1.1 *Viscosity subsolution:*
$u \in BUC(\Omega)$ (set of bounded and uniformly continuous functions) is a viscosity subsolution of equation (1.7) if:

$$\forall \phi \in C^1(\Omega), \forall (x_0, y_0) \in \Omega \text{ local maximum of } (u - \phi),$$

$$H(x_0, y_0, u(x_0, y_0), \nabla \phi(x_0, y_0)) \leq 0$$

Definition 1.2 *Viscosity supersolution:*
$u \in BUC(\Omega)$ is a viscosity supersolution of equation (1.7) if:

$$\forall \phi \in C^1(\Omega), \forall (x_0, y_0) \in \Omega \text{ local minimum of } (u - \phi),$$

$$H(x_0, y_0, u(x_0, y_0), \nabla \phi(x_0, y_0)) \geq 0$$

Definition 1.3 *Viscosity solution:*
u is a viscosity solution of equation (1.7) if it is both subsolution and supersolution of (1.7).

1.2.2 Existence and uniqueness of continuous viscosity solutions

As we have seen, the classical modelisation of SfS problem results in an Hamilton-Jacobi equation where the Hamiltonian does not depend on u considering the differential formulation (1.4).

We present here an uniqueness result due to Ishii [44]. This result has been proved later in a different manner by Lions [41]. Rouy and Tourin have also given this uniqueness result for Hamiltonian H which do not depend upon u (see [21]). For more general condition, see [9].

Theorem 1.4 *Let $u, v \in BUC(\overline{\Omega})$ respectively subsolution and supersolution of the equation:*

$$H(x, y, \nabla u(x, y)) = 0 \text{ on the bounded open } \Omega \subset \mathbb{R}^2. \tag{1.8}$$

If the following hypotheses are verified:

- $\forall (x_1, y_1), (x_2, y_2) \in \Omega$, $\forall p \in \mathbb{R}^2$, $|H(x_1, y_1, p) - H(x_2, y_2, p)| \leq \rho(|(x_1 - x_2, y_1 - y_2)|(1+|p|))$, *where ρ is a continuous nondecreasing function such that $\rho(0) = 0$;*

- *H is continuous in $\overline{\Omega} \times \mathbb{R}^2$ and convex with respect to ∇u;*
- *there exists a strict viscosity subsolution $\underline{u} \in C^1(\Omega) \int C(\overline{\Omega})$ of (1.8) (i.e. such that $H(x, y, \nabla u(x, y)) < 0$ for all $(x, y) \in \Omega$);*

then there exists at most one continuous viscosity solution of (1.8) verifying $u = g$ in $\partial\Omega$ where $g \in C(\partial\Omega)$ (it is to say a continuous solution of (1.4)).

In the eikonal equation case, it is easy to show that the previous theorem is sharp: there exists many solutions if there are singular points in Ω. Recall that in this context, a singular point is a point $(x, y) \in \Omega$ such that $I(x, y) = 1$.

Starting from the paper by Rouy and Tourin [21], the most recent approach to the resolution of SfS uses the notion of viscosity solutions to first order PDEs. These are almost-everywhere solution (a.e. solutions) which can be obtained as the limit in a family of solutions of regularized second order problems (the so-called "vanishing viscosity" method). These solution are typical Lipschitz continuous solutions (but discontinuous viscosity solutions have also been considered in the literature [43]. The development of the theory of viscosity solutions for Hamilton-Jacobi type equations provides a good framework for the analysis of the SfS problem.

Moreover, several algorithms have been proposed to compute viscosity solutions. Finite difference numerical methods have been used in [21, 9] for the resolution of (1.5) and generalized to the resolution of (1.3) in [45]. Similar results have been obtained by Oliensis and Dupuis [46] with an algorithm based on the Markow Chain approximation. Unfortunately, the Dirichlet problem (1.4) can have several weak solutions in the viscosity sense and also several classic solutions (due to the so-called concave/convex ambiguity, see [3]. As an example, all the surfaces represented in Fig. 1.2 are viscosity solutions of the same equation which is a particular case of (1.4) (in fact the equation is $|u'| = -2x$ with homogenous Dirichlet boundary condition). The solution represented in Fig. 1.2-a is the maximal solution and is smooth. All the non-smooth a.e. solutions which can be obtained by a reflection with respect to a horizontal axis, are still admissible weak solutions Fig. 1.2-b. In this example, the lack of uniqueness of the viscosity solutions is due to the existence of a singular point where the right hand side of (1.5) vanishes. An additional effort is then needed to define which the preferable solution since the lack of uniqueness is also a big drawback when trying to compute a numerical solution. In order to circumvent these difficulties, the problem is usually solved by adding some information such as height at each singular point [9].

More recently, an attempt has been made to eliminate the need for a priori additional information. In recent results in the theory of viscosity solutions, the "maximal solution" without additional information apart from the equation was characterized, as was the construction of an algorithm which converges to that solution. A result by Ishii and Ramaswamy [47] applied to SfS guarantees that if the function I is continuous and the number of singular points is finite, then a unique maximal solution (in the viscosity sense) of (1.4) exists. It should be noted that their result on the characterization of the maximal solution does not apply to the general situation when the set of singular points has a positive measure. More general uniqueness results for maximal solution have been recently obtained by Camilli et al. [48, 49]. Several papers have followed this approach providing different

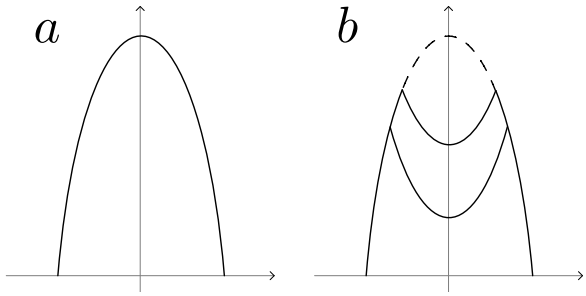

Figure 1.2. Illustration of the concave/convex ambiguity: (a) maximal solution and (b) a.e. solutions giving the same image.

algorithms to compute the maximal solution, which has been shown to be unique, see [50, 51] and the references therein.

We conclude this section by mentioning a few other extensions in the framework of viscosity solutions. All the theoretical results mentioned above use the regularity of the grey level function I, which is supposed to be (at least) continuous. Naturally, real images do not fit that assumption, even in the case of Lambertian objects. The continuity assumption for I has been removed in paper by Kain and Ostrov [52] and by Prados and Faugeras [53]. Both these papers also contain a scheme and some numerical example. At the end we note that, considering the SfS like an inverse problem, if we want to approximate a Lipschitz surface we must have (except for very spacial cases) a discontinuous function image I. This means that the Hamiltonian H of (1.4) is not continuous at all, so it is not possible to study the SfS problem with the aim to find the unique Lipschitz solution if the Hamiltonian is not discontinuous.

In our new differential approach we arrive to find a robust model that permits us to study a discontinuous Hamiltonian and that find a unique Lipschitz solution passing through the photometric stereo technique applied to the SfS problem. We arrive to the solution (and also to an efficient numerical scheme) using the characteristic strip expansion that will be introduced below.

1.3 Characteristic strip expansion

The first mention of 3D reconstruction using photometric cues is due to the Dutch astronomer Van Diggelen [4]. The first resolution was suggested by Rindfleisch [6] who demonstrated that if the photometric behavior of a surface follows certain properties, then the shape can be expressed as an integral along a set of convergent straight lines. He implemented this computation on images of the Moon, claiming that its surface verifies the necessary photometric properties reasonably well. Later, Horn suggested calling this problem "shape-form-shading", and showed that the resolution proposed by Rindfleisch in a particular case could be generalized, while still using the characteristic strip expansion [3], under the following two confition:

- the function u has to be of class C^2;
- the 5-uplet $(x, y, u, \frac{\partial u}{\partial x}, \frac{\partial u}{\partial y})$ has to be known at every point of a curve called the initial curve, which means in fact that two boundary condition are needed

simultaneously, one on u (Dirichlet boundary condition) and other on $(\frac{\partial u}{\partial x}, \frac{\partial u}{\partial y})$ (Neumann boundary condition).

The characteristic lines (which are the lines along which the integration has to be performed) can be of any form in the image domain, and this differs from the case studied by Rindfleisch.

Besides the inherent defect of error accumulation, which is typical of every method of resolution using integration, the determination of these characteristic lines is a new problem itself, since they also are defined through integration. Therefore, the accuracy of boundary conditions is much more crucial than for other methods. It follows that a certain number of obstacles must be overcome (i.e. the crossing of a characteristic lines) which should normally occur only at a singular points, or the presence of holes in Ω, which must be filled using secondary lines [3].

Finally this method has been essentially used for the theoretical study of the number of solutions of class C^2 of the eikonal equation: a number of uniqueness results have been provided (see [54, 55, 56, 57] and the reference therein).

The characteristic method is an important instrument useful to solve a particular class of PDE. The one more suitable are the partial differential equations where the information is propagated with finite velocity: hyperbolic equation which belong the wave equation and the transport equation are an example.

The simpler way to introduce this method, that convey understandable its intrinsic means in particular for our problem, is to introduce the characteristic considering directly the problem (1.4) where we suppose $\partial\Omega$ and $g : \partial\Omega \subset \mathbb{R}^2 \to \mathbb{R}$ known. Furthermore we suppose that H and g are regular functions. The characteristics method solve (1.4) converting the partial differential equation in a opportune ordinary differential equations system. We suppose that u solves (1.4) and we fix a point $(x, y) \in \Omega$. We want to compute $u(x, y)$ finding a curve that lies in Ω, which connects (x, y) to a point $(x_0, y_0) \in \partial\Omega$. and along which is possible to calculate u. Since the boundary condition, we know the value of u in (x_0, y_0). We want to calculate u along all the curve and in particular in (x, y). But, how we chose this curve? We suppose that it is parametrically described by the function $(x_c(s), y_c(s))$; the parameter s belong to an interval of $\mathbb{R}$. We suppose $u \in C^2$ solution of the equation of the problem (1.4). We define also:

$$z(s) = u(x_c(s), y_c(s)). \tag{1.9}$$

In addition we set:

$$p(s) = \nabla u(x_c(s), y_c(s)); \tag{1.10}$$

that is $p(s) = (p^1(s), p^2(s))$ where

$$p^1(s) = \frac{\partial u}{\partial x}(x_c(s), y_c(s)), \quad p^2(s) = \frac{\partial u}{\partial y}(x_c(s), y_c(s)). \tag{1.11}$$

In this way $z(\cdot)$ gives the value of u along the curve and $p(\cdot)$ records the values of the gradient ∇u. We must choose the function $(x_c(\cdot), y_c(\cdot))$ in such a way that we can compute $z(\cdot)$ and $p(\cdot)$.

If we differentiate (1.11) with respect to s, the equation of the problem (1.4) with respect to x and y and (1.9), making opportune substitutions, we arrive to the

following equations:

$$\begin{cases} \text{(a)} & (\dot{p}^1(s), \dot{p}^2(s)) = -D_z H(p(s), z(s), x_c(s), y_c(s))p(s) \\ & \quad -(D_{x_c} H(p(s), z(s), x_c(s), y_c(s)), D_{y_c} H(p(s), z(s), x_c(s), y_c(s))) \\ \text{(b)} & \dot{z}(s) = D_p H(p(s), z(s), x_c(s), y_c(s)) \cdot p(s) \\ \text{(c)} & (\dot{x}_c(s), \dot{y}_c(s)) = D_p H(p(s), z(s), x_c(s), y_c(s)). \end{cases} \tag{1.12}$$

this system of $2n + 1$ ODEs of the first order include the characteristic equations of the first order PDE of the problem (1.4). The functions $p(\cdot) = (p^1(\cdot), p^2(\cdot))$, $z(\cdot)$, $(x_c(\cdot), y_c(\cdot))$ are called characteristics. We will refer to $(x_c(\cdot), y_c(\cdot))$ as projected characteristic: it is the projection of the characteristic $(p(\cdot), z(\cdot), x_c(\cdot), y_c(\cdot)) \subset \mathbb{R}^5$ on the domain $\Omega \subset \mathbb{R}^2$.

We have seen how can be impossible to have a unique solution of the problem (1.4) through the viscosity solution notion. This kind of impossibility can also be seen considering the characteristic method. In fact, the singular points represent source (or well) where the information get out (or is sucked in). That is why we need to add information about the heigh of the surface in these points [58]. In the next part we will explain in a much more exhaustive way the

1.3.1 Other PDE methods

Another approach which produces a global solution to SfS consists in the search for equal-height contours, originally proposed by Bruckstein [59] and later re-introduced by Kimmel and Bruckstein [60, 61]. The method consists of two major steps: the computation of weighted distance functions from all the singular points, using a level set method, and the merging of these surfaces. The algorithm can compute a global solution (which is an a.e. solution) of eikonal equation (1.5) in the reconstruction domain, only combining the local solutions obtained during the first step. Interestingly, this method has been extended to the case of near light source [36].

Finally, the idea of solving the eikonal equation using a power series expansion at a regular point, in the case of a grey level function of class C^∞, has been introduced by Bruss [15] and has been extended to the analytical grey level functions by Durou and Piau, which could exhibit a "non-visible deformation" (i.e., a continuous family of analytical shapes giving the same image [19]). This is an important theoretical result but, nevertheless, no algorithm has been derived from this method of resolution.

1.3.2 Boundary condition

The use of PDE methods for the resolution of the SfS problem leads necessarily to the definition of some sort of boundary conditions. This is one of the differences with respect to the methods using optimization, since for those methods boundary conditions can be imposed but are not compulsory. A detailed analysis of the well-posedness of the boundary value problem for nonlinear PDEs in the framework of the weak solutions (in the viscosity sense) can be found in Barles' book [43] and in the references therein. It is important to note that the addiction of boundary conditions does not solve the concave/convex ambiguity and that in practical applications boundary conditions are seldom known.

Te choice between the different types of boundary conditions is a question of appropriateness and simplicity, or depends on the additional information available

on the object (if any). The Dirichlet boundary condition is typically used when the object is standing on a flat background and the surfaces meets the background at $\partial\Omega$, or if the height on $\partial\Omega$ is known (or assumed, for example by symmetry). Neumann boundary conditions correspond to $\frac{\partial u}{\partial \nu}(x,y) = m(x,y)$, where $\nu(\cdot)$ represents the outward normal to domain Ω. A typical use of it is when we know (or we presume) that the level curves of the surface are orthogonal to the boundary $\partial\Omega$ or to a subset of it where we simply choose $m(x,y) = 0$. The Neumann boundary condition gives more freedom in the computation since it only imposes the value of a derivative and does not fix the height of the surface at the boundary. Naturally, also this condition modifies the surface. State constraint boundary conditions differ from the previous ones since the do not impose a value either for the height or for its normal derivative. In this respect, it has been interpreted as a "no boundary condition" choice [62], although this interpretation is rather superficial. In fact, a real function u bounded and uniformly continuous is said to be a "state constraint viscosity solution" if and only if it is a subsolution (in the viscosity sense) in Ω and a supersolution in $\overline{\Omega}$ (i.e. up to the boundary). It can also be stated as a Dirichlet boundary condition, simply setting $g(x,y) = g_c$ on $\partial\Omega$, where g_c is a constant, provided:

$$g_c > \max_{(x,y)\in\Omega}\{u(x,y)\}$$

Note that in our problem, this is a mild assumption since we can easily fix an upper bound for the height of the object. The effect of the state constraint boundary condition is to produce solutions that grow inwards from the boundary $\partial\Omega$. This choice ca be appropriate in some situations and wrong in other situations, in any case also this boundary condition affects the computation.

1.4 Methods using optimization

Another class of algorithms which have been suggested are optimization method based on the variational approach. Note that these algorithms can work in the most general case of (1.1), contrary to the PDE method. In this class of methods, three basic ingredients must be chosen: the unknowns, the functional which has to be optimized (in fact, minimized), and the minimization method. Surprisingly, a certain number of paper flling within the domain of optimization do not clearly show the implications of these choices, so that the choice of a functional is something only guided by considerations on convergence. Even in [63], which is a major reference in the field, the discussion of several functionals is based on the possibility of finding an algorithm that converges toward a minimum. Indeed, it is possible a priori to freely combine any functional and any minimization algorithm.

1.4.1 Unknowns

The first difficulty encountered in the SfS problem is the choice of the unknown. The natural unknown (i.e. height u) is already used [64]: problems of convergence [63] or of slowness [65] are mentioned. Many papers dealing with optimization use $p = \frac{\partial u}{\partial x}$ and $q = \frac{\partial u}{\partial y}$ as unknowns (see [63, 65, 66, 67]), because u appears in the image irradiance equation only through its first derivativs; however, if u is supposed

to be of class C^2, p and q are two non-independent functions, since:

$$\frac{\partial p}{\partial y} = \frac{\partial q}{\partial x}. \tag{1.13}$$

Other unknowns have been used: the three unknowns (u, p, q) have been dealt with simultaneously [13, 68]; the stereographic coordinates of the normal [14, 69] present the great interest of being bounded on the occluding boundarues, contrary to (p, q); the normal itself is sometimes used [70, 71]. Finally, several model.based approaches have been proposed, such as quadratic models [72], triangular elements [73], deformable models [74] or B-splines [75].

When dealing with other unknowns than u itself, an additional problem is then to compute u. For instance, using (p, q) as unknown, the following equations must solved:

$$\begin{cases} \dfrac{\partial u}{\partial x} = p, \\ \dfrac{\partial u}{\partial y} = q, \end{cases} \tag{1.14}$$

which give (1.13) by elimination of u. Nevertheless, since (1.14) are linear in u, the problem of integration is much easier to solve than the SfS problem.

1.4.2 Functionals

The only quantity which has to be minimized, whatever the unknowns, is the "brightness error". Using u as unknown, defining function r so that $R(n(x, y)) = r(p(x, y), q(x, y))$, and using least square error, this term can be expressed as:

$$\mathcal{F}_1(u) = \int_{(x,y)\in\overline{\Omega}} \left(r\left(\frac{\partial u}{\partial x}(x, y), \frac{\partial u}{\partial y}(x, y)\right) - I(x, y)\right)^2 dxdy.$$

Using (p, q), a strictly equivalent functional to $\mathcal{F}_1$ is:

$$\begin{aligned} \mathcal{F}_2(p, q, \mu) = &\int_{(x,y)\in\overline{\Omega}} (r(p(x, y), q(x, y)) - I(x, y))^2 dxdy + \\ &+ \int_{(x,y)\in\overline{\Omega}} \mu(x, y)\left(\frac{\partial p}{\partial y}(x, y) - \frac{\partial q}{\partial x}(x, y)\right) dxdy, \end{aligned}$$

where μ is a Lagrange multiplier (i.e. a new unknown [63]). this last functional is often approximated by another one (for numerical reason) where the constraint term becomes a least square penalty term, often called the "integrability term" [63]:

$$\begin{aligned} \mathcal{F}_3(p, q, u) = &\int_{(x,y)\in\overline{\Omega}} (r(p(x, y), q(x, y)) - I(x, y))^2 dxdy + \\ &+ \lambda_i \int_{(x,y)\in\overline{\Omega}} \left(\frac{\partial p}{\partial y}(x, y) - \frac{\partial q}{\partial x}(x, y)\right)^2 dxdy. \end{aligned}$$

Several discrete implementations of this functional have been proposed [63, 66]. A problem is that it is parametric, contrary to $\mathcal{F}_1(u)$ and $\mathcal{F}_2(p, q, u)$, depending on parameter λ_i which is called the "integrability factor". Another way to translating functional (1.4.2), without introducing any parameter, consists in imposing the

hard constraint (1.13) in an iterative process: this leads to the well-known method Frankot and Chellappa [67], where integrability is forced at each step. Symmetrically, it has recently been proposed in [71] to impose (1.5) at each step of an iterative optimization method. Another least square penalty term which has been much used is the "smoothness term" [62]:

$$\mathcal{F}_4(p,q) = \int_{(x,y)\in\overline{\Omega}} (r(p(x,y),q(x,y)) - I(x,y))^2 dxdy + \\ + \lambda_s \int_{(x,y)\in\overline{\Omega}} (|\nabla p(x,y)|^2 + |\nabla q(x,y)|^2) dxdy$$

where λ_s is a second parameter given the name of "smoothing factor". Incidentally, one critical point of the optimization approach is that, given a noise-less image with assumptions satisfied, the true surface will minimize functionals $\mathcal{F}_1$ and $\mathcal{F}_2(p,q,\mu)$, but the same may not be said of the "improvement" that results in functional $\mathcal{F}_4(p,q)$. This can be avoided by progressibely decreasing λ_s as long as the brightness error decreases [64, 13]. Of course, some authors have used the functional combining both least square penalty terms [65, 68]:

$$\mathcal{F}_5(p,q) = \int_{(x,y)\in\overline{\Omega}} (r(p(x,y),q(x,y)) - I(x,y))^2 dxdy + \\ + \lambda_i \int_{(x,y)\in\overline{\Omega}} \left(\frac{\partial p}{\partial y}(x,y) - \frac{\partial q}{\partial x}(x,y)\right)^2 dxdy + \\ + \lambda_s \int_{(x,y)\in\overline{\Omega}} (|\nabla p(x,y)|^2 + |\nabla q(x,y)|^2) dxdy.$$

FInally, some other least square penalty terms have been used, as for example the "image intensity gradient constraint" [76] and, beside the classical least square estimator, robust estimator have also been used [77].

1.4.3 Methods of minimization

When a given functional is chosen, two main strategies to find its minimum exist, as recalled in [68]: either the Euler equations associated with the functional are solved, or the functional is directly minimized. The first strategy has been used much more often than the second one (see [13, 63, 66, 67, 14]), since it is easier to implement and generally faster, but its main drawback is possible possible divergence [18], because convergence is hard to prove for a Jacobi iteration. Neverthless, on the one hand, such a method is proved to be convergent in [69] and, on the other hand, linearizing the reflectance function renders the associated Euler equations linear [73], thus avoiding possible problems of divergence. Conjugate gradient descent has been used as a method of direct minimization in [64, 67], providing results of rather good quality, but convergence is not guaranteed, contrary to the classical gradient descent method combined with line search [65].

The approximate solutions computed are typically local minima of the functional. To obtain a global minimum, a global optimization algorithm has to be used, typically a stochastic algorithm like simulated annealing [75, 78] or genetic algorithms [79]. Naturally, the price to pay is a longer CPU time for the computation. This problem of a long computing time has been partially solved either using multiresolution

[68, 74, 78] or dealing with a parametric model with few parameters [75]. Finally, Courteille et al. [80] have extended some minimization algorithms to PSFS, showing some applications to documents digitization.

1.5 Not unique solution using one image. Photometric stereo introduction

We want to emphasize one more time that using only one images, because of the presence of singular points, it is not possible to find the unique solution of the SfS problem. With the purpose to try to find the unique solution, we increase the information about the surface in a natural way (i.e. starting with the same data types of the SfS problem). There are two techniques that permit us an increasing in this sense, that is we consider two images (I_1 e I_2) taken:

- from two different points of view, but using only one light source for both (stereo vision [10])
- from the same point of view, but using a different light source for each image (photometric stereo)

In this work we want to study the photometric stereo SfS problem (SfS-PS), where we can use more than one image of the same surface. In this problem the images will correspond to the *same* point of view but to *different* light sources. Let us assume that we have k different pictures of the same surface, this will produce k equations similar to (1.3), i.e.

$$I_i(x,y) = n(x,y)\cdot\omega^i \quad \forall (x,y)\in\Omega \quad ,i=1,\dots,k \tag{1.15}$$

As we will see in the following section, this will result in a system of nonlinear partial differential equations. Several points have to be clarified: what is the minimal number k which allows to reconstruct the a generic surface $z = u(x,y)$ without ambiguities? Which are the assumptions on light sources directions ω_i in order to obtain uniqueness? How can the surface be reconstructed? How can we deal with black shadows in the image?
Let us mention that some results of existence and uniqueness are already been proved by Onn and Bruckstein ([81]) and by Kozera ([11]). These theorems however have some important drawbacks as regards the class of functions where the solution is found and also as regards some hypothesis that threshold the use of these results in the real applications. Our purpose is to weaken all the hypothesis for try to prove the existence and the uniqueness, and to find some numerical convergent schemes for a function in a less regular space (i.e. Lipschitz functions space).

1.5.1 Photometric Stereo existing results

The concept of photometric stereo technique in this SfS characterization, will be taken as the possibility to take advantage of the light not in a physical sense (i.e. considering the intrinsic features of the ray of light like the wavelength), but in a simpler way. In fact, the purpose is to determine the surface starting from two

its images (I_1 and I_2) taken from the same point of view, changing every time the direction of the light source (ω' and ω'' respectively).

There are many possible approaches to make a model of the SfS-PS problem. In this work we will concentrate the dissertation on the possibility to arrive, through at least two nonlinear Hamilton-Jacobi equations, at the solution of the problem. This means that we are considering the hypotheses of the previous modelization of the SfS problem, that is:

1. the light sources are at infinity;
2. the surface is *Lambertian*, which means that the intensity reflected by a point of the surface is proportional only to the cosine of the angle between the direction of the illumination and the normal vector to the surface;
3. there are no self-reflections on the surface;
4. there are no black shadows on the surface.
5. the optical point is sufficiently far from the surface so that perspective deformations can be neglegted.

The condition of the complete illumination of the surface from the light source ω is guaranteed from the following

$$u((x,y)+t\widetilde{\omega}) < u(x,y)+t\omega_3 \quad \forall t>0. \tag{1.16}$$

We consider the SfS-PS problem for two light sources (ω' e ω'') and what we obtain is a system of the following type:

$$\begin{cases} \dfrac{-\nabla u(x,y)\cdot\widetilde{\omega}'+\omega_3'}{\sqrt{1+||\nabla u(x,y)||^2}} = I_1(x,y), & \forall (x,y)\in\Omega; \\ \dfrac{-\nabla u(x,y)\cdot\widetilde{\omega}''+\omega_3''}{\sqrt{1+||\nabla u(x,y)||^2}} = I_2(x,y), & \forall (x,y)\in\Omega. \end{cases} \tag{1.17}$$

with the Dirichlet boundary condition $u(x,y)=g(x,y)$ known for all $(x,y)\in\partial\Omega$.

Some results of uniqueness will be enunciate below ([11]):

Lemma 1.5 *The first derivatives of u can be expressed in terms of I_1, I_2, ω' and ω'' in the following form:*

$$u_x^{\pm} = \frac{(\omega_1''(\omega'\cdot\omega'')-\omega_1')I_1+(\omega_1'(\omega'\cdot\omega'')-\omega_1'')I_2 \pm (\omega_3'\omega_2''-\omega_2'\omega_3'')\varepsilon\sqrt{\Lambda}}{(\omega_3'-\omega_3''(\omega'\cdot\omega''))I_1+(\omega_3''-\omega_3'(\omega'\cdot\omega''))I_2 \pm (\omega_1'\omega_2''-\omega_2'\omega_1'')\varepsilon\sqrt{\Lambda}} \tag{1.18}$$

$$u_y^{\pm} = \frac{(\omega_2''(\omega'\cdot\omega'')-\omega_2')I_1+(\omega_2'(\omega'\cdot\omega'')-\omega_2'')I_2 \pm (\omega_1'\omega_3''-\omega_3'\omega_1'')\varepsilon\sqrt{\Lambda}}{(\omega_3'-\omega_3''(\omega'\cdot\omega''))I_1+(\omega_3''-\omega_3'(\omega'\cdot\omega''))I_2 \pm (\omega_1'\omega_2''-\omega_2'\omega_1'')\varepsilon\sqrt{\Lambda}} \tag{1.19}$$

where

$$\Lambda=\Lambda(x,y)=1-I_1^2(x,y)-I_2^2(x,y)-(\omega'\cdot\omega'')[\omega'\cdot\omega''-2I_1(x,y)I_2(x,y)] \tag{1.20}$$

and the function $\varepsilon=\varepsilon(x,y)$ take only the values ±1 in such a way that the function $f(x,y)=\varepsilon(x,y)\sqrt{\Lambda(x,y)}$ is continuous.

Theorem 1.6 *Let I_1 and I_2 be functions of class C^1 over a simply connected region Ω of $\mathbb{R}^2$ with values in $[0,1]$. Suppose that $\Lambda > 0$ on Ω and that for each choice of sign,*

$$\sigma^{\pm} = (\omega_3' - \omega_3''(\omega' \cdot \omega''))I_1 + (\omega_3'' - \omega_3'(\omega' \cdot \omega''))I_2 \pm (\omega_1'\omega_2'' - \omega_2'\omega_1'')\sqrt{\Lambda} \tag{1.21}$$

does not vanish over Ω. Then a necessary and sufficient condition for the existence of exactly two solutions to (1.17) of class C^2 is, for each choice of sign,

$$\frac{\partial}{\partial y}u_x^{\pm}(x,y) = \frac{\partial}{\partial x}u_y^{\pm}(x,y) \tag{1.22}$$

with $u_x^{\pm}$ and $u_y^{\pm}$ defined respectively from (1.18) and (1.19).

Corollary 1.7 *Let I_1 and I_2 be functions of class C^1 over a simply connecter region Ω of $\mathbb{R}^2$ with values in $[0,1]$. Suppose that $\Lambda \equiv 0$ on Ω and that*

$$\sigma = (\omega_3' - \omega_3''(\omega' \cdot \omega''))I_1 + (\omega_3'' - \omega_3'(\omega' \cdot \omega''))I_2 \tag{1.23}$$

does not vanish over Ω. Then a necessary and sufficient condition for the existence of exactly one solution of class C^2 to (1.17) is

$$\frac{\partial}{\partial y}u_x(x,y) = \frac{\partial}{\partial x}u_y(x,y) \tag{1.24}$$

with u_x and u_y defined respectively in (1.18) and (1.19) taken with $\Lambda \equiv 0$.

We note that the hypothesis of a regular starting data (in this case I_1 and I_2 taken in $C^1(\Omega)$) is not a sufficient condition in order to prove the uniqueness of u because of the strong hypothesis $\Lambda \equiv 0$ on all the domain Ω. Another thing where we want to focus the attention is the regularity of the surface. In fact these results arrive to obtain a solution $u \in C^2(\Omega)$. The next and the original part of the thesis is based on the study of this problem but based on a different approach. Our aim is to reduce the strong hypotheses with the contemporary objective to obtain a weaker solution.

Let consider now two cases:

- a non - physical case where we wonder if exist a function u related to any images I_1 and I_2 and any light vector ω' and ω'' not correlated among them;
- a physical case when we assume the existence of a surface u and we think that the images I_1 and I_2 are not generic since they are expressed in terms of two light vector ω' and ω'' like this:

$$I_1(x,y) = \frac{-\nabla u(x,y) \cdot \widetilde{\omega}' + \omega_3'}{\sqrt{1 + ||\nabla u(x,y)||^2}}, \quad I_2(x,y) = \frac{-\nabla u(x,y) \cdot \widetilde{\omega}'' + \omega_3''}{\sqrt{1 + ||\nabla u(x,y)||^2}} \tag{1.25}$$

In the next part we will use the more applicable case that is the physical one.

Chapter 2

A new differential approach to the **photometric stereo** using two images

Let's start the introduction of our new model from a first one-dimensional case (where $\overline{\Omega} = [a, b]$ and $\omega' = (\omega'_1, \omega'_2)$, $\omega'' = (\omega''_1, \omega''_2)$). The SfS problem transforms itself in the following system

$$\begin{cases} \dfrac{-u_x(x)\omega'_1 + \omega'_2}{\sqrt{1+u_x(x)^2}} = I_1(x), & \text{a.e. } x \in \Omega; \\ \dfrac{-u_x(x)\omega''_1 + \omega''_2}{\sqrt{1+u_x(x)^2}} = I_2(x), & \text{a.e. } x \in \Omega. \\ u(a) = u_a, u(b) = u_b & \text{with } u_a, u_b \in \mathbb{R}; \end{cases} \tag{2.1}$$

We want to emphasize that now and in the sequel all the partial differential equation are of the first order . We consider then the function set of the solutions, strictly connected with the definition of the problem. That is, if we define the equation almost everywhere we are searching for a function differentiable almost everywhere in Ω, that is a Lipschitz function [82].

For the non-linear system (2.1) the next result stands:

Theorem 2.1 *Let ω' and ω'' be two linearly independent (light) vectors. Let $I_1(x)$, $I_2(x) \in L^\infty(\Omega)$ and such that $0 < I_1(x), I_2(x) \leq 1$ for $x \in \Omega \subset \mathbb{R}$ connected. Then exist unique the lipschitz function $u(x)$ solution of the system (2.1) determined from a single boundary condition.*

Proof.
If we consider

$$\nu_1 = -\frac{u_x}{\sqrt{1+u_x^2}} \quad \text{and} \quad \nu_2 = \frac{1}{\sqrt{1+u_x^2}} \tag{2.2}$$

then it is possible to rewrite the system (2.1) like this:

$$\begin{pmatrix} \omega'_1 & \omega'_2 \\ \omega''_1 & \omega''_2 \end{pmatrix} \begin{pmatrix} \nu_1 \\ \nu_2 \end{pmatrix} = \begin{pmatrix} I_1 \\ I_2 \end{pmatrix} \tag{2.3}$$

If the light source vectors are linear independents, is possible calculate the unique solution (ν_1, ν_2) from which is easy to get the u_x; in fact: $u_x = -\frac{\nu_1}{\nu_2}$.

If we know the first derivative we can calculate the function from the fundamental theorem of calculus:

$$u(x) = u_a + \int_a^x u_x(s)ds \tag{2.4}$$

otherwise

$$u(x) = u_b - \int_x^b u_x(s)ds \tag{2.5}$$

□

We observe that if we repeat the same reasoning with space dimension n (where we are studying the problem) and considering a number of light sources equal to $n+1$, we can note that is always possible to write a formula for the first partial derivative ([11]).

The problem is to reduce, as possible, the number of light sources (i.e. the number of images, i.e. the information about the surface). The next step will be to consider the two-dimensional case and repeat the elimination of the non linearity and try to reduce the space dimension of the problem looking for find the unique solution when we use only two light sources.

That is, we consider the system (1.17) and we eliminate the non linearity considering, for example, from the first equation the following:

$$\sqrt{1 + ||\nabla u(x,y)||^2} = \frac{-\nabla u(x,y) \cdot \widetilde{\omega}' + \omega_3'}{I_1(x,y)} \tag{2.6}$$

Replacing it into the other equation we obtain the following linear equation:

$$(I_2(x,y)\omega_1' - I_1(x,y)\omega_1'')\frac{\partial u}{\partial x} + (I_2(x,y)\omega_2' - I_1(x,y)\omega_2'')\frac{\partial u}{\partial y} = (I_2(x,y)\omega_3' - I_1(x,y)\omega_3'') \quad \forall (x,y) \in \Omega \tag{2.7}$$

considering also the same boundary condition the previous (1.17), that is:

$$\begin{cases} b(x,y) \cdot \nabla u(x,y) = f(x,y), & \forall (x,y) \in \Omega; \\ u(x,y) = g(x,y) & \forall (x,y) \in \partial\Omega. \end{cases} \tag{2.8}$$

where

$$b(x,y) = (I_2(x,y)\omega_1' - I_1(x,y)\omega_1'', I_2(x,y)\omega_2' - I_1(x,y)\omega_2'') \tag{2.9}$$

and

$$f(x,y) = I_2(x,y)\omega_3' - I_1(x,y)\omega_3''. \tag{2.10}$$

We note that the fact that $b(x,y)$ doesn't vanish in Ω imply the absence of attracting or source points in the domain. We will see in the next part a better result that permits us to have a weaker solution.

In order to pass from a two dimensional to a one dimensional problem, exploiting the previous result, we solve the equation along the characteristics curve. In the general case the characteristics relative to the linear differential equation (2.8) results to be dependent on the shape of the surface. This inconvenient makes particularly

complicated the reconstruction of the surface. We can have a considerable simplification choosing opportunely the light sources in order to have a light information that propagates in a linear way (i.e. the characteristics are straight lines).

Example 1

We consider now a particular position of the light sources. Let's take the two light vectors $\omega' = (0, 0, 1)$ and $\omega'' = (\sin(\varphi), 0, \cos(\varphi))$ $(\varphi \in (-\frac{\pi}{2}, 0) \cup (0, \frac{\pi}{2}))$; the equation becomes:

$$-I_1(x,y)\sin(\varphi)\frac{\partial u}{\partial x} = (I_2(x,y) - I_1(x,y)\cos(\varphi)) \quad \forall (x,y) \in \Omega \tag{2.11}$$

This example is useful to understand how the information about the surface is given by the light. We can see that the main information is given in the direction of the vector $\widetilde{\omega}''$ that in our case coincides with the direction of the X axis (the same thing, but with the Y axis, happens if we take the second light source $\omega'' = (0, \sin(\varphi), \cos(\varphi))$). The approximation schemes give, like we will see in the next paragraph, good results also for finite difference methods with low order convergence because of their numerical integration along the characteristic lines. This allows us to study a two-dimensional problem like a one-dimensional case considering it along the characteristic curves.

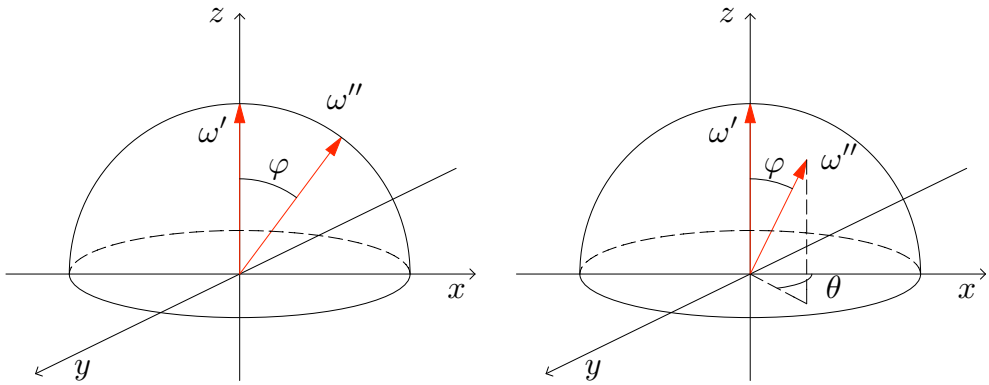

Figure 2.1. On the left the two light sources of the first example (that is coplanar to the xz plane) and on the right the light vectors of the second example.

Example 2

When the second light is any unitary vector (i.e. $\omega'' = (\sin(\varphi)\cos(\theta), \sin(\theta)\sin(\varphi), \cos(\varphi))$ with $\varphi \in (-\frac{\pi}{2}, 0) \cup (0, \frac{\pi}{2})$ and $\theta \in [0, 2\pi]$), we can note that the equation becomes

$$-I_1(x,y)\omega_1''\frac{\partial u}{\partial x} - I_1(x,y)\omega_2''\frac{\partial u}{\partial y} = I_2(x,y) - I_1(x,y)\omega_3'' \quad \forall (x,y) \in \Omega \tag{2.12}$$

and the curves where the luminous information travel (i.e. the characteristic field) is the same as before and for $\theta \neq k\frac{\pi}{2}$ (with $k = 0, 1, 2, 3$) we lose the complete coordination with the axis. This inconvenient does not change the type of problem to solve, that is, the characteristic curves continue to be straight lines. In particular now they are an improper sheaf of lines defined by the angle θ. The approximation

of the linear equation (2.7) in fact is very difficult if we don't consider schemes that take care of the direction of the luminous information.

Lemma 2.2 *If there are not any points $(x, y) \in \Omega$ of black shadows for the image functions (i.e. $I_1(x, y) \neq 0$ and $I_2(x, y) \neq 0$), we have that $||b(x, y)|| \neq 0$ (i.e. the vectorial function does not vanish in Ω).*

Proof. Now, considering the definition of the function $b(x, y)$, suppose for absurd that there exists a point $(\overline{x}, \overline{y}) \in \Omega$ such that $b(\overline{x}, \overline{y}) = 0$, that is:

$$\begin{cases} I_2(\overline{x}, \overline{y})\omega_1' - I_1(\overline{x}, \overline{y})\omega_1'' = 0 \\ I_2(\overline{x}, \overline{y})\omega_2' - I_1(\overline{x}, \overline{y})\omega_2'' = 0 \end{cases} \tag{2.13}$$

If $\widetilde{\omega}' = \widetilde{\omega}''$ then also $\omega_3' = \omega_3''$ because we are considering this vector on the upper semi sphere. This is redundant with the conclusion of (2.13) (that is $I_1(x, y) = I_2(x, y)$) since

$$\begin{cases} I_2(x, y)\omega_1 = I_1(x, y)\omega_1 \\ I_2(x, y)\omega_2 = I_1(x, y)\omega_2 \end{cases}$$

where $(\omega_1, \omega_2) = \widetilde{\omega}' = \widetilde{\omega}''$, but it is not the situation of the photometric stereo technique.

In this case it is necessary to consider only the case when $\widetilde{\omega}' \neq \widetilde{\omega}''$, that is

$$\begin{cases} (I_1(\overline{x}, \overline{y}), -I_2(\overline{x}, \overline{y})) \cdot (\omega_1'', \omega_1') = 0 \\ (I_1(\overline{x}, \overline{y}), -I_2(\overline{x}, \overline{y})) \cdot (\omega_2'', \omega_2') = 0 \end{cases}$$

This means that the vector $(I_1(\overline{x}, \overline{y}), -I_2(\overline{x}, \overline{y}))$ is in the same time orthogonal to (ω_1'', ω_1') and (ω_2'', ω_2'). We can distinguish two cases:

1. the vectors (ω_1'', ω_1') and (ω_2'', ω_2') are orthogonal and coincident (that is $(\omega_1'', \omega_1') \equiv (\omega_2'', \omega_2')$), see Fig. 2.2;

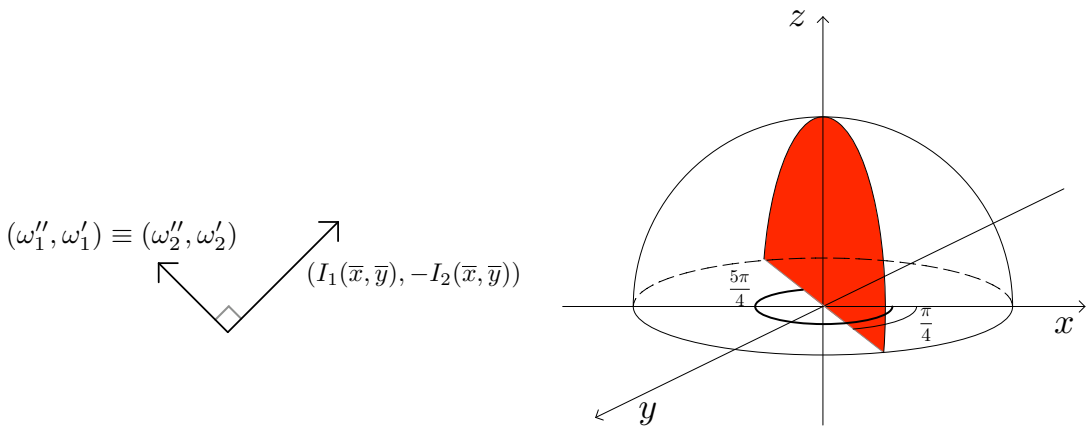

Figure 2.2. On the left the disposition of the orthogonal vector relatively to the first case. On the right, in red, the set of all the possible light sources respect this situation.

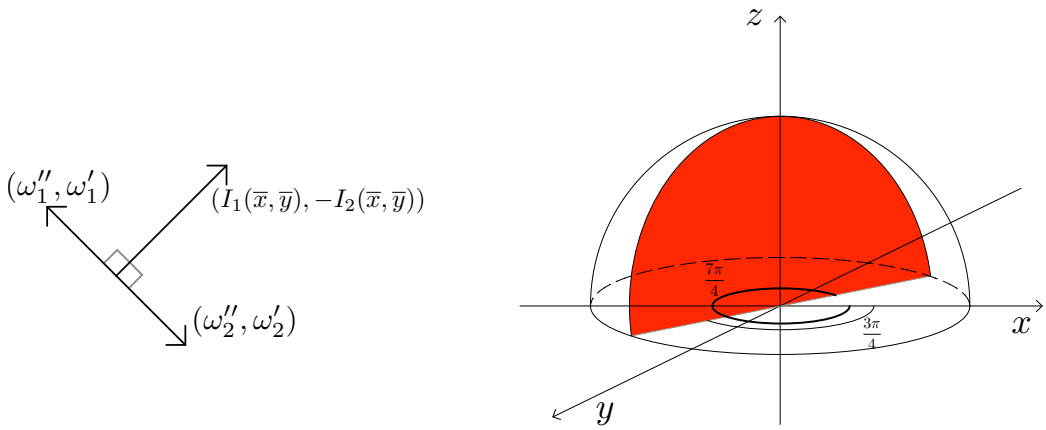

Figure 2.3. On the left the second case explained by the disposition of the vectors. On the right se set of all the possible light sources in the unitary sphere.

2. the two vectors (ω_1'', ω_1') and (ω_2'', ω_2') are orthogonal and placed in the opposite direction (that is $\omega_1'' = -\omega_2''$ and $\omega_1' = -\omega_2'$), see Fig. 2.3.

For both cases we arrive to keep, instead of the two null component of the vector b in (2.13), only one equation (because it is easy to see that in this two cases they are the same). Let us take, for example, the first. That is:

$$I_2(\overline{x}, \overline{y})\omega_1' - I_1(\overline{x}, \overline{y})\omega_1'' = 0 \tag{2.14}$$

Now, in order to complete the proof we consider the definition of images I_1 and I_2 like for the physic case. This means that, replacing their definition we have:

$$\frac{-\nabla u(\overline{x}, \overline{y}) \cdot \widetilde{\omega}'' + \omega_3''}{\sqrt{1 + ||\nabla u(\overline{x}, \overline{y})||^2}}\omega_1' - \frac{-\nabla u(\overline{x}, \overline{y}) \cdot \widetilde{\omega}' + \omega_3'}{\sqrt{1 + ||\nabla u(\overline{x}, \overline{y})||^2}}\omega_1'' = 0$$

$$\frac{-\nabla u(\overline{x}, \overline{y}) \cdot (\omega_1'', \omega_2'') + \omega_3''}{\sqrt{1 + ||\nabla u(\overline{x}, \overline{y})||^2}}\omega_1' - \frac{-\nabla u(\overline{x}, \overline{y}) \cdot (\omega_1', \omega_2') + \omega_3'}{\sqrt{1 + ||\nabla u(\overline{x}, \overline{y})||^2}}\omega_1'' = 0$$

$$\frac{\partial u}{\partial x}(\overline{x}, \overline{y})\omega_1''\omega_1' - \frac{\partial u}{\partial y}(\overline{x}, \overline{y})\omega_2''\omega_1' + \omega_3''\omega_1' + \frac{\partial u}{\partial x}(\overline{x}, \overline{y})\omega_1'\omega_1'' + \frac{\partial u}{\partial y}(\overline{x}, \overline{y})\omega_2'\omega_1'' - \omega_3'\omega_1'' = 0$$

$$\frac{\partial u}{\partial x}(\overline{x}, \overline{y})\omega_1''\omega_1' - \frac{\partial u}{\partial y}(\overline{x}, \overline{y})\omega_1''\omega_1' + \omega_3''\omega_1' + \frac{\partial u}{\partial x}(\overline{x}, \overline{y})\omega_1'\omega_1'' + \frac{\partial u}{\partial y}(\overline{x}, \overline{y})\omega_1'\omega_1'' - \omega_3'\omega_1'' = 0$$

Then we finally arrive to:

$$\frac{\omega_3''}{\omega_3'} = \frac{\omega_1''}{\omega_1'} = \frac{\omega_2''}{\omega_2'}$$

and if we consider the previous equivalence using the spherical coordinates for the light source vectors we obtain:

$$\frac{\cos\varphi_2}{\cos\varphi_1} = \frac{\sin\varphi_2\cos\theta_2}{\sin\varphi_1\cos\theta_1} = \frac{\sin\varphi_2\sin\theta_2}{\sin\varphi_1\sin\theta_1}. \tag{2.15}$$

In the first case we have that $\theta_1, \theta_2 \in \{\frac{\pi}{4}, \frac{5\pi}{4}\}$ whereas in the second case $\theta_1, \theta_2 \in \{\frac{3\pi}{4}, \frac{7\pi}{4}\}$. Our target is to prove that $\theta_1 = \theta_2$ in order to obtain the absurd considering

that in this case it results that $\widetilde{\omega}' = \widetilde{\omega}''$ (i.e. $\omega' = \omega''$) and it is not the case of the photometric stereo.

It is clear that, for both cases, if $\frac{\cos\theta_2}{\cos\theta_1} = +1$ then $\theta_1 = \theta_2$ while $\frac{\cos\theta_2}{\cos\theta_1} = -1$ means $\theta_1 \neq \theta_2$.

Let us suppose, for absurd again, that $\theta_1 \neq \theta_2$. Then, from (2.15) we have:

$$\frac{\cos\varphi_2}{\cos\varphi_1} = -\frac{\sin\varphi_2}{\sin\varphi_1}$$

and it is not possible because $\varphi_1, \varphi_2 \in [0, \frac{\pi}{2}]$.

□

We will see that this lemma will be useful in two important points in the next parts: the first is for the proof of the uniqueness of the weakest admissible solution of the problem and, the second, is related to an important consideration related to the semi-lagrangian numerical scheme.

One way to prove the existence and the uniqueness of the solution of the problem (2.8) is to consider the characteristics method ([58]). This kind of proof gives us the possibility to use a numerical scheme that retraces this method to construct an approximation of the solution.

If we consider the function that describes the previous linear problem as the (1.4) one, that is

$$H(x, y, p) = b(x, y) \cdot p - f(x, y) = 0 \tag{2.16}$$

we can write the uniqueness theorem like this:

Theorem 2.3 *If we consider $H(x, y, p) = b(x, y) \cdot p - f(x, y)$ with $b(x, y)$, $f(x, y)$ and $g(x, y)$ Lipschitz functions, then the problem*

$$\begin{cases} H(x, y, \nabla u) = 0, & \forall (x, y) \in \Omega; \\ u(x, y) = g(x, y) & \forall (x, y) \in \partial\Omega. \end{cases} \tag{2.17}$$

admits an unique solution $u(x, y) \in C^1(\Omega)$.

We have rewritten the problem (1.4) just for emphasize that, if we want to arrive to find the unique smooth solution of this kind of differential problem, we need to have the equation defined $\forall (x, y) \in \Omega$. In the next sections we will see as the weakening of the regularity of the solution for the same problem allow us to write that the equation of the problem must be verified $a.e.(x, y) \in \Omega$. This is because the equation depends only from the gradient on u and also because we want to weakening the solution till the Lipschitz continuity space.

2.1 Existence and uniqueness of the weak solution

As seen before, for the problem (2.8) it is possible to prove the existence and the uniqueness of a regular solution that is a classical smooth solution. In order to complete the analysis and try to make this approach applicable in practice, we will extend the uniqueness results also in the case of weak solution. In our case we denote by weak solutions the set of Lipschitz functions defined on Ω. In real

applications indeed the most part of the objects that we can take a picture can be considered without points of discontinuity, and only with points where they are not differentiable.

Let's observe that the SfS problem, when we use only one image, fails its target (the reconstruction of the surface) even if we consider the restriction of the problem to the classical solutions that is to the $C^1(\Omega)$ functions ([2, 9]).

If we remain in the context of the applications, it is possible to consider the advantage of the study of an inverse problem like the SfS. In this case (that is the physical case), in fact, we can understand what happens to the function coefficients $b(x, y)$ and $f(x, y)$. If we consider as a solution surface u a Lipschitz one, and we consider the points where it is not differentiable as the family of piecewise regular curves $(\gamma_1(t), \ldots, \gamma_k(t))$ where t is the argument of the parametric representation, it is clear that this curve contains also the points of discontinuity of the functions $b(x, y)$ and $f(x, y)$ because of their definition depends by $I_1(x, y)$ and $I_2(x, y)$. This means that our problem (2.8) has, in the linear equation, discontinuous coefficients. That is, if we consider our differential problem like an inverse problem of SfS with photometric stereo technique, searching for a weak solution implies a study of the linear partial differential equation with discontinuous coefficients. Moreover there is a relation between the set of points of discontinuity of $b(x, y)$ and $f(x, y)$ and the set of points where the solution u is not differentiable in fact they are the same (see Fig. 2.4). Another feature about the discontinuity type of $b(x, y)$ and $f(x, y)$ is always related to the fact that we are considering an inverse problem where it is proposed to find a Lipschitz solution. This means that it must be a jump discontinuity.

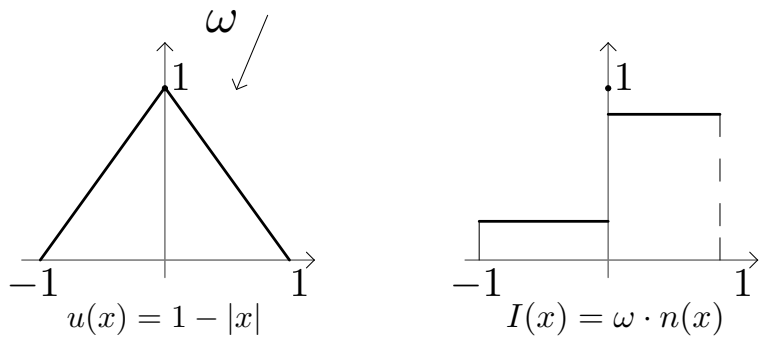

Figure 2.4. A schematic example shows that the points where the image function I is discontinuous are the same for which the solution u is not differentiable. On the left the Lipschitz function, on the right the associated image through the light ω.

Theorem 2.4 *Let us consider two points* $(\hat{x}, \hat{y})$, $(\widetilde{x}, \widetilde{y}) \in \Omega \backslash (\gamma_1(t), \ldots, \gamma_k(t))$ *(where* $(\gamma_1(t), \ldots, \gamma_k(t))$ *represents the family of jump discontinuity curves for b) and let us define the following quantities:*

$$\hat{I}_1 = I_1(\hat{x}, \hat{y}), \quad \widetilde{I}_1 = I_1(\widetilde{x}, \widetilde{y})$$
$$\hat{I}_2 = I_2(\hat{x}, \hat{y}), \quad \widetilde{I}_2 = I_2(\widetilde{x}, \widetilde{y}).$$

Replacing them in the analytical form of $b(x,y)$ *(2.9)*

$$\hat{b} = (b_1(\hat{x},\hat{y}), b_2(\hat{x},\hat{y})) = (\hat{I}_2\omega_1' - \hat{I}_1\omega_1'', \hat{I}_2\omega_2' - \hat{I}_1\omega_2'')$$
$$\widetilde{b} = (b_1(\widetilde{x},\widetilde{y}), b_2(\widetilde{x},\widetilde{y})) = (\widetilde{I}_2\omega_1' - \widetilde{I}_1\omega_1'', \widetilde{I}_2\omega_2' - \widetilde{I}_1\omega_2'')$$

we have

$$\hat{b}\cdot\widetilde{b} \geq 0. \tag{2.18}$$

Proof.
Let us start the prove writing (2.18) in its complete analytical form. We obtain:

$$(\hat{I}_2\omega_1' - \hat{I}_1\omega_1'', \hat{I}_2\omega_2' - \hat{I}_1\omega_2'')\cdot(\widetilde{I}_2\omega_1' - \widetilde{I}_1\omega_1'', \widetilde{I}_2\omega_2' - \widetilde{I}_1\omega_2'') \geq 0$$
$$(\hat{I}_2\omega_1' - \hat{I}_1\omega_1'')(\widetilde{I}_2\omega_1' - \widetilde{I}_1\omega_1'') + (\hat{I}_2\omega_2' - \hat{I}_1\omega_2'')(\widetilde{I}_2\omega_2' - \widetilde{I}_1\omega_2'') \geq 0$$

that is

$$\hat{I}_2\widetilde{I}_2(\omega_2')^2 - \widetilde{I}_1\hat{I}_2\omega_1'\omega_1'' - \hat{I}_1\widetilde{I}_2\omega_1'\omega_1'' + \hat{I}_1\widetilde{I}_1(\omega_1'')^2 + \\ + \hat{I}_2\widetilde{I}_2(\omega_2')^2 - \widetilde{I}_1\hat{I}_2\omega_2'\omega_2'' - \hat{I}_1\widetilde{I}_2\omega_2'\omega_2'' + \hat{I}_1\widetilde{I}_1(\omega_2'')^2 \geq 0$$

that can be showed as follow:

$$\hat{I}_2\widetilde{I}_2((\omega_1')^2 + (\omega_2')^2) - \widetilde{I}_1\hat{I}_2(\omega_1'\omega_1'' + \omega_2'\omega_2'') - \\ - \hat{I}_1\widetilde{I}_2(\omega_1'\omega_1'' + \omega_2'\omega_2'') + \hat{I}_1\widetilde{I}_1((\omega_1'')^2 + (\omega_2'')^2) \geq 0$$

so in the end we study the inequality below

$$\hat{I}_2\widetilde{I}_2||\widetilde{\omega}'||^2 + \hat{I}_1\widetilde{I}_1||\widetilde{\omega}''||^2 \geq (\hat{I}_1\widetilde{I}_2 + \widetilde{I}_1\hat{I}_2)\widetilde{\omega}'\cdot\widetilde{\omega}''. \tag{2.19}$$

Now we have to take into account that our image functions have all bounded values in $(0,1]$. The only way to have the left side of (2.19) equal to zero consists to take $\widetilde{\omega}'$ and $\widetilde{\omega}''$ such that $||\widetilde{\omega}'||$ and $||\widetilde{\omega}''||$ are equal to zero at the same time. But this is not permitted by the photometric stereo technique definition used to solve the problem (i.e. the light sources must be different).

It is clear that if we take the two light vectors such that $\widetilde{\omega}'\cdot\widetilde{\omega}'' \leq 0$ we obtain (2.18) verified, but now we want to prove it (through the (2.19) formulation) in a more general case.

Let us recall the definition of the image function (in the interested points) in the physic case:

$$\hat{I}_1 = \frac{-\nabla u(\hat{x},\hat{y})\cdot\widetilde{\omega}' + \omega_3'}{\sqrt{1+||\nabla u(\hat{x},\hat{y})||^2}}, \qquad \widetilde{I}_1 = \frac{-\nabla u(\widetilde{x},\widetilde{y})\cdot\widetilde{\omega}' + \omega_3'}{\sqrt{1+||\nabla u(\widetilde{x},\widetilde{y})||^2}},$$
$$\hat{I}_2 = \frac{-\nabla u(\hat{x},\hat{y})\cdot\widetilde{\omega}'' + \omega_3''}{\sqrt{1+||\nabla u(\hat{x},\hat{y})||^2}}, \qquad \widetilde{I}_2 = \frac{-\nabla u(\widetilde{x},\widetilde{y})\cdot\widetilde{\omega}'' + \omega_3''}{\sqrt{1+||\nabla u(\widetilde{x},\widetilde{y})||^2}}.$$

replacing them into (2.19), we observe that the denominator of all the terms of both sides is the same, that is:

$$\sqrt{1+||\nabla u(\widetilde{x},\widetilde{y})||^2}\sqrt{1+||\nabla u(\hat{x},\hat{y})||^2}$$

and we can study the inequality without it because it is always different from zero (and in particular it is positive). Let us define the following quantities (positive by definition):

$$\begin{aligned} \hat{i}_1 &= -\nabla u(\hat{x},\hat{y})\cdot\widetilde{\omega}' + \omega_3', \qquad \widetilde{i}_1 = -\nabla u(\widetilde{x},\widetilde{y})\cdot\widetilde{\omega}' + \omega_3', \\ \hat{i}_2 &= -\nabla u(\hat{x},\hat{y})\cdot\widetilde{\omega}'' + \omega_3'', \qquad \widetilde{i}_2 = -\nabla u(\widetilde{x},\widetilde{y})\cdot\widetilde{\omega}'' + \omega_3'', \end{aligned} \tag{2.20}$$

for which is possible to calculate the differences below:

$$\begin{aligned} |\hat{i}_1 - \widetilde{i}_1| &= |(\nabla u(\hat{x},\hat{y})\cdot\widetilde{\omega}' + \omega_3') - (-\nabla u(\widetilde{x},\widetilde{y})\cdot\widetilde{\omega}' + \omega_3')| = \\ &= |(\nabla u(\widetilde{x},\widetilde{y}) - \nabla u(\hat{x},\hat{y}))\cdot\widetilde{\omega}'| \le ||\nabla u(\widetilde{x},\widetilde{y}) - \nabla u(\hat{x},\hat{y})||||\widetilde{\omega}'|| \le \Delta_L||\widetilde{\omega}'|| \end{aligned} \tag{2.21}$$

$$\begin{aligned} |\hat{i}_2 - \widetilde{i}_2| &= |(\nabla u(\hat{x},\hat{y})\cdot\widetilde{\omega}'' + \omega_3'') - (-\nabla u(\widetilde{x},\widetilde{y})\cdot\widetilde{\omega}'' + \omega_3'')| = \\ &= |(\nabla u(\widetilde{x},\widetilde{y}) - \nabla u(\hat{x},\hat{y}))\cdot\widetilde{\omega}''| \le ||\nabla u(\widetilde{x},\widetilde{y}) - \nabla u(\hat{x},\hat{y})||||\widetilde{\omega}''|| \le \Delta_L||\widetilde{\omega}''|| \end{aligned} \tag{2.22}$$

that permit to write that

$$\exists!\quad \xi\in[-\Delta_L,\Delta_L] \quad : \quad \hat{i}_1 = \widetilde{i}_1 + \xi||\widetilde{\omega}'||, \quad \hat{i}_2 = \widetilde{i}_2 + \xi||\widetilde{\omega}''||. \tag{2.23}$$

Now, replacing the equalities of (2.23) in (2.19) we obtain:

$$\begin{gathered} (\widetilde{i}_2+\xi||\widetilde{\omega}''||)\widetilde{i}_2||\widetilde{\omega}'||^2+(\widetilde{i}_1+\xi||\widetilde{\omega}'||)\widetilde{i}_1||\widetilde{\omega}''||^2-\Big[(\widetilde{i}_1+\xi||\widetilde{\omega}'||)\widetilde{i}_2+(\widetilde{i}_2+\xi||\widetilde{\omega}''||)\widetilde{i}_1\Big]\widetilde{\omega}'\cdot\widetilde{\omega}'' \ge 0 \\ (\widetilde{i}_2)^2||\widetilde{\omega}'||^2 + \widetilde{i}_2\xi||\widetilde{\omega}''||||\widetilde{\omega}'||^2 + (\widetilde{i}_1)^2||\widetilde{\omega}''||^2 + \widetilde{i}_1\xi||\widetilde{\omega}'||||\widetilde{\omega}''|| - \\ - \Big[\widetilde{i}_1\widetilde{i}_2 + \widetilde{i}_2\xi||\widetilde{\omega}'|| + \widetilde{i}_1\widetilde{i}_2 + \widetilde{i}_1\xi||\widetilde{\omega}''||\Big]\widetilde{\omega}'\cdot\widetilde{\omega}'' \ge 0 \\ (\widetilde{i}_2\widetilde{\omega}' - \widetilde{i}_1\widetilde{\omega}'')^2 + \xi\Big[\widetilde{i}_2||\widetilde{\omega}''||||\widetilde{\omega}'||^2 + \widetilde{i}_1||\widetilde{\omega}'||||\widetilde{\omega}''||^2 - \Big(\widetilde{i}_2||\widetilde{\omega}'|| + \widetilde{i}_1||\widetilde{\omega}''||\Big)\widetilde{\omega}'\cdot\widetilde{\omega}''\Big] \ge 0 \\ (\widetilde{i}_2\widetilde{\omega}' - \widetilde{i}_1\widetilde{\omega}'')^2 + \xi\Big[||\widetilde{\omega}'||||\widetilde{\omega}''||(\widetilde{i}_2||\widetilde{\omega}'|| + \widetilde{i}_1||\widetilde{\omega}''||) - \Big(\widetilde{i}_2||\widetilde{\omega}'|| + \widetilde{i}_1||\widetilde{\omega}''||\Big)\widetilde{\omega}'\cdot\widetilde{\omega}''\Big] \ge 0 \end{gathered}$$

$$(\widetilde{i}_2\widetilde{\omega}' - \widetilde{i}_1\widetilde{\omega}'')^2 + \xi\Big[(\widetilde{i}_2||\widetilde{\omega}'|| + \widetilde{i}_1||\widetilde{\omega}''||)(||\widetilde{\omega}'||||\widetilde{\omega}''|| - \widetilde{\omega}'\cdot\widetilde{\omega}'')\Big] \ge 0. \tag{2.24}$$

Considering that $||\widetilde{\omega}'||||\widetilde{\omega}''|| - \widetilde{\omega}'\cdot\widetilde{\omega}'' \ge 0$ (for the Cauchy-Schwarz inequality), we have that the (2.24) is verified if $\xi \ge 0$. Now we can obtain the appropriate sign of this coefficient considering the most appropriate relation between $\widetilde{i}_j$ and $\hat{i}_j$ for $j = 1, 2$. That is, let us suppose that $\xi \in [-\Delta_L, 0)$, it is clear that we can choose the following relation

$$\widetilde{i}_1 = \hat{i}_1 - \xi||\widetilde{\omega}'||, \quad \widetilde{i}_2 = \hat{i}_2 - \xi||\widetilde{\omega}''||$$

(or the others intermediate relations) and repeat the substitutions in order to obtain the (2.24) satisfied.

□

It is clear that is very important the structure of the vector field $b(x, y)$ near the points of discontinuity because the characteristics have not to meet any obstacle for the propagation of the information across the domain. In Fig. 2.5 we summarize the possibles cases of behavior of $b(x, y)$ around a point $(\overline{x}, \overline{y})$ of a fixed discontinuity

curve $\gamma(t)$. In the picture of Fig. 2.5(a) and Fig. 2.5(b) we consider the vector field well structured for the information flow because in these cases we can obtain the uniqueness of a weak solution for the linear problem (2.17). In the others two cases of Fig. 2.5(c) and Fig. 2.5(d) we are not able to obtain a unique continuous solution without know additional information about the height of the surface on the curve $\gamma(t)$.

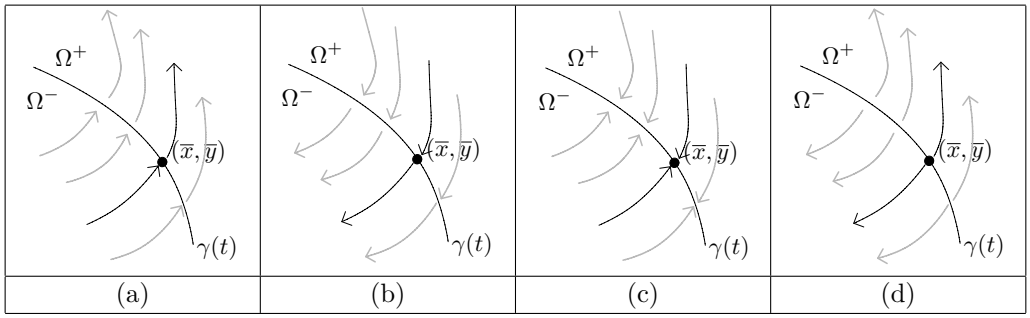

Figure 2.5. The vector field with respect to the discontinuity curve $\gamma(t)$.

Let us start proving a result regarding the global structure of $b(x,y)$. We will emphasize later the importance of this result respect the curves of its discontinuity. In fact it is possible to prove that the characteristic field has the features of the Fig.2.5(a) or Fig.2.5(b).

Theorem 2.5 *Let $\gamma(t)$ be a curve of discontinuity for the function $b(x,y)$ (and $f(x,y)$) and let $(\overline{x},\overline{y})$ be a point of this curve. Let $n(\overline{x},\overline{y})$ be the outgoing normal with respect to the set Ω^+, than we have*

$$\left[\lim_{(x,y)\in\Omega^+\to(\overline{x},\overline{y})} b(x,y)\cdot n(\overline{x},\overline{y})\right]\left[\lim_{(x,y)\in\Omega^-\to(\overline{x},\overline{y})} b(x,y)\cdot n(\overline{x},\overline{y})\right]\geq 0 \tag{2.25}$$

Proof.
Let us define the following quantities:

$$\begin{aligned} I_1^+ &= \lim_{(x,y)\in\Omega^+\to(\overline{x},\overline{y})} I_1(x,y), \qquad I_1^- = \lim_{(x,y)\in\Omega^-\to(\overline{x},\overline{y})} I_1(x,y),\\ I_2^+ &= \lim_{(x,y)\in\Omega^+\to(\overline{x},\overline{y})} I_2(x,y), \qquad I_2^- = \lim_{(x,y)\in\Omega^-\to(\overline{x},\overline{y})} I_2(x,y), \end{aligned}$$

in order to work with the vector field $b(x,y)$ in the limit zone of $(\overline{x},\overline{y})$ considering:

$$\begin{aligned} \lim_{(x,y)\in\Omega^+\to(\overline{x},\overline{y})} b(x,y) = (b_1^+,b_2^+) &= (I_2^+\omega_1' - I_1^+\omega_1'', I_2^+\omega_2' - I_1^+\omega_2''),\\ \lim_{(x,y)\in\Omega^-\to(\overline{x},\overline{y})} b(x,y) = (b_1^-,b_2^-) &= (I_2^-\omega_1' - I_1^-\omega_1'', I_2^-\omega_2' - I_1^-\omega_2''). \end{aligned} \tag{2.26}$$

Calling as $(n_1,n_2) = (n_1(\overline{x},\overline{y}), n_2(\overline{x},\overline{y}))$ the two coordinates of $n(\overline{x},\overline{y})$ and replacing these last identity in the inequality (2.25) it is possible to write the following passages:

$$\begin{aligned} (b_1^+n_1 + b_2^+n_2)(b_1^-n_1 + b_2^-n_2) &\geq 0\\ b_1^+b_1^-n_1^2 + b_2^+b_2^-n_2^2 + n_1n_2(b_1^+b_2^- + b_2^+b_1^-) &\geq 0 \end{aligned}$$

and now, using (2.26), we have

$$(I_2^+\omega_1' - I_1^+\omega_1'')(I_2^-\omega_1' - I_1^-\omega_1'')n_1^2 + (I_2^+\omega_2' - I_1^+\omega_2'')(I_2^-\omega_2' - I_1^-\omega_2'')n_2^2 + \\ \Big[(I_2^+\omega_1' - I_1^+\omega_1'')(I_2^-\omega_2' - I_1^-\omega_2'') + (I_2^-\omega_1' - I_1^-\omega_1'')(I_2^+\omega_2' - I_1^+\omega_2'')\Big]n_1n_2 \geq 0 \quad (2.27)$$

For a better understanding, let us separate the coefficients that multiply n_1^2 (2.28), n_2^2 (2.29) and n_1n_2 (2.30). We can write them respectively below:

$$I_2^+I_2^-(\omega_1')^2 - I_2 + I_1^-\omega_1'\omega_1'' - I_1^+I_2^-\omega_1'\omega_1'' + I_1^+I_1^-(\omega_1'')^2 = \\ = I_2^+I_2^-(\omega_1')^2 - (I_2^+I_1^- + I_1^+I_2^-)\omega_1'\omega_1'' + I_1^+I_1^-(\omega_1'')^2 \quad (2.28)$$

$$I_2^+I_2^-(\omega_2')^2 - I_2^+I_1^-\omega_2'\omega_2'' - I_1^+I_2^-\omega_2'\omega_2'' + I_1^+I_1^-(\omega_2'')^2 = \\ I_2^+I_2^-(\omega_2')^2 - \omega_2'\omega_2''(I_1^+I_2^- + I_2^+I_1^-) + I_1^+I_1^-(\omega_2'')^2 \quad (2.29)$$

$$I_2^+I_2^-\omega_1'\omega_2' - I_1^-I_2^+\omega_1'\omega_2'' - I_1^+I_2^-\omega_1''\omega_2' + I_1^+I_1^-\omega_1''\omega_2'' + \\ + I_2^+I_2^-\omega_2'\omega_1' - I_2^+I_1^-\omega_2'\omega_1'' - I_1^+I_2^-\omega_2''\omega_1' + I_1^+I_1^-\omega_1''\omega_2'' = \\ = 2I_2^+I_2^-\omega_1'\omega_2' - \omega_1'\omega_2''(I_1^-I_2^+ + I_1^+I_2^-) - \omega_1''\omega_2'(I_1^-I_2^2 + I_1^+I_2^-) + 2I_1^+I_1^-\omega_1''\omega_2'' = \\ = 2I_2^+I_2^-\omega_1'\omega_2' - (\omega_1'\omega_2'' + \omega_1''\omega_2')(I_1^-I_2^+ + I_1^+I_2^-) + 2I_1^+I_1^-\omega_1''\omega_2'' \quad (2.30)$$

In order to proceed with the prove in the physic case, we consider the following equality for the image functions:

$$I_1^+ = \lim_{(x,y)\in\Omega^+\to(\overline{x},\overline{y})} I_1(x,y) = \lim_{(x,y)\in\Omega^+\to(\overline{x},\overline{y})} \frac{-\nabla u(x,y)\cdot\widetilde{\omega}' + \omega_3'}{\sqrt{1+||\nabla u(x,y)||^2}} = \frac{-\nabla u^+\cdot\widetilde{\omega}' + \omega_3'}{\sqrt{1+||\nabla u^+||^2}},$$
$$I_1^- = \lim_{(x,y)\in\Omega^-\to(\overline{x},\overline{y})} I_1(x,y) = \lim_{(x,y)\in\Omega^-\to(\overline{x},\overline{y})} \frac{-\nabla u(x,y)\cdot\widetilde{\omega}' + \omega_3'}{\sqrt{1+||\nabla u(x,y)||^2}} = \frac{-\nabla u^-\cdot\widetilde{\omega}' + \omega_3'}{\sqrt{1+||\nabla u^-||^2}},$$
$$I_2^+ = \lim_{(x,y)\in\Omega^+\to(\overline{x},\overline{y})} I_2(x,y) = \lim_{(x,y)\in\Omega^+\to(\overline{x},\overline{y})} \frac{-\nabla u(x,y)\cdot\widetilde{\omega}'' + \omega_3''}{\sqrt{1+||\nabla u(x,y)||^2}} = \frac{-\nabla u^+\cdot\widetilde{\omega}'' + \omega_3''}{\sqrt{1+||\nabla u^+||^2}},$$
$$I_2^- = \lim_{(x,y)\in\Omega^-\to(\overline{x},\overline{y})} I_2(x,y) = \lim_{(x,y)\in\Omega^-\to(\overline{x},\overline{y})} \frac{-\nabla u(x,y)\cdot\widetilde{\omega}'' + \omega_3''}{\sqrt{1+||\nabla u(x,y)||^2}} = \frac{-\nabla u^-\cdot\widetilde{\omega}'' + \omega_3''}{\sqrt{1+||\nabla u^-||^2}}.$$

Since in the coefficients (2.28), (2.29) and (2.30) there are all terms divided by a common denominator always strictly positive

$$\sqrt{1+||\nabla u^+||^2}\sqrt{1+||\nabla u^-||^2}$$

we can eliminate it and consider the following quantities (always positive because of the absence of the black shadows):

$$\begin{aligned} i_1^+ &= -\nabla u^+\cdot\widetilde{\omega}' + \omega_3', \qquad & i_1^- &= -\nabla u^-\cdot\widetilde{\omega}' + \omega_3', \\ i_2^+ &= -\nabla u^+\cdot\widetilde{\omega}'' + \omega_3'', \qquad & i_2^- &= -\nabla u^-\cdot\widetilde{\omega}'' + \omega_3'', \end{aligned} \quad (2.31)$$

and, considering the same differences (as in the Theorem 2.4)

$$|i_1^+ - i_1^-| = |(\nabla u^+\cdot\widetilde{\omega}' + \omega_3') - (-\nabla u^-\cdot\widetilde{\omega}' + \omega_3')| = \\ = |(\nabla u^- - \nabla u^+)\cdot\widetilde{\omega}'| \leq ||\nabla u^- - \nabla u^+||||\widetilde{\omega}'|| \leq \Delta^{\pm}||\widetilde{\omega}'|| \quad (2.32)$$

$$|i_2^+ - i_2^-| = |(\nabla u^+ \cdot \widetilde{\omega}'' + \omega_3'') - (-\nabla u^- \cdot \widetilde{\omega}'' + \omega_3'')| = \\ = |(\nabla u^- - \nabla u^+) \cdot \widetilde{\omega}''| \leq ||\nabla u^- - \nabla u^+|| ||\widetilde{\omega}''|| \leq \Delta^{\pm} ||\widetilde{\omega}''|| \tag{2.33}$$

we can write that

$$\exists! \quad \eta \in [-\Delta^{\pm}, 0) \cup (0, \Delta^{\pm}] \quad : \quad i_1^+ = i_1^- + \eta ||\widetilde{\omega}'||, \quad i_2^+ = i_2^- + \eta ||\widetilde{\omega}''||. \tag{2.34}$$

We are excluding the case $\eta = 0$ because it corresponds to the case of a regular point for the surface u (i.e. $\eta = 0$ if and only if $(\overline{x}, \overline{y}) \notin \gamma(t)$). Now, replacing the equalities of (2.34) in (2.28), (2.29) and (2.30) we obtain respectively:

$$(i_2^-)^2(\omega_1')^2 + i_2^-(\omega_1')^2||\widetilde{\omega}''||\eta + (i_1^-)^2(\omega_1'')^2 + i_1^-(\omega_1'')^2||\widetilde{\omega}'||\eta - \\ - \Big[i_2^- i_1^- + i_1^-||\widetilde{\omega}''||\eta + i_1^- i_2^- + i_2^-||\widetilde{\omega}'||\eta\Big]\omega_1'\omega_1'' = \\ = (i_1^-\omega_1'' - i_2^-\omega_1')^2 + \eta\Big[i_2^-(\omega_1')^2||\widetilde{\omega}''|| + i_1^-(\omega_1'')^2||\widetilde{\omega}'|| - \omega_1'\omega_1''(i_1^-||\widetilde{\omega}''|| + i_2^-||\widetilde{\omega}'||)\Big]$$

$$(i_2^-)^2(\omega_2')^2 + i_2^-(\omega_2')^2||\widetilde{\omega}''||\eta + (i_1^-)^2(\omega_2'')^2 + i_1^-(\omega_2'')^2||\widetilde{\omega}'||\eta - \\ - \Big[i_1^- i_2^- + i_2^-||\widetilde{\omega}'||\eta + i_2^- i_1^- + i_1^-||\widetilde{\omega}''||\eta\Big]\omega_2'\omega_2'' = \\ = (i_2^-\omega_2' - i_1^-\omega_2'')^2 + \eta\Big[i_2^-(\omega_2')^2||\widetilde{\omega}''|| - i_1^-(\omega_2'')^2||\widetilde{\omega}'|| - \omega_2'\omega_2''(i_1^-||\widetilde{\omega}''|| + i_2^-||\widetilde{\omega}'||)\Big]$$

$$2(i_2^-)^2\omega_1'\omega_2' + 2i_2^-\omega_1'\omega_2'||\widetilde{\omega}''||\eta + 2(i_1^-)^2\omega_1''\omega_2'' + 2i_1^-\omega_1''\omega_2''||\widetilde{\omega}''||\eta - \\ - (\omega_1'\omega_2'' + \omega_1''\omega_2')\Big[i_1^- i_2^- + i_1^-||\widetilde{\omega}''||\eta + i_1^- i_2^- + i_2^-||\widetilde{\omega}'||\eta\Big] = \\ = 2(i_1^-)^2\omega_1''\omega_2'' + 2(i_2^-)^2\omega_1'\omega_2' - 2i_1^- i_2^-(\omega_1'\omega_2'' + \omega_1''\omega_2') + \\ + \eta\Big[2i_2^-\omega_1'\omega_2'||\widetilde{\omega}''|| + 2i_1^-\omega_1''\omega_2''||\widetilde{\omega}''|| - (\omega_1'\omega_2'' + \omega_1''\omega_2')(i_1^-||\widetilde{\omega}''|| + i_2^-||\widetilde{\omega}'||)\Big] = \\ = -2i_1^- i_2^-\omega_1''\omega_2' + 2(i_1^-)^2\omega_1''\omega_2'' + 2(i_2^-)^2\omega_1'\omega_2' - 2i_1^- i_2^-\omega_1'\omega_2'' + \\ + \eta\Big[2i_2^-\omega_1'\omega_2'||\widetilde{\omega}''|| + 2i_1^-\omega_1''\omega_2''||\widetilde{\omega}''|| - (\omega_1'\omega_2'' + \omega_1''\omega_2')(i_1^-||\widetilde{\omega}''|| + i_2^-||\widetilde{\omega}'||)\Big] = \\ = -2(i_1^-\omega_1'' - i_2\omega_1')(i_2^-\omega_2' - i_1^-\omega_2'') + \\ + \eta\Big[2i_2^-\omega_1'\omega_2'||\widetilde{\omega}''|| + 2i_1^-\omega_1''\omega_2''||\widetilde{\omega}''|| - (\omega_1'\omega_2'' + \omega_1''\omega_2')(i_1^-||\widetilde{\omega}''|| + i_2^-||\widetilde{\omega}'||)\Big]$$

Replacing them into (2.27), we have:

$$\Big[(i_1^-\omega_1'' - i_2^-\omega_1')n_1 - (i_2^-\omega_2 - i_1^-\omega_2'')n_2\Big]^2 + \\ + \eta\Big[(i_2^-(\omega_1')||\widetilde{\omega}''|| - (i_2^-||\widetilde{\omega}'|| + i_1^-||\widetilde{\omega}'')\omega_1'\omega_1'' + i_1^-(\omega_1'')^2||\widetilde{\omega}'||)n_1^2 + \\ + (i_2^-(\omega_2')^2||\widetilde{\omega}''|| - (i_2^-||\widetilde{\omega}'|| + i_1^-||\widetilde{\omega}''||)\omega_2'\omega_2'' + i_1(\omega_2'')^2||\widetilde{\omega}'||)n_2^2 + \\ + (2i_2^-\omega_1'\omega_2'||\widetilde{\omega}''|| + 2i_1^-\omega_1''\omega_2''||\widetilde{\omega}'|| - (\omega_1'\omega_2'' + \omega_1''\omega_2')(i_2^-||\widetilde{\omega}'|| + i_1^-||\widetilde{\omega}''||)n_1 n_2\Big] \geq 0.$$

In order to verify the previous inequality we continue to manipulate the left side obtaining

$$\begin{aligned}\Big[(i_1^-\omega_1'' - i_2^-\omega_1')n_1 - (i_2^-\omega_2 - i_1^-\omega_2'')n_2\Big]^2 + \\ + \eta\Big[i_2^-||\widetilde{\omega}''||((\omega_1')^2n_1^2 + (\omega_2')^2n_2^2 + 2\omega_1'\omega_2'n_1n_2) + \\ + i_1^-||\widetilde{\omega}'||((\omega_1'')^2n_1^2 + (\omega_2'')^2n_2^2 + 2\omega_1''\omega_2''n_1n_2) - \\ - (i_2^-||\widetilde{\omega}'|| + i_1^-||\widetilde{\omega}''||)(\omega_1'\omega_1''n_1^2 + \omega_2'\omega_2''n_2^2 + (\omega_1'\omega_2'' + \omega_1''\omega_2')n_1n_2)\Big] \geq 0\end{aligned}$$

that in the end becomes

$$\begin{aligned}\Big[(i_1^-\omega_1'' - i_2^-\omega_1')n_1 - (i_2^-\omega_2 - i_1^-\omega_2'')n_2\Big]^2 + \\ + \eta\Big[i_2^-||\widetilde{\omega}''||(\omega_1'n_1 + \omega_2'n_2)^2 + i_1^-||\widetilde{\omega}'||(\omega_1''n_1 + \omega_2''n_2)^2 - \\ - (i_2^-||\widetilde{\omega}'|| + i_1^-||\widetilde{\omega}''||)(\omega_1'\omega_1''n_1^2 + \omega_2'\omega_2''n_2^2 + (\omega_1'\omega_2'' + \omega_1''\omega_2')n_1n_2)\Big] \geq 0.\end{aligned}$$

Now, with the aim to have the inequality verified, (as in the Theorem 2.4) it is possible to choose the appropriate representation of the numerator of the images valued by the limit in $(\overline{x}, \overline{y})$ (that is i_1^+, i_1^-, i_2^+ and i_2^-) in order to have an η of an appropriate sign.

□

The conclusion of the previous theorem is related to the structure of the vector field $b(x, y)$. In fact, near the points of discontinuity, the condition (2.18) permits to respects the structure represented in Fig. 2.5(a) and Fig. 2.5(b). Instead, in a global sense, some difficult structures (like in Fig. 2.6) for $b(x, y)$ are avoided. However this condition on the vector field b is necessary for the construction of a unique Lipschitz solution shown in the following result.

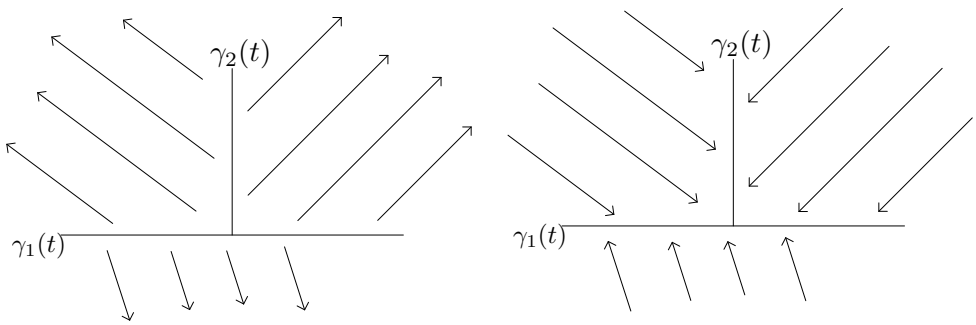

Figure 2.6. Two example of impossible structures for the vector field $b(x, y)$.

Theorem 2.6 *Let us consider the problem*

$$\begin{cases} b(x,y)\cdot\nabla u(x,y) = f(x,y), & a.e.\ (x,y)\in\Omega; \\ u(x,y) = g(x,y) & \forall (x,y)\in\partial\Omega. \end{cases} \tag{2.35}$$

Let us suppose that $(\gamma_1(t), \dots, \gamma_k(t))$*, the family of discontinuity curves for* $b(x, y)$ *and* $f(x, y)$*, are not characteristic curves (with respect to the previous problem). Then there exists a unique Lipschitz solution of the problem.*

Proof.

We start the proof considering the problem written like (2.17). The following system of ordinary differential equation permits to obtain the characteristics:

$$\begin{cases} \text{(a)} & \dot{z}(s) = D_p H(p(s), x_c(s), y_c(s)) \cdot p(s) \\ \text{(b)} & \dot{x}_c(s) = D_p H(p(s), x_c(s), y_c(s))_1 \\ \text{(c)} & \dot{y}_c(s) = D_p H(p(s), x_c(s), y_c(s))_2 \end{cases} \tag{2.36}$$

where s is the variable of the parameterization and $z(s)$, $p(s)$ are respectively the value of u and ∇u on the projected characteristic (that is $z(s) = u(x_c(s), y_c(s))$ and $p(s) = \nabla u((x({}_c s), y_c(s)))$. The (2.36) in our case becomes

$$\begin{cases} \text{(a)} & \dot{z}(s) = f(x_c(s), y_c(s)) \\ \text{(b)} & \dot{x}_c(s) = b_1(x_c(s), y_c(s)) \\ \text{(c)} & \dot{y}_c(s) = b_2(x_c(s), y_c(s)) \end{cases} \tag{2.37}$$

The initial condition to integrate this system of ordinary differential equations is taken from the values of the function u known on the boundary. Then

$$\begin{cases} \text{(a}_0\text{)} & u(x_c(0), y_c(0)) = g(x_0, y_0) \\ \text{(b}_0\text{)} & x_c(0) = x_0 \\ \text{(c}_0\text{)} & y_c(0) = y_0 \end{cases}$$

with $(x_0, y_0) \in \partial\Omega$. It is possible now to use the result (2.2) considering that there is no possibility to have attracting or source points in the domain Ω since the vector field $b(x, y)$ is always different from the null vector inside this domain.

Starting from the boundary, it is possible to integrate till the first point of intersection between the projection of the characteristic and the first jump discontinuity curve using the standard method ([58]). Let's consider the point $(x_1, y_1) \in \gamma_j$ also a point of the characteristic passing through (x_0, y_0), that is, there exists $\bar{s}$ and $\bar{t}_j$ such that $(x_1, y_1) = (x_c(\bar{s}), y_c(\bar{s})) = \gamma_j(\bar{t}_j)$, see Fig. 2.7.

Now we can begin to solve another Dirichlet problem on the characteristic, very similar to the starting one:

$$\begin{cases} F(\nabla u(x, y), x, y) = 0, & \forall (x, y) \in (x_c(s), y_c(s)) \text{ with } s > \bar{s}; \\ u(x_c(\bar{s}), y_c(\bar{s})) = \lim\limits_{s \to \bar{s}} u(x_c(s), y_c(s)) \end{cases} \tag{2.38}$$

The well posedness of (2.38) is guaranteed from the type of discontinuity of the functions $b(x, y)$ and $f(x, y)$. In fact the jump discontinuity permits to work with prolongation by the limit. This problem is a simplification of the previous one (2.17) because we are studying it only on a specific characteristic taking like initial starting value the limit of $z(s)_{s \to \bar{s}}$ for the system of ordinary differential equation (2.37). Using the Theorem 2.5 is possible to understand that we don't need of additional information about the solution u inside the domain. In fact, the only information we need to reconstruct the surface all over the domain Ω is the Dirichlet boundary condition.

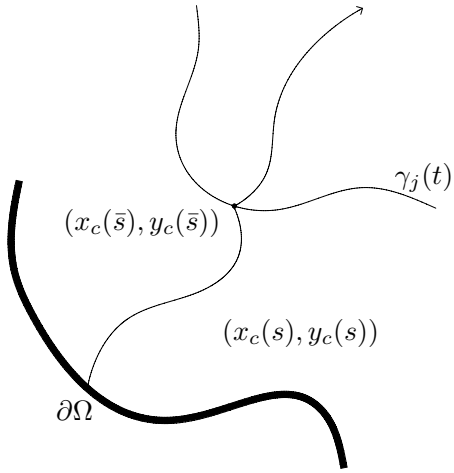

Figure 2.7. A schematic representation of a first intersection point $(x_c(\bar{s}), y_c(\bar{s}))$ between the projected characteristic and the curve of discontinuity $\gamma(t)$.

The reasoning can be extended to all the discontinuity points, that is for all the points of $(\gamma_1(t), \dots \gamma_k(t))$. This means that the integration along the characteristic $s > \bar{s}$ is intended till a new point of discontinuity of the functions $b(x, y)$ and $f(x, y)$, that is till a new intersection point between the characteristic and one of the γ_i curve.

□

Now we want to explain that these kind of solution are the weakest possible to obtain using this type of model for the SfS. If we continue to consider the problem in the physical case, it is much easier to understand the impossibility to have a discontinuous function of the problem (2.35). Let's now use the one dimensional case (always having reference to the two dimensional one) taking for example these two functions:

$$u_1(x) = \begin{cases} x+1, & \text{if } x \leq 1, \\ -x+3, & \text{if } x > 1. \end{cases} \qquad u_2(x) = \begin{cases} x+1, & \text{if } x \leq 1, \\ -x+2, & \text{if } x > 1. \end{cases}$$

If we choose a two dimensional light source ω such that there is no shadow for both the functions, it is then possible to write the respective image functions:

$$I(u_1(x)) = \frac{(-u_1'(x), 1)}{\sqrt{1 + (u_1'(x)^2)}} \cdot (\omega_1, \omega_2) = \frac{(-u_1'(x)\omega_1 + \omega_2)}{\sqrt{1 + (u_1'(x)^2)}} =$$
$$= \frac{(-u_2'(x)\omega_1 + \omega_2)}{\sqrt{1 + (u_2'(x)^2)}} = \frac{(-u_2'(x), 1)}{\sqrt{1 + (u_2'(x)^2)}} \cdot (\omega_1, \omega_2) = I(u_2(x))$$

This is because of the derivative of $u_1(x)$ and $u_2(x)$ (where they are derivable) coincide.

It is clear that these two functions, when we fix the Ω domain, differ from the values they assume on the boundary $\partial\Omega$, but we will see in the next section that not all the boundary is necessary to find the solution. Then, following the previous

constructive demonstration with the aim to obtain a weaker solution, we need to know the value of the jump of u in every point of discontinuity for u. Then, this limitation implies that we are not able to consider discontinuous functions is relative to this kind of model of SfS. In fact, by using a light placed at infinity it is not possible to obtain an associate image that distinguishes from different discontinuous surfaces with the same derivative.

2.2 Consistent boundary condition

In this section we want to introduce the concept of consistent boundary condition with the purpose to define it for our differential problem.

In the previous section we have presented a way to find the unique solution using the characteristic field across all the domain Ω. This approach can be used in two different ways depending on the direction of the characteristic field we want take into account.

If we call $\nu(x,y)$ the unit outgoing normal vector to $\partial\Omega$, it is possible define the following subsets of $\partial\Omega$:

$$\Gamma_{in} = \{(x,y) \in \partial\Omega : \nu(x,y) \cdot \lim_{(\widetilde{x},\widetilde{y})\in\Omega\to(x,y)} b(\widetilde{x},\widetilde{y}) < 0\}$$

$$\Gamma_{out} = \{(x,y) \in \partial\Omega : \nu(x,y) \cdot \lim_{(\widetilde{x},\widetilde{y})\in\Omega\to(x,y)} b(\widetilde{x},\widetilde{y}) > 0\}$$

they are, respectively, the sets of points where the characteristic field is incoming and outgoing respect to Ω. Let us recall that, in our hypotheses, the vector field b is not continuous. This means that in all the discontinuous points of b belonging to $\partial\Omega$ we have to consider the limit vector from the inside of the domain. Let us emphasize once more Theorem 2.5 ensure us any ambiguous case about the sets Γ_{in} and Γ_{out} in fact, as said before, if a curve of discontinuity coincides on a part of the boundary, we have to consider the limit vector of $b(x,y)$.

Then, we can write,

$$\partial\Omega = \Gamma_{out} \cup \Gamma_{in} \cup \Gamma_{tan}$$

where Γ_{tan} is the sets of points where the characteristic field is tangent to $\partial\Omega$.

Let us explain what happens in a simple case going back to a previous example where the light sources are: $\omega' = (0,0,1)$ and $\omega'' = (\omega_1'', \omega_2'', \omega_3'') = (\widetilde{\omega}'', \omega_3'') = (\sin(\varphi)\cos(\theta), \sin(\theta)\sin(\varphi), \cos(\varphi))$. Then, the vector field that defines the characteristic field, that is $b(x,y) = (-I_1(x,y)\omega_1'', -I_1(x,y)\omega_2'') = -I_1(x,y)\widetilde{\omega}''$, can be represented by straight lines all parallels to $\widetilde{\omega}''$ but with the head in the opposite side of it. In this case it is possible to see the two sets Γ_{in} and Γ_{out} of a particular domain Ω (i.e. image domain) like in Fig. 2.8.

As we have seen before, we get to the uniqueness of the weak solution through the characteristic method. In the proof we have not specified the orientation of this field, giving for certain that the direction we consider is orientated as the vector field b. In other words, the problem we solved in the proof is the forward problem, that is:

$$\begin{cases} b(x,y) \cdot \nabla u(x,y) = f(x,y), & \text{a.e. } (x,y) \in \Omega; \\ u(x,y) = g_{in}(x,y) & \forall (x,y) \in \Gamma_{in}. \end{cases} \tag{2.39}$$

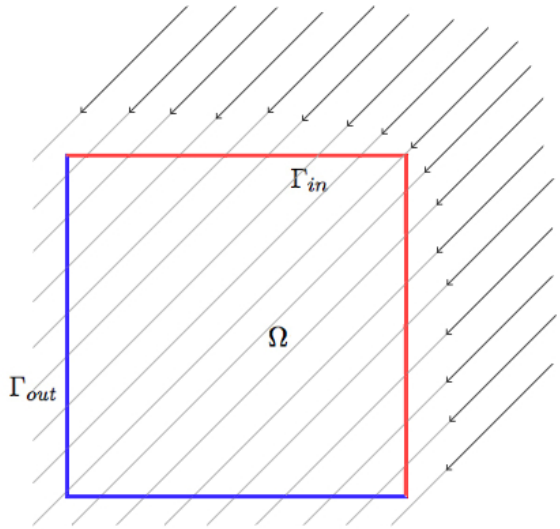

Figure 2.8. An example of image domain Ω and the distribution of the Γ_{In} and Γ_{Out} sets considering a constant characteristic field (represented by the arrows) like in the previous example.

In the same way we can consider the opposite direction and repeat the proof of the uniqueness theorem obtaining the same result. Let us consider then the following backward problem:

$$\begin{cases} b(x,y)\cdot\nabla u(x,y) = f(x,y), & \text{a.e. } (x,y)\in\Omega; \\ u(x,y) = g_{out}(x,y) & \forall (x,y)\in\Gamma_{out}. \end{cases} \tag{2.40}$$

It is clear that, when we consider a global boundary condition $g(x,y)$ (like in the general problem (2.35)) defined all over the boundary domain $\partial\Omega$, we need to define the consistence of this function with both the previous cases. That is, when we start to solve the solution from Γ_{in}, for example, we need to obtain, through the characteristic method, the exact value of $g(x,y)$ on the "other side" of the boundary, that is Γ_{out}. With the aim to define the condition of compatibility of this boundary condition we will define all the constraints that it has to respect to make the problem well posed.

Let us emphasize that all the points of Ω which are not points of discontinuity for b, can be reached by a characteristic curve, that is, for all these points the solution can be univocally determined. We start considering (2.39). We define $\widetilde{\Gamma}^{(x_0,y_0)}(t)$ as the characteristic curve passing through $(x_0,y_0)\in\Gamma_{in}$ and $(x_1,y_1)\in\Gamma_{out}\cap\widetilde{\Gamma}^{(x_0,y_0)}(t)$. Now, following the characteristic method, we determine the value of u_{in} at the point (x_1,y_1). Fixing $g_{in}(x_1,y_1) = u_{in}(x_1,y_1)$ we obtain the boundary condition $g_{in}(x,y)$ defined in $\Gamma_{in}\cup\Gamma_{out}$. Let us call it $\bar{g}_{in}(x,y)$. In the same way we can repeat the reasoning and build $\bar{g}_{out}(x,y)$ defined in $\Gamma_{in}\cup\Gamma_{out}$.

Definition 2.7 *A function $g(x,y)\in C(\Gamma_{in})\cap C(\Gamma_{out})$ is a consistent boundary condition if $\bar{g}_{out}(x,y) = \bar{g}_{in}(x,y)$ and we setting it equal to them.*

Let us emphasize that this kind of definition of consistent boundary condition does not allow us to characterize a unique $g(x,y)$ all over the boundary. That is,

once we set it on Γ_{in} and Γ_{out} like explained before, there is not a unique way to define it globally on all $\partial\Omega$ because of Γ_{tan}. However, this ambiguity does not prevent to reconstruct the solution on all the open domain, on the contrary, using the solution $u(x,y)$ calculated on the open set Ω we can extend continuously the surface also in Γ_{tan}.

That is, if we consider $(x_{tan}, y_{tan}) \in \Gamma_{tan}$ we can call $\nu(x_{tan}, y_{tan})$ the normal unitary vector defined through its polar coordinates, that is: $\nu(x_{tan}, y_{tan}) = (\cos(\theta_{tan}), \sin(\theta_{tan}))$. Let us define the continuous extension of u by the limit:

$$u(x_{tan}, y_{tan}) = \lim_{\rho \to 0} U(x_{tan} + \rho\cos(\theta_{tan}), y_{tan} + \rho\sin(\theta_{tan})) \tag{2.41}$$

where U is the composed function after the polar coordinates substitution.

2.3 Equivalence between the non-linear problem and the linear one

Now we want to prove the equivalence between the problem (2.35) and the following

$$\begin{cases} \dfrac{-\nabla u(x,y)\cdot\widetilde{\omega}' + \omega_3'}{\sqrt{1+||\nabla u(x,y)||^2}} = I_1(x,y), & a.e.(x,y)\in\Omega; \\ \dfrac{-\nabla u(x,y)\cdot\widetilde{\omega}'' + \omega_3''}{\sqrt{1+||\nabla u(x,y)||^2}} = I_2(x,y), & a.e.(x,y)\in\Omega; \\ u(x,y) = g(x,y) & \forall (x,y)\in\partial\Omega. \end{cases} \tag{2.42}$$

Proposition 2.8 *If $v(x,y)$ is a solution of the nonlinear system (2.42) than it is a solution also of (2.35).*

Proof.

We will prove that the two problems are equivalent in the physical case, that is when we consider the relation between the two images and the surface:

$$\begin{cases} I_1(x,y) = G_{\omega'}(v) = \dfrac{-\nabla v(x,y)\cdot\widetilde{\omega}' + \omega_3'}{\sqrt{1+|\nabla v(x,y)|^2}}, & (x,y)\in\Omega; \\ I_2(x,y) = G_{\omega''}(v) = \dfrac{-\nabla v(x,y)\cdot\widetilde{\omega}'' + \omega_3''}{\sqrt{1+|\nabla v(x,y)|^2}}, & (x,y)\in\Omega; \end{cases} \tag{2.43}$$

Let's call $G_{\omega'}(v)$ and $G_{\omega''}(v)$ the operators that describe the SfS classical problem applied to the surface v. We want now to emphasize how the functions $I_1(x,y)$, $I_2(x,y)$ and the function u, solution of the problem (2.35), are correlated between them. First, we fix the light sources, so the applications $G_{\omega'}(v)$ and $G_{\omega''}(v)$ are univocally determined (that is, if we assign a surface v, it is always possible to calculate the bringhtness images I_1 and I_2 respectively for the light vectors ω' e ω''), but they are not bijective (because it's not possible to determine the surface v only by the single function of the bringhtness and the value of the surface on the boundary of the set Ω). Now we want to verify that, if u satisfies (2.35) and we add the condition $u(x,y) = v(x,y)$ for the $(x,y)\in\partial\Omega$, then $u(x,y) = v(x,y)$ in Ω. If we consider v as the solution of the non-linear system, we can use the fact that it generates the image functions I_1 and I_2. Then, by substitution we have:

$$\nabla u(x,y)\cdot(\widetilde{\omega}' G_{\omega''}(v) - \widetilde{\omega}'' G_{\omega'}(v)) = \omega_3' G_{\omega''}(v) - \omega_3'' G_{\omega'}(v) \tag{2.44}$$

then

$$\nabla u(x,y)\cdot\left(\widetilde{\omega}'\frac{-\nabla v(x,y)\cdot\widetilde{\omega}''+\omega_3''}{\sqrt{1+|\nabla v(x,y)|^2}}-\widetilde{\omega}''\frac{-\nabla v(x,y)\cdot\widetilde{\omega}'+\omega_3'}{\sqrt{1+|\nabla v(x,y)|^2}}\right)=$$
$$=\omega_3'\frac{-\nabla v(x,y)\cdot\widetilde{\omega}''+\omega_3''}{\sqrt{1+|\nabla v(x,y)|^2}}-\omega_3''\frac{-\nabla v(x,y)\cdot\widetilde{\omega}'+\omega_3'}{\sqrt{1+|\nabla v(x,y)|^2}}$$

$$\nabla u(x,y)\cdot((-\nabla v(x,y)\cdot\widetilde{\omega}'')\widetilde{\omega}'+\omega_3''\widetilde{\omega}'+(\nabla v(x,y)\cdot\widetilde{\omega}')\widetilde{\omega}''-\omega_3'\widetilde{\omega}'')=$$
$$=-\nabla v(x,y)\cdot\widetilde{\omega}''\omega_3'+\omega_3'\omega_3''+\nabla v(x,y)\cdot\widetilde{\omega}'\omega_3''-\omega_3'\omega_3''$$

$$\nabla u(x,y)\cdot((-\nabla v(x,y)\cdot\widetilde{\omega}'+\nabla v(x,y)\cdot\widetilde{\omega}')\widetilde{\omega}''+\omega_3''\widetilde{\omega}'-\omega_3'\widetilde{\omega}'')=-\nabla v(x,y)\cdot(\widetilde{\omega}''\omega_3'-\widetilde{\omega}'\omega_3'')$$

for which

$$\nabla u(x,y)\cdot(\omega_3''\widetilde{\omega}'-\omega_3'\widetilde{\omega}'')=\nabla v(x,y)\cdot(\widetilde{\omega}'\omega_3''-\widetilde{\omega}''\omega_3')$$

and this implies the equality $\nabla u(x,y)=\nabla v(x,y)$ in Ω. If we consider the condition $u(x,y)=v(x,y)$ for the points $(x,y)\in\partial\Omega$, we obtain the extention of the equality also in all the domain.

□

We will use now this result for the uniqueness of solution of the problem (2.42), that is:

Corollary 2.9 *The nonlinear system (2.42) admits only one solution.*

Proof.

If, for absurd, we take two solutions of the problem (2.42) called $v_1(x,y)$ and $v_2(x,y)$ then, by (2.8) we can also say that both of them are solutions of the problem (2.35). But, by the uniqueness result Theorem 2.6, we have that $v_1(x,y)=v_2(x,y)$ $\forall(x,y)\in\Omega$.

□

2.4 Analysis of some approximation schemes

Now we consider the numerical methods through which we have obtained the numerical results on artificial images.

For all the numerical schemes we consider a square domain Ω like the set $[a,b]^2$ and with a uniform discretization space step $\Delta=(b-a)/n$ where n is the number of intervals divides the side of the square (that is $x_i=-1+i\Delta$, $y_j=-1+j\Delta$ with $i,j=0,\ldots,n$). We use this uniform discretization calling by $\overline{\Omega}_d$ all the points of the lattice belonging to Ω, by Ω_d all the internal points and by $\partial\Omega_d$ all the points boundary points.

2.4.1 Finite difference

First of all we start with the approximation of u via the following discretization of the first derivative: $u_x(x_i, y_j) = \frac{u(x_{i+1},y_j)-u(x_{i-1},y_j)}{2\Delta} + \mathcal{O}(\Delta^2)$ and $u_y(x_i, y_j) = \frac{u(x_i,y_{j+1})-u(x_i,y_j)}{\Delta} + \mathcal{O}(\Delta)$. We can write a discretization (2.35) as

$$U^1(x_i, y_{j+1}) = U^1(x_i, y_j) + \left[f(x_i, y_j) - b_1(x_i, y_j) \frac{U^1(x_{i+1}, y_j) - U^1(x_{i-1}, y_j)}{2\Delta} \right] \frac{\Delta}{b_2(x_i, y_j)} \tag{2.45}$$

and solve it for $i = 1, \ldots, n-1$ and $j = 0, \ldots, n-1$. In this case, the only necessary boundary conditions are those on the left, right and inferior sides of the square.

For this first method the approximation of the surface is better when the characteristics of the problem are vertical (or almost vertical).

A second method discretizes backward with respect to the y variable rather then forward (i.e. $u_y(x_i, y_j) = \frac{u(x_i,y_j)-u(x_i,y_{j-1})}{\Delta} + \mathcal{O}(\Delta)$), the derivative with respect to x is descritized in the same way. We obtain then:

$$U^2(x_i, y_{j-1}) = U^2(x_i, y_j) - \left[f(x_i, y_j) - b_1(x_i, y_j) \frac{U^2(x_{i+1}, y_j) - U^2(x_{i-1}, y_j)}{2\Delta} \right] \frac{\Delta}{b_2(x_i, y_j)} \tag{2.46}$$

and approximate the solution taking the index in this order: $i = 1, \ldots, n-1$ and $j = n, \ldots, 1$. The difference compared with the previous one is that the approximation is done from top to bottom. In this case the only boundary conditions we need are those on the left, right and superior sides of the square.

Now we consider, on the same previous idea, a finite difference discretization of the equation (2.35) of the second order with respect to the y variable and a first order discretization of the first derivative in x. That is: $u_x(x_i, y_j) = \frac{u(x_{i+1},y_j)-u(x_i,y_j)}{\Delta} + \mathcal{O}(\Delta)$ and $u_y(x_i, y_j) = \frac{u(x_i,y_{j+1})-u(x_i,y_{j-1})}{2\Delta} + \mathcal{O}(\Delta^2)$; we obtain the following scheme:

$$U^3(x_{i+1}, y_j) = U^3(x_i, y_j) + \left[f(x_i, y_j) - b_2(x_i, y_j) \frac{U^3(x_i, y_{j+1}) - U^3(x_i, y_{j-1})}{2h} \right] \frac{\Delta}{b_1(x_i, y_j)} \tag{2.47}$$

for $i = 0, \ldots, n-1$ and $j = 1, \ldots, n-1$. For this case the only necessary boundary conditions are those on the left, upper and bottom sides of the square.

In the end we consider the last finite difference explicit method where the difference compared with the previous one is that the first derivative in x is approximated by $u_x(x_i, y_j) = \frac{u(x_i,y_j)-u(x_{i-1},y_j)}{\Delta} + \mathcal{O}(\Delta)$. Then the scheme becomes:

$$U^4(x_{i-1}, y_j) = U^4(x_i, y_j) - \left[f(x_i, y_j) - b_2(x_i, y_j) \frac{U^4(x_i, y_{j+1}) - U^4(x_i, y_{j-1})}{2\Delta} \right] \frac{\Delta}{b_1(x_i, y_j)} \tag{2.48}$$

for $i = n, \ldots, 1$ and $j = 1, \ldots, n-1$. The only boundary conditions that we need are on the left, upper and bottom sides of the square.

From the numerical tests one can see that the good approximation of the surface (at least in the case of a vertical ω') depends only on the direction of the characteristics (i.e. $\widetilde{\omega}_2$). It is clear that this way to solve numerically the problem has all the limits well known of the approximation of the solution relative to the transport equation. In particular, the velocity function depends by the ratio between the two

components of the vector field b, that is b_1 and b_2. Furthermore, in our case there is not a real dependence on the time, but, in the previous schemes, the role of the evolution parameter is given to x for the approximation U^3 and U^4, and to y for the approximation U^1 and U^2.

See [83] and [84] for others results about the stability, consistence and convergence of this kind of numerical schemes.

Now, we want to explain that even if we use the implicit finite difference schemes (usually used to ameliorate the stability of this kind of techniques) we have to continue to respect some constraints in order to reach the convergence [85].

Let us consider the following two discretization for the first derivative of u:

$$\frac{\partial u}{\partial x}(x_i, y_j) = \frac{u(x_{i+1}, y_{j+1}) - u(x_{i-1}, y_{j+1})}{2\Delta} + \mathcal{O}(\Delta^2),$$
$$\frac{\partial u}{\partial y}(x_i, y_j) = \frac{u(x_i, y_{j+1}) - u(x_i, y_j)}{\Delta} + \mathcal{O}(\Delta).$$

This time, starting with the knowledge of the boundary condition in the left, right and inferior sides of the domain, we apply the previous two approximations to the equation of the hyperbolic problem (2.8) and we get the following implicit scheme:

$$U^5(x_i, y_{j+1}) + \frac{b_1(x_i, y_{j+1})}{2b_2(x_i, y_j)}(U^5(x_{i+1}, y_{j+1}) - U^5(x_{i-1}, y_{j+1})) = \\ = U^5(x_i, y_j) + \frac{\Delta}{b_2(x_i, y_j)} f(x_i, y_j). \quad (2.49)$$

Since that for this scheme we should divide by the second component of the vector field b, if it exists a point (x_i, y_j) such that $b_2(x_i, y_j) = 0$ it is clear that the numerical scheme is ill-posed.

Then, for every line of the domain (and for $j = 0, \ldots, n-1$) we have to solve the following tridiagonal linear systems:

$$\begin{pmatrix} 1 & \frac{b^1_{1,j+1}}{2b^2_{1,j}} & 0 & 0 & \cdots & 0 \\ -\frac{b^1_{2,j+1}}{2b^2_{2,j}} & 1 & \frac{b^1_{2,j+1}}{2b^2_{2,j}} & 0 & \cdots & 0 \\ 0 & \ddots & \ddots & \ddots & \ddots & \vdots \\ \vdots & \ddots & \ddots & \ddots & \ddots & 0 \\ 0 & \cdots & 0 & -\frac{b^1_{n-2,j+1}}{2b^2_{n-2,j}} & 1 & \frac{b^1_{n-2,j+1}}{2b^2_{n-2,j}} \\ 0 & \cdots & \cdots & 0 & -\frac{b^1_{n-1,j+1}}{2b^2_{n-1,j}} & 1 \end{pmatrix} \begin{pmatrix} U^5_{1,j+1} \\ U^5_{2,j+1} \\ \vdots \\ \vdots \\ U^5_{n-2,j+1} \\ U^5_{n-1,j+1} \end{pmatrix} =$$
$$= \begin{pmatrix} U^5_{1,j} + \frac{\Delta}{b^2_{1,j}} f_{1,j} + \frac{b^1_{1,j+1}}{2b^2_{1,j}} U^5_{0,j+1} \\ U^5_{2,j} + \frac{\Delta}{b^2_{2,j}} f_{2,j} \\ \vdots \\ \vdots \\ U^5_{n-2,j} + \frac{\Delta}{b^2_{n-2,j}} f_{n-2,j} \\ U^5_{n-1,j} + \frac{\Delta}{b^2_{n-1,j}} f_{n-1,j} - \frac{b^1_{n,j+1}}{2b^2_{n,j}} U^5_{n,j+1} \end{pmatrix} \quad (2.50)$$

where we are calling $b_1(x_i, y_j)$ and $b_2(x_i, y_j)$ respectively as $b^1_{i,j}$ and $b^2_{i,j}$.

In order to increase the efficiency of calculus we optimize the Thomas' algorithm for the computation of the solution using the LU factorization ($M = LU$). In particular, instead of use matrix structure, we store all the coefficients in the less number of vectors and adapt the calculus to this particular case. That is, once we rewrite the diagonal, superior and inferior coefficients of the previous matrix as follow:

$$\begin{aligned} m^{diag} &= (1, \ldots, 1); \\ m^{sup} &= \left(\frac{b^1_{1,j+1}}{2b^2_{1,j}}, \ldots, \frac{b^1_{n-2,j+1}}{2b^2_{n-2,j}} \right); \\ m^{inf} &= \left(-\frac{b^1_{2,j+1}}{2b^2_{2,j}}, \ldots, -\frac{b^1_{n-1,j+1}}{2b^2_{n-1,j}} \right); \end{aligned} \tag{2.51}$$

it is possible to compute easily the coefficients of the two matrices L and U (respectively lower triangular and upper triangular). In fact, if we fix the diagonal coefficients of L equal to 1 and $u^{diag}_1 = m^{diag}_1$, we have that:

$$\begin{aligned} u^{sup}_k &= m^{sup}_k; \\ l^{sup}_k &= \frac{m^{sup}_k}{u^{diag}_k}; \\ u^{diag}_{k+1} &= m^{diag}_{k+1} - l^{sup}_k u^{sup}_k; \end{aligned} \tag{2.52}$$

for $k = 1, \ldots, n-1$. As we explain in the numerical tests part, this kind of algorithm optimization permits to be efficient and increase the speedup of the numerical scheme in order to solve the problem of the approximation of the solution U^5 in less than one second even if we are using images of size 800×800.

In order to complete the computation of the values of U^5 for the row j we have to solve two triangular linear systems which is a very standard issue for the numerical analysis.

With the aim to study the stability of this scheme we will use the Fourier-method. Let us consider the homogenous differential equation

$$b(x, y) \cdot \nabla u(x, y) = 0. \tag{2.53}$$

With the use of of discretization (2.49) this leads to the following implicit scheme:

$$U^5(x_i, y_{j+1}) + \frac{b_1(x_i, y_{j+1})}{2b_2(x_i, y_j)} (U^5(x_{i+1}, y_{j+1}) - U^5(x_{i-1}, y_{j+1})) = U^5(x_i, y_j). \tag{2.54}$$

with $u(x_0, y_j)$, $u(x_n, y_j)$ and $u(x_i, y_0)$ given for $i, j = 0, \ldots, n$.

If we prove the stability for this scheme, we can use the principle of Duhamel [86], which states, that the scheme for the inhomogeneous problem is stable if the corresponding scheme for the homogenous scheme is stable. Let $u(x_i, y_j)$ be the theoretical solution of the finite difference scheme (2.54) and $U^5(x_i, y_j)$ the solution of the scheme which is actually obtained, so that $U^5(x_i, y_j)$ contains rounding errors. Thus the error at every mesh point (x_i, y_j) is defined as:

$$err(x_i, y_j) = u(x_i, y_j) - U^5(x_i, y_j).$$

If we substitute

$$err(x_i, y_j) = e^{\alpha j\Delta} e^{I\beta i\Delta} \tag{2.55}$$

where $I^2 = -1$, then a finite difference scheme with constant coefficients is stable if

$$|e^{\alpha\Delta}| \leq 1 \quad \forall \alpha \in \mathbb{R}. \tag{2.56}$$

This is the Von Neumann (Fourier) criterion of stability.

Theorem 2.10 *The numerical scheme (2.54) is unconditionally stable.*

Proof. Once we have defined the error at every mesh point as $err(x_i, y_j)$, with the substitution (2.55), it remains to show that condition (2.56) is satisfied. Taking the scheme (2.54) we have:

$$e^{\alpha(j+1)\Delta} e^{I\beta i\Delta} + \frac{\overline{b}}{2}(e^{\alpha(j+1)\Delta} e^{I\beta(i+1)\Delta} - e^{\alpha(j+1)\Delta} e^{I\beta(i-1)\Delta}) = e^{\alpha j\Delta} e^{I\beta i\Delta}$$

where $\overline{b} = \max_{(x_i,y_j)\in\Omega_d} \frac{b_1(x_i,y_{j+1})}{b_2(x_i,y_j)}$. Division by $e^{\alpha(j+1)\Delta} e^{I\beta i\Delta}$ yields:

$$1 + \frac{\overline{b}}{2}(e^{I\beta\Delta} - e^{-I\beta\Delta}) = e^{-\alpha\Delta},$$

and with $\theta = e^{\alpha\Delta}$:

$$1 + \frac{\overline{b}}{2}(2I\sin(\beta\Delta)) = \frac{1}{\theta}.$$

Thus we obtain for θ:

$$\theta = \frac{1 - \overline{b}I\sin(\beta\Delta)}{1 + \overline{b}^2\sin^2(\beta\Delta)}$$

and

$$|\theta| \leq 1.$$

□

It is clear that even if the stability can be reached if there exists a point (x_i, y_j) such that $b_2(x_i, y_j) = 0$, in this case the discretized problem (2.50) can not be solved.

In order to use a numerical scheme that works without consider the variability of the vector field b we introduce in the next session the semi-Lagrangian scheme used to solve the SfS-PS problem with very efficient results.

2.4.2 An efficient numerical scheme: semi-lagrangian discretization

A second numerical approach to the solve equation (2.35) is to mimic the solution along the characteristics in th general case, i.e. when they are not parallel to the axis as in the finite difference case. We pass then to consider the following equivalent equation obtained dividing the two sides of (2.35) by the norm of $b(x, y)$:

$$\nabla_\rho u(x, y) = \frac{f(x, y)}{||b(x, y)||} \quad \forall (x, y) \in \Omega \tag{2.57}$$

with $\rho(x, y) = \frac{b(x,y)}{||b(x,y)||}$.

We observe that the division by $||b(x,y)||$ doesn't involve any kind of difficulties for the numerical scheme (Lemma 2.2). Now, considering the definition of directional derivative, we can write:

$$\lim_{h\to 0} \frac{u(x+h\rho_1(x,y), y+h\rho_2(x,y)) - u(x,y)}{h} = \frac{f(x,y)}{||b(x,y)||} \quad \forall (x,y) \in \Omega \tag{2.58}$$

for which is true the next approximation

$$\frac{u(x+h\rho_1(x,y), y+h\rho_2(x,y)) - u(x,y)}{h} \simeq \frac{f(x,y)}{||b(x,y)||} \quad \forall (x,y) \in \Omega \tag{2.59}$$

Considering a uniform discretization $\overline{\Omega}_d$ as in the previous section, we can finally write the semi-lagrangian schemes:

$$u(x_i,y_j) \simeq u(x_i+h\rho_1(x_i,y_j), y_j+h\rho_2(x_i,y_j)) - \frac{f(x_i,y_j)}{||b(x_i,y_j)||}h \tag{2.60}$$

for all $(x_i,y_j) \equiv (-1+i\Delta, -1+j\Delta)$ with $i,j = 1,\dots,n-1$ (namely $\forall (x_i,y_j) \in \Omega_d$) where n represents the number of intervals whereby $[-1,1]$ is been divided (if we talk about digial images, $(n+1)\times(n+1)$ represents the resolution) and $h > 0$.

This scheme has the advantage to follow a numerical integration along the characteristics of the equation (2.35), but it has some computational drawback:

- it resolves for every point $(x_i,y_j) \in \Omega_d$ a linear system for the interpolation of the point $u(x_i+h\rho_1(x_i,y_j), y_j+h\rho_2(x_i,y_j))$ with respect to the uniform grid;
- it is iterative, because it is a fixed point scheme.

Now we describe the algorithm in detail in order to explain the difficulties written above.

We introduce two discrete functions $u^n(x_i,y_j) = u^n_{i,j}$ and $u^{n+1}(x_i,y_j) = u^{n+1}_{i,j}$ defined only on the grid nodes. Therefore, the iterative scheme (2.60) is corresponding to:

$$u^{n+1}_{i,j} = u^n(x_i+h\rho_1(x_i,y_j), y_j+h\rho_2(x_i,y_j)) - \frac{f_{i,j}}{||b_{i,j}||}h \quad \forall (x_i,y_j) \in \Omega_d \tag{2.61}$$

If we assign an initial function $u^0_{i,j}$, such that $u^0(x_i,y_j) = g(x_i,y_j)\ \forall (x_i,y_j) \in \partial\Omega_d$, it is possible to start the iterations computing the successive approximation $u^{n+1}_{i,j}$ like described in (2.61).

With the same construction of the previous algorithm (*forward semi-lagrangian scheme*), we can write a second type of semi-lagrangian scheme which works backward. Taking into account the equation (2.35), we now modify the orientation of the characteristic field without changing the equation. We multiply by minus one both the sides and dividing by $||b(x,y)||$ we obtain:

$$\nabla_{-\rho} u(x,y) = -\frac{f(x,y)}{||b(x,y)||} \quad \forall (x,y) \in \Omega \tag{2.62}$$

with $\rho(x,y)$ the same as before. Considering the definition of directional derivative now with respect to $-\rho(x,y)$, we can write:

$$\lim_{h\to 0} \frac{u(x-h\rho_1(x,y), y-h\rho_2(x,y)) - u(x,y)}{h} = -\frac{f(x,y)}{||b(x,y)||} \quad \forall (x,y) \in \Omega \tag{2.63}$$

for which is true the next approximation

$$\frac{u(x-h\rho_1(x,y),y-h\rho_2(x,y))-u(x,y)}{h}\simeq-\frac{f(x,y)}{||b(x,y)||}\quad\forall(x,y)\in\Omega \tag{2.64}$$

Like before we have obtained a scheme that approximates the solution along the characteristics direction, but this time from the inflow verse. The fix point scheme that comes out is the following:

$$u_{i,j}^{n+1}=u^n(x_i-h\rho_1(x_i,y_j),y_j-h\rho_2(x_i,y_j))+\frac{f_{i,j}}{||b_{i,j}||}h\quad\forall(x_i,y_j)\in\Omega_d \tag{2.65}$$

Let us explain the difference between the forward (2.61) and backward (2.65)method. The substantial difference is in the way they use the starting data u^0 and in the use of the information stored in the boundary condition. Let's take first the forward scheme; if we consider the vector $(\rho_1(x_i,y_j),\rho_2(x_i,y_j))$ like the linear approximation of the characteristics field (defined by the vector field $b(x,y)$) in the point (x_i,y_j), it is easy to see that the value $u^{n+1}(x_i,y_j)$ depends on the value of the previous one u^n at the point $(x_i+h\rho_1(x_i,y_j),y_j+h\rho_2(x_i,y_j))$. This means that the information is propagated in the opposite toward to the characteristic field (i.e. it solves (2.40)). For the backward one it is possible to consider the same way to intend the different problem solved by the scheme. It is clear that the use of the point $(x_i-h\rho_1(x_i,y_j),y_j-h\rho_2(x_i,y_j))$ implies that the information for the calculation of u^{n+1}, considering the verse of the characteristics, will be taken back from the point (x_i,y_j). This means that the approximation of the surface will follow the same orientation of the problem (2.39).

Consistency and convergence

For every point it will be necessary to compute $u^n(x_i+h\rho_1(x_i,y_j),y_j+h\rho_2(x_i,y_j))$ and thus to approximate with an interpolation method the function u^n at a point not belonging to the grid Ω_d. For this purpose we consider the bilinear interpolation which needs of the coefficients $(a,b,c,d)\in\mathbb{R}^4$ to express the function value $u^n(x_s,y_s)=u^n(x_i+h\rho_1(x_i,y_j),y_j+h\rho_2(x_i,y_j))$ in the bilinear combination $ax_sy_s+bx_s+cy_s+d$. We choose this kind of interpolation because every point $(x_s,y_s)\in(\Omega\setminus\Omega_d)$ falls inside a cell of four nodes and we assume as the reference vertex the one in the bottom on the left that we will call $(x_k,y_k)\in\Omega_d$. If we impose the interpolation condition for the nearest four points of (x_s,y_s) inside this cell is thus possible to obtain the following system:

$$\begin{cases}ax_ky_k+bx_k+cy_k+d=u^n(x_k,y_k)\\ ax_{k+1}y_k+bx_{k+1}+cy_k+d=u^n(x_{k+1},y_k)\\ ax_{k+1}y_{k+1}+bx_{k+1}+cy_{k+1}+d=u^n(x_{k+1},y_{k+1})\\ ax_ky_{k+1}+bx_k+cy_{k+1}+d=u^n(x_k,y_{k+1})\end{cases} \tag{2.66}$$

that is

$$\begin{pmatrix}x_ky_k & x_k & y_k & 1\\ x_{k+1}y_k & x_{k+1} & y_k & 1\\ x_{k+1}y_{k+1} & x_{k+1} & y_{k+1} & 1\\ x_ky_{k+1} & x_k & y_{k+1} & 1\end{pmatrix}\begin{pmatrix}a\\b\\c\\d\end{pmatrix}=\begin{pmatrix}u^n(x_k,y_k)\\u^n(x_{k+1},y_k)\\u^n(x_{k+1},y_{k+1})\\u^n(x_k,y_{k+1})\end{pmatrix}. \tag{2.67}$$

Let us emphasize an interpolation results based on the uniqueness of bilinear interpolation on this kind of data:

Lemma 2.11 *The system (2.67) admits a unique solution.*

Proof. The proof is simply based on the computation of the determinant of the matrix. We want to prove that the necessary conditions to make it be zero are not possibles to obtain considering a discretization like our.

$$\det\begin{pmatrix} x_k y_k & x_k & y_k & 1 \\ x_{k+1} y_k & x_{k+1} & y_k & 1 \\ x_{k+1} y_{k+1} & x_{k+1} & y_{k+1} & 1 \\ x_k y_{k+1} & x_k & y_{k+1} & 1 \end{pmatrix} =$$

$$\begin{aligned}
&= -(x_{k+1}y_k x_{k+1}y_{k+1} + x_{k+1}y_{k+1}x_k y_{k+1} + x_{k+1}y_{k+1}x_k y_k - \\
&\quad - x_k y_{k+1}x_{k+1}y_k - x_{k+1}y_{k+1}x_{k+1}y_{k+1} - x_k y_{k+1}x_{k+1}y_k) + \\
&\quad + x_k y_k x_{k+1}y_{k+1} + x_k y_{k+1}x_k y_{k+1} + x_{k+1}y_{k+1}x_k y_k \\
&\quad - x_k y_{k+1}x_{k+1}y_k - x_{k+1}y_{k+1}x_k y_{k+1} - x_k y_{k+1}x_k y_k - \\
&\quad - (x_k y_k x_{k+1}y_{k+1} + x_k y_k x_k y_{k+1} + x_{k+1}y_k x_k y_k - \\
&\quad - x_k y_{k+1}x_{k+1}y_k - x_{k+1}y_k x_k y_{k+1} - x_k y_k x_k y_k) + \\
&\quad + x_k y_k x_{k+1}y_{k+1} + x_k y_k x_{k+1}y_{k+1} + x_{k+1}y_k x_{k+1}y_k - \\
&\quad - x_{k+1}y_{k+1}x_{k+1}y_k - x_{k+1}y_k x_k y_{k+1} - x_{k+1}y_k x_k y_k = \\
&= -2x_{k+1}^2 y_k y_{k+1} - 2x_k x_{k+1}y_{k+1}^2 + x_{k+1}^2 y_{k+1}^2 + 4x_k x_{k+1}y_k y_{k+1} + \\
&\quad + x_k^2 y_{k+1}^2 - 2x_k^2 y_k y_{k+1} - 2x_k x_{k+1}y_k^2 + x_k^2 y_k^2 + x_{k+1}^2 y_k^2 = \\
&= x_{k+1}^2 (y_k - y_{k+1})^2 + x_k^2 (y_k - y_{k+1})^2 - 2x_k x_{k+1}(y_k - y_{k+1})^2 = \\
&= (y_k - y_{k+1})^2 (x_k - x_{k+1})^2.
\end{aligned}$$

Therefore the matrix has the determinant equal to zero if and only if

$$y_k = y_{k+1} \quad \text{or} \quad x_k = x_{k+1}.$$

Then it concludes the proof.

□

Let us call the unique solution of the previous system (a^*, b^*, c^*, d^*) for every point $(x_i, y_j) \in \Omega_d$. Now it is possible to calculate the bilinear form in the evaluation point (x_s, y_s), that is:

$$a^* x_s y_s + b^* x_s + c^* y_s + d^* = u^n(x_s, y_s) = u^n(x_i + h\rho_1(x_i, y_j), y_j + h\rho_2(x_i, y_j)) \quad (2.68)$$

If we consider a linear interpolation (that has the same order as of the bilinear interpolation) in dimension one with the purpose to obtain an estimation of the order of consistency, we can use the following

$$\begin{aligned}
|I[q](x) - q(x)| &= \left| q(x_i) + \frac{q(x_{i+1}) - q(x_i)}{x_{i+1} - x_i}(x - x_i) - q(x) \right| \leq \\
&\leq |q'(\xi)(x_i - x) + q'(\eta)(x - x_i)| \leq |q''(\tau)||\eta - \xi||x - x_i| \leq M\Delta^2
\end{aligned}$$

With $I[q]$ we consider the linear interpolation of a function $q \in C^2(x_i, x_{i+1})$, τ, η and ξ are points in (x_i, x_{i+1}) and $M = \max_{(x_i,x_{i+1})} |q''(x)|$. Now, if we take into account that

$$\frac{u(x + h\rho_1(x,y), y + h\rho_2(x,y)) - u(x,y)}{h} = \nabla u(x,y) \cdot \rho + \mathcal{O}(h).$$

Let us define the following two quantities:

$$M(x,y) = \nabla_\rho u - \frac{f(x,y)}{||b(x,y)||}$$
$$P_{h,\Delta}u(x,y) = \frac{I[u](x + h\rho_1(x,y), y + h\rho_2(x,y)) - u(x,y)}{h} - \frac{f(x,y)}{||b(x,y)||}$$

that permit us to calculate the consistency error considering the difference $M(x,y) - P_{h,\Delta}u(x,y)$ calculated in the domain Ω_d, that is

$$M_{i,j} - P_{h,\Delta}u_{i,j} =$$
$$= \nabla_\rho u_{i,j} - \frac{f_{i,j}}{||b_{i,j}||} - \frac{I[u](x_i + h\rho_1(x_i,y_j), y_j + h\rho_2(x_i,y_j)) - u_{i,j}}{h} + \frac{f_{i,j}}{||b_{i,j}||} =$$
$$= \frac{u(x_i + h\rho_1(x_i,y_j), y_j + h\rho_2(x_i,y_j)) - u_{i,j}}{h} + \mathcal{O}(h) -$$
$$- \frac{I[u](x_i + h\rho_1(x_i,y_j), y_j + h\rho_2(x_i,y_j)) - u_{i,j}}{h} =$$
$$= \frac{u(x_i + h\rho_1(x_i,y_j), y_j + h\rho_2(x_i,y_j)) - I[u](x_i + h\rho_1(x_i,y_j), y_j + h\rho_2(x_i,y_j))}{h} + \mathcal{O}(h) =$$
$$= \mathcal{O}(h) + \mathcal{O}\left(\frac{\Delta^2}{h}\right).$$

We can obtain an order one of consistency if we take $h = \Delta$.

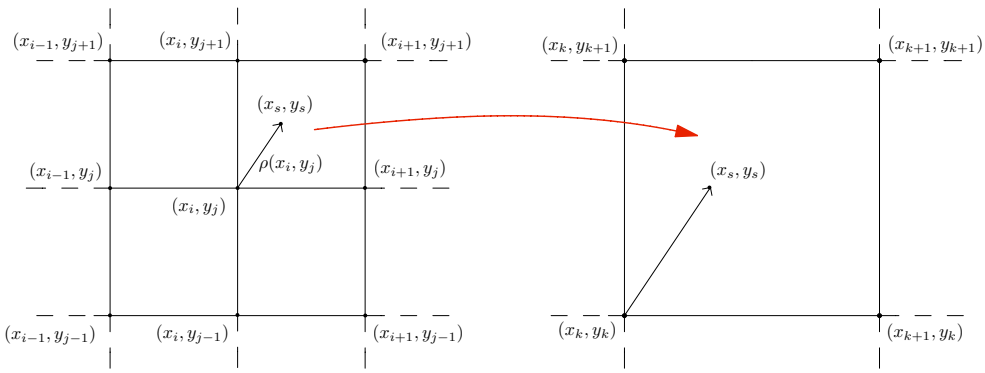

Figure 2.9. The picture explains the position of the different points for the bilinear interpolation to determine the value $u^n(x_s, y_s)$ in the case where $\rho_1(x_i, y_j)$ and $\rho_2(x_i, y_j)$ are both positive. On the left the part of the lattice centered on $(x_i.y_j)$, on the right the zooming of the interesting square with the reference coordinate.

Let now give a proof of the convergence of this method. In this case we will show that the numerical algorithm is a non increasing map in $L^\infty(\Omega)$ on the Banach

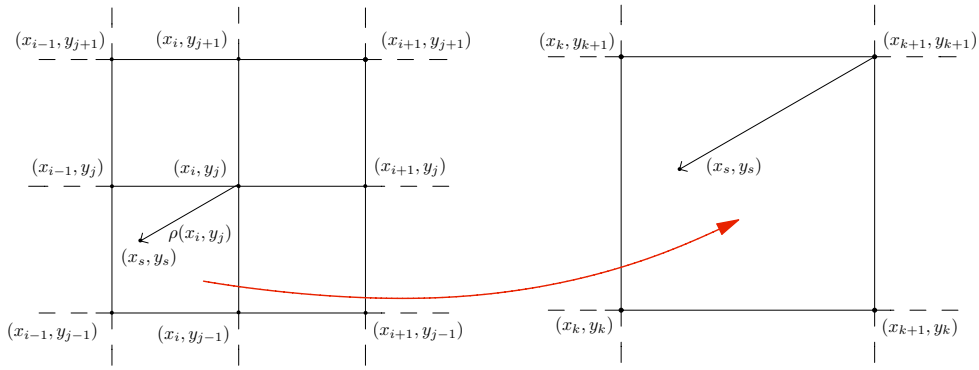

Figure 2.10. The structure of this picture is the same of the (2.9) but in the case when $\rho_1(x_i, y_j)$ and $\rho_2(x_i, y_j)$ are both negative.

space function $W^{1,\infty}(\Omega)$, that is the Sobolev space notation for the Lipschitz type functions.

In order to prove the convergence of the scheme using the existence of a unique fixed point for the nonexpansive map [89] we give the following

Definition 2.12 *If D is a subset of a Banach space X, T is a mapping from D into X, and $x_1 \in D$, then $M(x_1, t_n, T)$ is the sequence $\{x_n\}_{n=1}^{\infty}$ defined by $x_{n+1} = (1 - t_n)x_n + t_n T x_n$, where $\{t_n\}_{n=1}^{\infty}$ is a real sequence. If a point x_1 and a sequence $\{t_n\}_{n=1}^{\infty}$ satisfy the following three conditions:*

$$\sum_{n=1}^{\infty} t_n = \infty, \tag{2.69}$$

$$0 \leq t_n \leq b < 1 \qquad \text{for all positive integers } n, \tag{2.70}$$

then x_1 and $\{t_n\}_{n=1}^{\infty}$ will be said to satisfy Condition A.

Note that if $t_n \in [a, b]$ for all positive integers n and $0 < a \leq b < 1$, then it is obvious that the sequence $\{t_n\}_{n=1}^{\infty}$ satisfies (2.69) and (2.70).

Theorem 2.13 *Let D be a closed subset of a Banach space X and let T be a nonexpansive mapping from D into a compact subset of X. If there exist x_1 and $\{t_n\}_{n=1}^{\infty}$ that satisfy Condition A, then T has a fixed point in D and $M(x_1, t_n, T)$ converges to a fixed point of T.*

Using the previous result we want to prove the convergence of the numerical semi-lagrangian schemes using the fact that the operator that defines the schemes satisfies Condition A.

Theorem 2.14 *The numerical scheme (2.61) (and (2.65)) converges to the unique weak solution of the problem (2.35)*

Proof. For first we define the map T described by the numerical scheme (2.61) on the Lipschitz functional space:

$$T(u)(x, y) = u((x, y) + h\rho(x, y)) - h\frac{f(x, y)}{||b(x, y)||} \tag{2.71}$$

It is easy to see that (2.71) is nonexpansive in $W^{1,\infty}(\Omega)$. In fact, if we take two functions u and w both in $W^{1,\infty}(\Omega)$, then

$$||T(u)(x,y) - T(w)(x,y)||_\infty =$$
$$= \left\| u((x,y) + h\rho(x,y)) - h\frac{f(x,y)}{||b(x,y)||} - w((x,y) + h\rho(x,y)) + h\frac{f(x,y)}{||b(x,y)||} \right\|_\infty =$$
$$= \|u((x,y) + h\rho(x,y)) - w((x,y) + h\rho(x,y))\|_\infty = ||u(x,y) - w(x,y)||_\infty$$

The iterative numerical method uses this map to build the sequence by the recursive scheme, that is: $u^{n+1} = T(u^n)$. In order to use the previous thorem we define some objects useful to this purpose. Let $M(v^0, t_n, T)$ be the sequence defined as follows:

$$v^{n+1} = (1 - t_n)v^n + t_n T(v^n) \tag{2.72}$$

where $v^0 \in W^{1,\infty}(\Omega)$ is the initial data and $\{t_n\}_{n=0}^\infty$ is a sequence of real numbers such that:

$$\sum_{n=0}^{\infty} t_n = \infty, \text{ with } 0 \leq t_n \leq b < 1$$

with $b \in \mathbb{R}$. In our case it is also possible to take it as a constant sequence (for example $t_n = \frac{1}{2}$).

In the weakest case (where we prove the existence and the uniqueness, Theorem 2.6) we consider that the functions $b(x,y)$ and $f(x,y)$ are discontinuous on the same curve $\gamma(t) \subset \Omega$. The operator T is applied on functions taken in a discrete domain Ω_d, then if we consider $\frac{f(x,y)}{||b(x,y)||}$ with $(x,y) \in \Omega_d$ as the values of a function in $W^{1,\infty}(\Omega)$, then the following can be considered true:

$$v^n \in W^{1,\infty}(\Omega) \quad \forall n \geq 0$$

We finally have all the necessary hypothesis satisfied in order to apply the previous theorem.

□

The computational cost for every iteration of both the schemes is considerable, taking into account that for every internal point of the grid we have to resolve a linear system whose dimension is small and constant for every point if we use a bilinear interpolation. In fact, for every pixel we solve a linear system of dimension four to find the coefficients (a^*, b^*, c^*, d^*) of the bilinear function.

The arrest criterion is based on the convergence of the succession of approximations u^n through the Cauchy criterion with the infinity norm, that is, since $u^n \to u$, then the algorithm will be stop when:

$$||u^n - u^{n+1}||_{\Delta_\infty} = \max_{(x_i,y_j)\in\Omega_d} ||u^n(x_i,y_j) - u^{n+1}(x_i,y_j)|| < \varepsilon \tag{2.73}$$

with ε opportunely chosen small.

2.4.3 Numerical tests

The numerical schemes previously described are tested on a set of surfaces and permit us to show how the approximation methods work well compared with the previous theorem of existence of a Lipschitz weak solution. In this purpose we use two kind of surfaces (see Fig. 4.4) and, for simplicity, both of them have an easy boundary condition (that is $u(x,y) = 0\ \forall (x,y) \in \partial\Omega$) that permits us to start with an initial guess u^0 which values are zero in all the domain (included the boundary). Both surfaces will be used also in the next next numerical tests because they have interesting features for this problem. In fact:

- v_{sym} has a big slope between the maximum and the minimum points;
- v^+_{lip} is a Lipschitz surface with an interesting disposition of the curves where it is not differentiable.

Figure 2.11. Set of surfaces used in the numerical tests

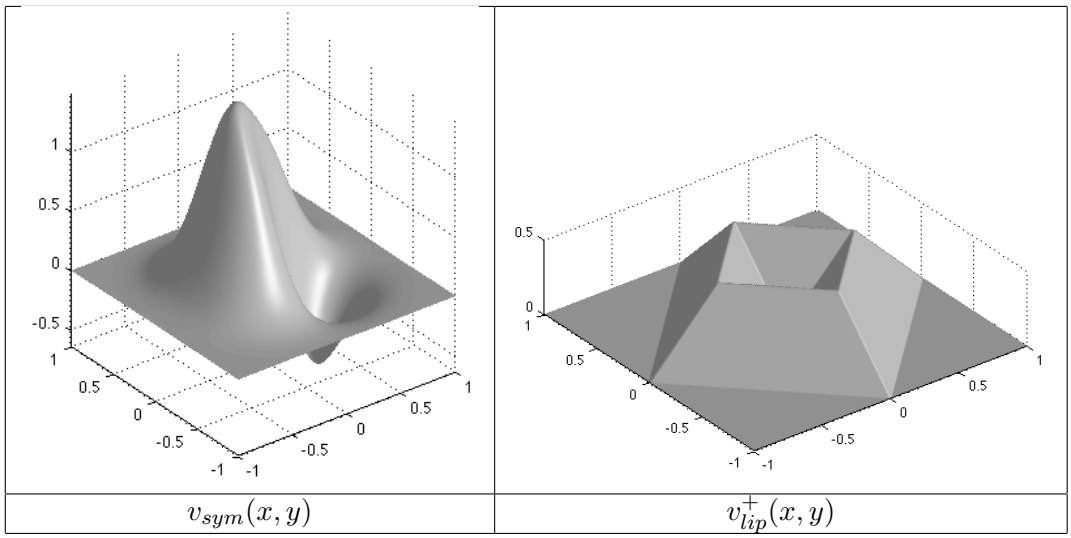

$v_{sym}(x,y)$ | $v^+_{lip}(x,y)$

The results presented in this chapter were first applied on synthetic surfaces. That is surfaces defined in their analytical form (let us call it $v(x,y)$) known till the beginning. In this case the mathematical approach is much more detailed and correct because, first of all, it is possible to eliminate the noise effect from the images and furthermore we can compare the exact solution to the approximate one. This permits an analysis on the convergence order for the adopted numerical scheme adopted.

For the synthetic case we consider the square domain $[-1,1]^2$ with uniform discretization space step $\Delta = 2/n$ where n represents the number of intervals that divide the square (that is $x_i = -1 + i\Delta$, $y_j = -1 + j\Delta$ with $i,j = 0,\ldots,n$). We call Ω_d the set that contains the internal (x_i, y_j) and $\partial\Omega_d$ the set of points (x_i, y_j) that discretize the boundary.

The procedure followed is resumed below:

1. we consider two light sources expressed in the spherical coordinates ($\omega = (\sin(\varphi)\cos(\theta), \sin(\theta)\sin(\varphi), \cos(\varphi))$) in order to obtain no black shadow using (1.16);

2. we construct the images from the analytical formula of the surface. Let us call its height $v(x, y)$;
3. we calculate the initial guess such that $u^0(x_i, y_j) = v(x_i, y_j)\ \forall (x_i, y_j) \in \partial\Omega_d$ and equal to zero inside Ω_d;
4. we start the iteration of (2.61) and (2.64) till (2.73) with $\varepsilon = 10^{-7}$. Let us note $\overline{n}$ the last iteration;
5. the error in the $L^\infty(\Omega_d)$ norm is calculated $err = \max_{(x_i,y_j)\in\Omega_d} |u^{\overline{n}}(x_i, y_j) - v(x_i, y_j)|$.

Finite difference schemes

Like described before, very good numerical integration results are obtained using the light source such that the propagation of the light information (i.e. the projected characteristics) is parallel to the direction of one of the coordinate axis. One first series of test are then carried out with a vertical light source (ω'), while the second light source (ω'') such that $\widetilde{\omega}''$ is been taken parallel to the x axis. It is possible to see the coordinates of the light vectors under every image used for the test.

Expressing the light source vector in spherical coordinates, like in the first case we consider this choice of angles $\theta_1 = 0.0$, $\varphi_1 = 0.0$, $\theta_2 = 0.0$ and $\varphi_2 = 0.1$ that is $\omega' = (0, 0, 1)$ and $\omega'' = (\sin(0.1), 0, \cos(0.1))$. The reason for which we take this kind of light sources is that the information propagated from the light sources generates a characteristic field of straight lines all parallel to the x axis. The starting images are then the following

Figure 2.12. On the left the image I_1, on the right the image I_2 of v_{sym}.

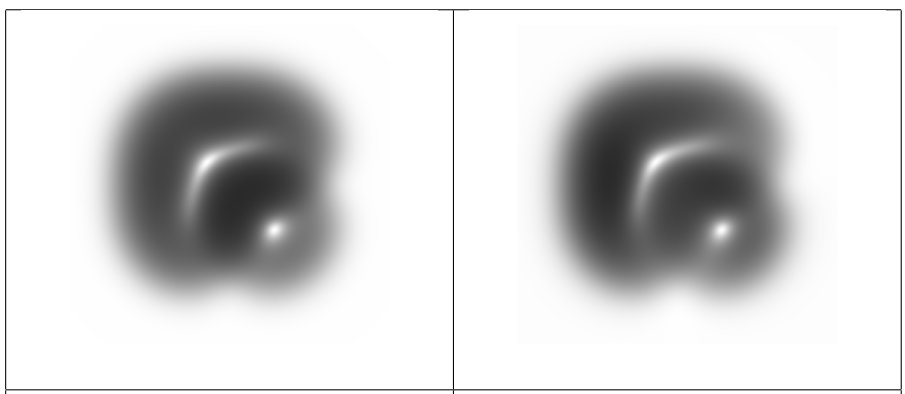

$\varphi_1 = 0.0,\ \theta_1 = 0.0 \rightarrow (I_1)$	$\varphi_2 = 0.0,\ \theta_2 = 0.0 \rightarrow (I_2)$

For the numerical integration we use a uniform step $\Delta = 0.02$ considering that in the application we have a uniform pixel's size for all the image domain. Then, we have the surfaces error of Fig. 2.13.

Repeating the numerical integration for v^+_{lip} we have that, starting from the two images of the Fig. 2.14 obtained from the same light sources we have the error of Fig. 2.15.

Similar results have been obtained considering like direction of propagation of light information the y axis (with the only difference that we use the finite difference schemes with U^1 and U^2).

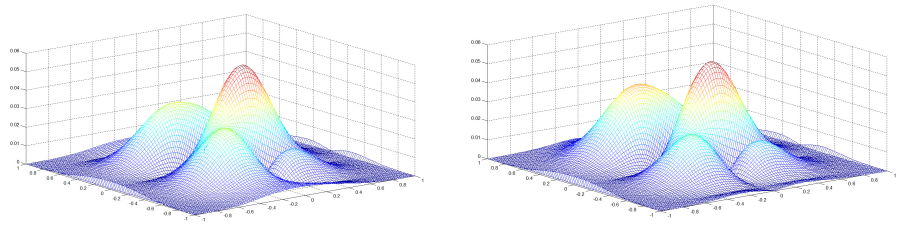

Figure 2.13. On the left the error for the approximate solution U^3, on the right the error for U^4 (the maximum errors on the grid with the exact solution are respectively 5.47×10^{-2} and 5.23×10^{-2})

Figure 2.14. On the left the image I_1, on the right the image I_2 of v_{lip}^+.

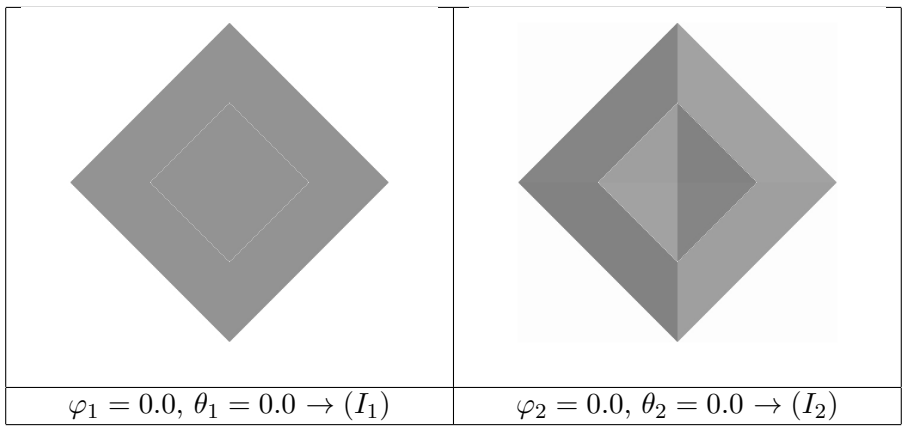

Figure 2.15. On the left the error for the approximate solution U^3, on the right the error for U^4 (the maximum errors on the grid with the exact solution are respectively 2.0×10^{-2} and 1.0×10^{-2})

In the end we want to stress that only the direction of the numerical integration is important for the convergence of the schemes and not the verse of the characteristics.

Semi-lagrangian schemes

In the case of the semi-lagrangian schemes instead, there isn't the problem of the placement of the light in a way to have the characteristics curve oriented parallel to the coordinate axis. This fact allows us to obtain important results for the reconstruction of surfaces with the SfS using the photometric stereo technique considering every type of light sources. The only constraints is that the light source must be taken so that we don't have shadows on the surface.

A first example for these schemes is related to the starting images of Fig. 2.16.

Figure 2.16. On the left the image I_1, on the right the image I_2 of v_{sym} for the semi-lagrangian approximation.

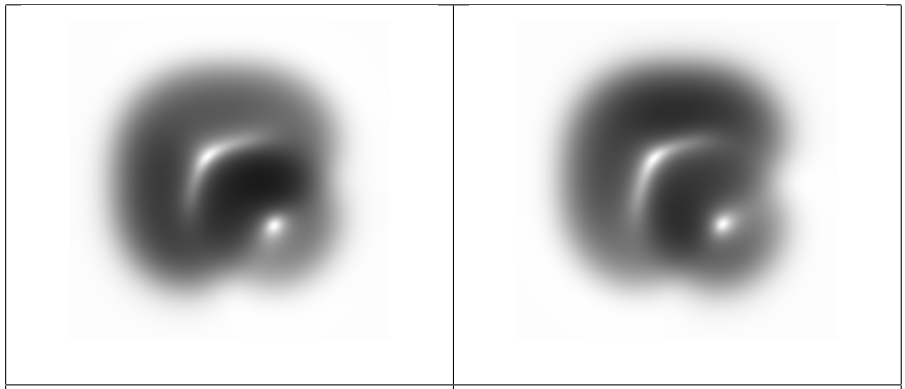

$\varphi_1 = 0.1,\ \theta_1 = \frac{\pi}{3} + 0.2 \rightarrow (I_1)$ | $\varphi_2 = -0.1,\ \theta_2 = \frac{\pi}{3} + 0.3 \rightarrow (I_2)$

With a uniform integration step $\Delta = 0.02$ and a semi-lagrangian step h equal to Δ we have obtained the error shown in Fig. 2.17 with 113 iterations (with $\varepsilon = 10^{-7}$).

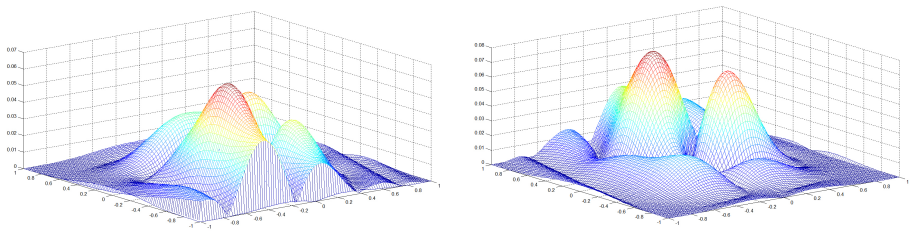

Figure 2.17. On the left the error of the numerical solution approximation with the forward-semi-lagrangian scheme where the maximum is 6.514×10^{-2}. On the right the error of the approximation with the backward ones where the maximum of this surface is 7.425×10^{-2}

Figure 2.18. On the left the image I_1, on the right the image I_2 of v_{lip}^{+} for the semi-lagrangian approximation.

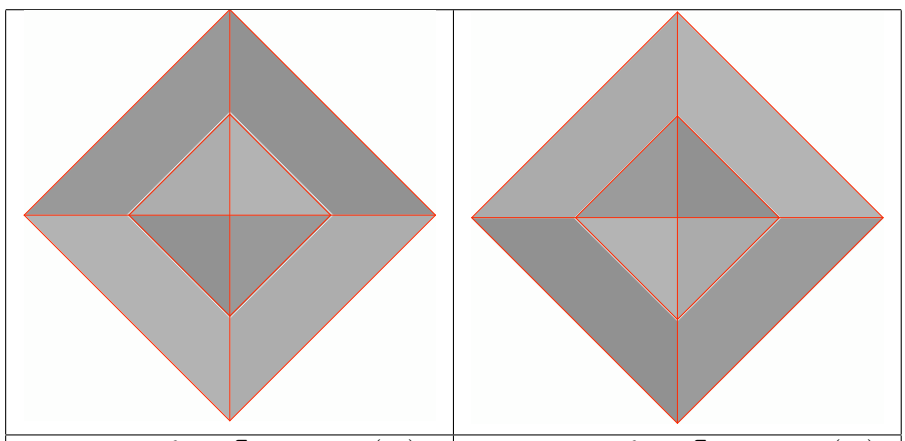

$\varphi_1 = 0.1,\ \theta_1 = \frac{\pi}{3} + 0.2 \rightarrow (I_1)$ | $\varphi_2 = -0.1,\ \theta_2 = \frac{\pi}{3} + 0.3 \rightarrow (I_2)$

For the other kind of surface we have obtained the convergence also considering

the discontinuity of $b(x,y)$ and $f(x,y)$. This is an application of the Theorem 2.6 where the discontinuity curve $\gamma(t)$ (i. e. the discontinuity set of points) can be represented with the red lines of Fig. 2.18.

With the same data used for v_{sym}, we repeat the approximation with the semi-lagrangian schemes starting from the images of Fig. 2.19 obtaining the errors of Fig. 2.19 with 114 iterations.

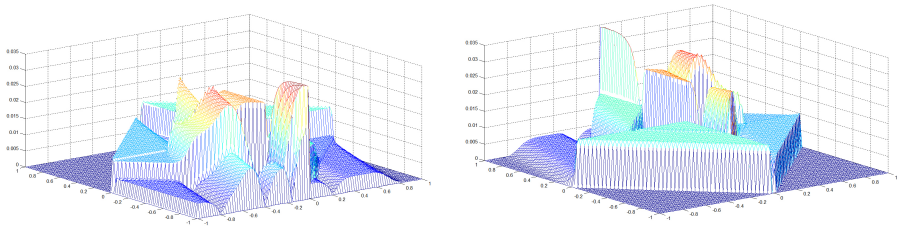

Figure 2.19. On the left the error of the numerical solution approximation with the forward-semi-lagrangian scheme where the maximum is 3.487×10^{-2}. On the right the error of the approximation with the backward ones where the maximum of this surface is 3.469×10^{-2}

In Tab. 2.1 and Tab. 2.2 we summarize the results obtained from the numerical integration of various examples where we fix the light socurces (with $\varphi_1 = 0.1$, $\theta_1 = \frac{\pi}{3} + 0.2$, $\varphi_2 = -0.1$ and $\theta_2 = \frac{\pi}{3} + 0.3$) and the $\varepsilon = 10^{-7}$. The test surfaces are always the same. The only parameters we change are the coefficient α of proportionality between Δ and h ($\alpha = \frac{\Delta}{h}$) and the grid step Δ. The rows of the tables are divided by for just for emphasize where the coefficient of proportionality α changes. That is, in the first four rows (for both tables) we have $\alpha = \frac{1}{2}$, in the second four $\alpha = 1$ and in the last four rows $\alpha = 2$. We can see that the bests results (about the errors) are in the middle part. This is bear out also from the consistency estimation (**??**) that can be minimize taking $\Delta = h$.

v_{sym}		Semi-lagrangian		Semi-lagrangian	
		Forward	Backward	Forward	Backward
h	Δ	$\overline{n}$		err	
0.04	0.02	160	126	8.951×10^{-2}	9.45×10^{-2}
0.02	0.01	159	118	4.542×10^{-2}	4.963×10^{-2}
0.01	0.005	217	216	2.348×10^{-2}	2.576×10^{-2}
0.005	0.0025	428	426	1.366×10^{-2}	1.39×10^{-2}
0.02	0.02	116	113	6.514×10^{-2}	7.425×10^{-2}
0.01	0.01	223	219	3.493×10^{-2}	3.853×10^{-2}
0.005	0.005	434	430	1.969×10^{-2}	2.032×10^{-2}
0.0025	0.0025	856	850	1.201×10^{-2}	1.116×10^{-2}
0.01	0.02	278	267	7.641×10^{-2}	8.691×10^{-2}
0.005	0.01	507	491	4.071×10^{-2}	4.571×10^{-2}
0.0025	0.005	949	929	2.259×10^{-2}	2.37×10^{-2}
0.00125	0.0025	1815	1788	1.346×10^{-2}	1.284×10^{-2}

Table 2.1. Numerical test on v_{sym}.

v^+_{lip}		Semi-lagrangian		Semi-lagrangian	
		Forward	Backward	Forward	Backward
h	Δ	$\overline{n}$		err	
0.04	0.02	150	113	4.808×10^{-2}	4.734×10^{-2}
0.02	0.01	152	133	2.392×10^{-2}	2.356×10^{-2}
0.01	0.005	217	217	1.196×10^{-2}	1.176×10^{-2}
0.005	0.0025	427	427	5.98×10^{-3}	5.88×10^{-3}
0.02	0.02	115	114	3.487×10^{-2}	3.469×10^{-2}
0.01	0.01	222	221	1.744×10^{-2}	1.736×10^{-2}
0.005	0.005	434	432	8.79×10^{-3}	8.76×10^{-3}
0.0025	0.0025	854	852	4.44×10^{-3}	4.46×10^{-3}
0.01	0.02	274	274	4.004×10^{-2}	4.01×10^{-2}
0.005	0.01	503	502	2.008×10^{-2}	2.012×10^{-2}
0.0025	0.005	945	945	1.004×10^{-2}	1.006×10^{-2}
0.00125	0.0025	1809	1812	5.02×10^{-3}	5.02×10^{-3}

Table 2.2. Numerical test on v^+_{lip}.

Chapter 3

Boundary condition approximation via normal field method

All the previous differential model use, in a very strong way, the information stored in the boundary condition of the height of the surface. In fact it is a very indispensable ingredient that let us start to build the solution. Instead, in the applications, is very difficult to obtain this kind of information. If we take a picture of a real object is not possible to obtain this precious data using only a digital photo camera. In this part we discuss about the impossibility to reconstruct the problem without the boundary condition.

Now we explain that the problem of SfS, that uses the photometric stereo techniques with only two images, is ill posed if the boundary condition is not take into account. Let us start considering two different surfaces $z_+ = u_+(x,y)$ and $z_- = u_-(x,y)$ defined as follow:

$$\begin{aligned} u_+(x,y) = &\quad q(x) + g(y) \\ u_-(x,y) = &\quad -q(x) + g(y) \end{aligned} \tag{3.1}$$

where q and g are two functions defined in a limited and connected intervals of $\mathbb{R}$ and these intervals can also be different.

If we calculate the unitary normal vector for both surfaces we obtain a particular case

$$\begin{cases} \mathbf{n}_+(x,y) = & \dfrac{1}{\sqrt{q'(x)^2 + g'(y)^2 + 1}} \left(-q'(x), -g'(y), 1\right) \\ \mathbf{n}_-(x,y) = & \dfrac{1}{\sqrt{q'(x)^2 + g'(y)^2 + 1}} \left(q'(x), -g'(y), 1\right) \end{cases} \tag{3.2}$$

writing with the symbol $q(x)'$ and $g(y)'$ the first derivative respect the correspondent variable (x for q and y for g). If we use this kind of light sources

$$\omega_\varphi = (0, \sin\varphi, \cos\varphi)$$

it is possible to obtain the same image function:

$$I_+^\varphi(x,y) = \omega_\varphi \cdot \mathbf{n}_+(x,y) = \frac{-g'(y)\sin\varphi + \cos\varphi}{\sqrt{q'(x)^2 + g'(y)^2 + 1}} = \omega_\varphi \cdot \mathbf{n}_-(x,y) = I_-^\varphi(x,y)$$

It is clear that the angle φ can be taken for every values where shadows do not appear, that is for all the values of φ that respect the illumination inequality (1.16). In general the admissible angles vary in an open interval, so we can chose infinity light sources. In our case, in the case of two images, it is sufficient to take two different values for φ.

This means that, for both the surfaces, we obtain the same image functions and this imply that the functions $b(x, y)$ and $f(x, y)$ that describe the problem are the same. In this case there is not the ambiguity relative to the regularity of the surfaces seen that we have no limited $q(x)$ and $g(y)$ to a particular class of functions. Then, this means that the complete problem admits only one solution (like proved before), but the problems connected to the two different surfaces differ only from the boundary condition. Here the dependence relative to the boundary condition of this kind of formulation of the problem.

Another case where is possible to see the same ambiguity (solved by the boundary condition) is this similar one:

$$\begin{aligned} u_+(x,y) &= \quad q(x) + g(y) \\ u_-(x,y) &= \quad q(x) - g(y) \end{aligned} \tag{3.3}$$

with this other kind of normal field

$$\begin{cases} \mathbf{n}_+(x,y) = & \dfrac{1}{\sqrt{q'(x)^2 + g'(y)^2 + 1}} \left(-q'(x), -g'(y), 1\right) \\ \mathbf{n}_-(x,y) = & \dfrac{1}{\sqrt{q'(x)^2 + g'(y)^2 + 1}} \left(-q'(x), g'(y), 1\right) \end{cases} \tag{3.4}$$

If we use this other kind of light sources

$$\omega_\varphi = (\sin\varphi, 0, \cos\varphi)$$

we obtain the following image functions:

$$I^\varphi_+(x,y) = \omega_\varphi \cdot \mathbf{n}_+(x,y) = \frac{-q'(y)\sin\varphi + \cos\varphi}{\sqrt{q'(x)^2 + g'(y)^2 + 1}} = \omega_\varphi \cdot \mathbf{n}_-(x,y) = I^\varphi_-(x,y)$$

and then we arrive to the same conclusion.

In the last years another kind of approach which has allowed to solve the SfS problem with stereo photometric techniques is been the determination of the surface through the approximation and the integration of its normal field.

Let us now consider this problem using three images. This means that we use another light source ω''' defined like the previous two. The number of equations that is possible to consider is now three and, for the normal field approximation, the way to solve the problem is based on the solution of the following linear system:

$$\begin{cases} \omega'_1 n_1 + \omega'_2 n_2 + \omega'_3 n_3 = I_1 \\ \omega''_1 n_1 + \omega''_2 n_2 + \omega''_3 n_3 = I_2 \\ \omega'''_1 n_1 + \omega'''_2 n_2 + \omega'''_3 n_3 = I_3 \end{cases} \tag{3.5}$$

These are the three irradiance equations considering the derivative of u inside the component of the normal vector $n = (n_1, n_2, n_3)$. In fact:

$$n = \left(\frac{-u_x}{\sqrt{1 + ||\nabla u||^2}}, \frac{-u_y}{\sqrt{1 + ||\nabla u||^2}}, \frac{1}{\sqrt{1 + ||\nabla u||^2}} \right) \tag{3.6}$$

with $u_x = -\frac{n_1}{n_3}$ and $u_y = -\frac{n_2}{n_3}$.

The procedure consists in solving the system (3.5) for every pixel (i, j), that is, solve the following linear systems:

$$\begin{cases} \omega_1' n_1(x_i, y_j) + \omega_2' n_2(x_i, y_j) + \omega_3' n_3(x_i, y_j) = I_1(x_i, y_j) \\ \omega_1'' n_1(x_i, y_j) + \omega_2'' n_2(x_i, y_j) + \omega_3'' n_3(x_i, y_j) = I_2(x_i, y_j) \\ \omega_1''' n_1(x_i, y_j) + \omega_2''' n_2(x_i, y_j) + \omega_3''' n_3(x_i, y_j) = I_3(x_i, y_j) \end{cases} \tag{3.7}$$

This permits to calculate the normal field n for every pixel; in others words we know the gradient vector for every pixel. The hypothesis on the previous system in order to obtain a unique solution is the linear independence of the light sources. From here it is possible to use interpolation method to obtain u from its normal field ([90, 91, 92]).

But this kind of approach uses three digital images in order to obtain the uniqueness of the solution, and this represents a drawback. The use of only two digital images, that is, to consider only the first two equations of (3.7), brings an ambiguity of the solution which involves for each pixel, the determination of two possible normal vectors. However, there are some areas in the image domain for which we can determine univocally the normal field.

On equal terms of image data, the difference between the normal field approximation and our differential approach is the resolution of the problem in a local way with the normal field's approximation. Each point (pixel) and the relative normal calculation is treated separately. This technique doesn't allow the propagation of any kind of information obtained through the calculation of the normal vectors to the surface, and this is a drawback. Through the technique which uses the PDE approximation we have two very important aspects which are different from the previous one: the first is that the differential equation which defines the problem is valid for each point in the image domain (that is for each pixel, so there is a "rule", suggested by the equation, which is valid uniformly for all the pixels), the second one is that we take into consideration a propagation of information related to the numerical approximation technique which approximates the surface through the characteristic method.

In order to use only two images to solve the problem we take into consideration both methods. Then we use the normal field approximation to determine the boundary conditions, while, for the surface approximation, we use the PDE numerical techniques.

3.1 Geometrical approach to the normal field approximation with two images

In this paragraph we study two different cases in which it is possible to determine the uniqueness of the normal field and then we develop a method used to identify these sets inside the images taken into account. The example we are going to illustrate take in consideration the artificial surfaces cases as well as real images cases.

We introduce the problem of normal field approximation emphasizing one more time that it is based on a local study of the image. For each pixel we approximate the unitary vector which represents the outgoing normal to the surface supposed

lambertian. Referring to a cartesian coordinates system (x, y, z) (which we will name from now on (n_1, n_2, n_3) in order to assimilate it to the set of possible normals for each pixel), we suppose that for each image used as a photo the camera's point of view is placed on the z axis. Therefore, in this image, we can determine, for each pixel, a set of visible unitary vectors detected like the sphere's superior part ($n_3 > 0$) centered in the origin and with radius one. We consider now the two light sources supposing them placed at the infinity. Therefore, we can write them like two vectors (for simplicity unitary) ω' and ω'' for which it is possible to determine two plans passing through the origin.

They are:

$$\begin{aligned} \pi' &: \omega'_1 n_1 + \omega'_2 n_2 + \omega'_3 n_3 = 0 \\ \pi'' &: \omega''_1 n_1 + \omega''_2 n_2 + \omega''_3 n_3 = 0 \end{aligned} \tag{3.8}$$

Now we can determine the set of the possible normals for each pixel, which can be sum up in the following non linear system:

$$\begin{cases} \omega'_1 n_1 + \omega'_2 n_2 + \omega'_3 n_3 \geq 0 \\ \omega''_1 n_1 + \omega''_2 n_2 + \omega''_3 n_3 \geq 0 \\ n_1^2 + n_2^2 + n_3^2 = 1 \\ n_3 > 0 \end{cases} \tag{3.9}$$

Naming $I_1(i, j)$ and $I_2(i, j)$ the grey level of the images (between 0 and 1) respectively obtained with ω' and ω'' for the pixel (i, j), we can say that the linear system

$$\begin{cases} \omega'_1 n_1 + \omega'_2 n_2 + \omega'_3 n_3 = I_1(i, j) \\ \omega''_1 n_1 + \omega''_2 n_2 + \omega''_3 n_3 = I_2(i, j) \\ n_1^2 + n_2^2 + n_3^2 = 1 \end{cases} \tag{3.10}$$

admits two solutions. An important study is carried out on the line relative to the line intersection of the two planes $r : \pi' \cap \pi''$, whose parameters are

$$\begin{aligned} k &= \omega'_2 \omega''_3 - \omega'_3 \omega''_2 \\ l &= \omega'_3 \omega''_1 - \omega'_1 \omega''_3 \\ m &= \omega'_1 \omega''_2 - \omega'_2 \omega''_1 \end{aligned} \tag{3.11}$$

This allows to establish the direct connection between the two solutions of the system (3.10). So, suppose we calculate one solution of the system (3.10), that is $\hat{n} = (\hat{n}_1, \hat{n}_2, \hat{n}_3)$. If we consider the line of parameters (k, l, m) passing through $\hat{n}$, then the second solution $(\hat{\hat{n}})$ will be its second intersection on the sphere.

3.1.1 Uniqueness of normal obtained by visibility (Σ_G)

Now we consider the first case in which we can obtain the normal field uniqueness using two images. This first case is explainable geometrically considering the set obtained changing the sign of the last inequality of the system (3.9) (which represents the condition of visibility) and then projecting it, through the line of the parameters (k, l, m), on the other side of the sphere. Clearly, we can obtain the uniqueness

because, in this situation, we are able to discard one of the solutions of the system (3.10) considering only the possible one.

Therefore, in order to determine these points, the first step is to determine the set so that

$$\begin{cases} \omega'_1 n_1 + \omega'_2 n_2 + \omega'_3 n_3 \geq 0 \\ \omega''_1 n_1 + \omega''_2 n_2 + \omega''_3 n_3 \geq 0 \\ n_1^2 + n_2^2 + n_3^2 = 1 \\ n_3 < 0 \end{cases} \tag{3.12}$$

Clearly, these set of points, which we will name $\hat{n}$, can't be considered as a possible candidate for the normal field at the surface taken into consideration (because they are placed on the part of the sphere which is not visible; see the yellow set in Fig. 3.1). The points which could be candidate for the normal field are the ones in the set in biunique correspondence with (3.12) through the intersection of the straight line of parameters (k, l, m) and passing through $\hat{n}$. It intersects the sphere in another point $\hat{\hat{n}}$ that we take into consideration inside the set of possibles surface normal vectors (see the green set in Fig. 3.1).

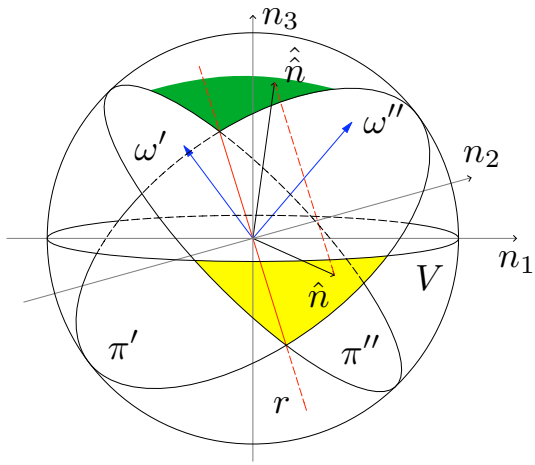

Figure 3.1. The planes π' and π'' are orthogonal, respectively, to the directions ω' and ω'' of the lightenings. The intersection between π' and π'' is denoted as r. Therefore, the three lines in red, which are supported by ω', ω'' and r, form an orthogonal basis. Each normal $\hat{\hat{n}}$ pointing to the green area is known without ambiguity, since the second possible normal $\hat{n}$ points to the yellow area, which is a twice lighted but non-visible part of the sphere, because it lies under the equator E.

Let's consider now the details of the calculus which is going to determine the point $\widetilde{n} = (\widetilde{n}_1, \widetilde{n}_2, \widetilde{n}_3)$. It is simple; between the two points determined from the intersection between the straight line r and the unitary sphere, the one which has the third component $\widetilde{n}_3$ negative is chosen. We note that the existence of this set is guaranteed by passing through origin of the straight line r. Considering the parametric equation of r

$$\begin{cases} n_1 = kt \\ n_2 = lt \\ n_3 = mt \end{cases}$$

it is possible to find the intersections with the sphere ($n_1^2 + n_2^2 + n_3^2 = 1$) if we consider the substitution

$$\begin{cases} n_1 = \dfrac{k}{m} n_3 \\ n_2 = \dfrac{l}{m} n_3 \end{cases}$$

which permits to determine the two values of

$$n_3 = \pm \sqrt{1 + \left(\frac{k}{m}\right)^2 + \left(\frac{l}{m}\right)^2}^{-1} \tag{3.13}$$

Then $\widetilde{n}_3$ is the negative determination of the previous square root.

Remark 3.1 *In order to avoid numerical instability when m is too close to zero, it is possible to calculate the $\widetilde{n}$ point in a similar way but dividing by k or l.*

Now it is possible to start the discretization of the set defined by (3.12). Let us consider a point we can imagine attached at one lattice that discretizes this set on the sphere; let's take $\bar{n}_3$ like one point that describes longitudinally this lattice ($\widetilde{n}_3 < \bar{n}_3 < 0$). We describe now the latitudinal discretization of this set. In this aim we consider the intersection of two planes π' e π'' with the section of the sphere horizontally cut at height $\bar{n}_3$ (see Fig. 3.2).

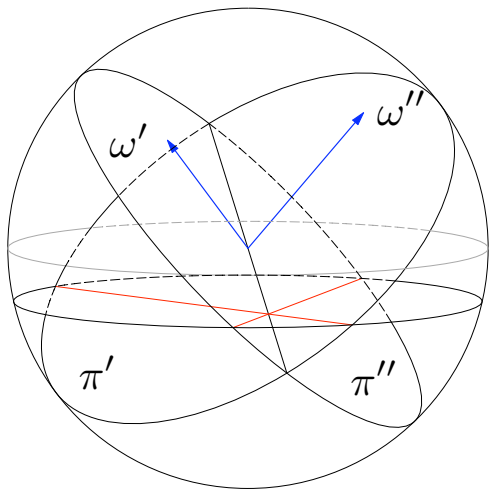

Figure 3.2. The intersections of a parallel plane with π' and π'' form the two straight lines in red.

Now we describe in detail the steps relative to the calculus of the intersection points among this sphere section and the light planes considering a generic plane of parameters $(\omega_1, \omega_2, \omega_3)$ (the diversification on our case is referred only to the application of the suitable apexes). To do this it is sufficient to solve the following nonlinear system:

$$\begin{cases} \omega_1 n_1 + \omega_2 n_2 + \omega_3 \bar{n}_3 = 0 \\ n_1^2 + n_2^2 = 1 - \bar{n}_3^2 \end{cases} \tag{3.14}$$

Changing it in an opportune way (for example $n_1 = (-\omega_2 n_2 - \omega_3 \bar{n}_3)\frac{1}{\omega_1}$ in the second equation) it is possible to determine the two solutions solving the second order equation (in the variable n_2) where the coefficients are:

$$\begin{aligned} a &= \left(\frac{\omega_2}{\omega_1}\right)^2 + 1 \\ b &= 2\frac{\omega_2\omega_3\bar{n}_3}{\omega_1^2} \\ c &= \left(\frac{\omega_3\bar{n}_3}{\omega_1}\right)^2 + \bar{n}_3^2 - 1 \end{aligned} \tag{3.15}$$

We find then the two intersections that we will call $P_1^* = (1n_1^*, 1n_2^*)$ and $P_2^* = (2n_1^*, 2n_2^*)$.

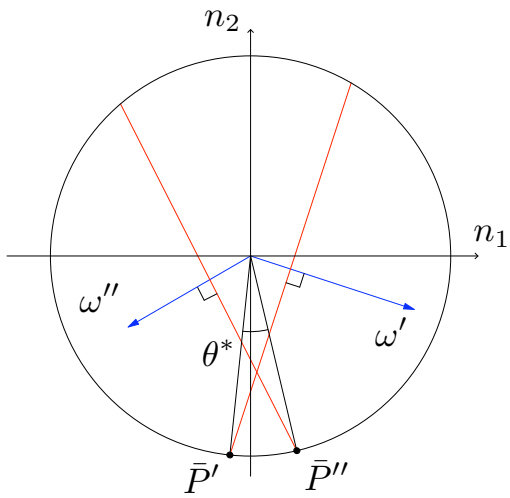

Figure 3.3. Seen from the direction of observation, these two intersections are orthogonal to the lightenings ω' and ω''. This allows us to define the angle θ^*.

Remark 3.2 *With the aim to decrease the bad conditioning relative to the calculus of these points, it is also possible to express in n_2 in order to divide by ω_2 in the case where ω_1 is computationally small.*

The point that interests us is the one nearest to $\widetilde{n}$. The point we consider will be determined by the distance criteria, that is:

$$P^* = arg \min_{i=1,2}(\text{dist}(P_i^*, (\widetilde{n}_1, \widetilde{n}_2))) = (n_1^*, n_2^*) \tag{3.16}$$

We can calculate it for both planes (π' and π'') obtaining the intersection points between them and the sphere section at quote $\bar{n}_3$. Let us call these points $\bar{P}' = (n_1', 1n_2', \bar{n}_3)$ and $\bar{P}'' = (n_1'', n_2'', \bar{n}_3)$.

After we have calculated the angles θ_1 and θ_2 determined by the axis n_1 and the segment connecting the origin of the plane $(n_1, n_2, \bar{n}_3)$ with, respectively $\bar{P}'$ and $\bar{P}''$, we consider like referential angle $\theta^* = |\theta_1 - \theta_2|$.

Now it is possible to express the vector $\hat{n}$ in the following way:

$$\begin{aligned}\hat{n}_1 &= \cos(\bar{\theta} + \min(\theta_1, \theta_2))\sqrt{1-\bar{n}_3^2}\\ \hat{n}_2 &= \sin(\bar{\theta} + \min(\theta_1, \theta_2))\sqrt{1-\bar{n}_3^2}\\ \hat{n}_3 &= \bar{n}_3\end{aligned} \tag{3.17}$$

We can make vary $\theta^* < \bar{\theta} < 0$ and $\hat{n}_3 < \bar{n}_3 < 0$, obtaining the discretization of the set (3.12). Now, for every of these points $\hat{n}$ it is necessary to find the correspondent point $\hat{\hat{n}}$ in the visible zone of the sphere.

In order to make this let us consider the equation of the straight line in the $\mathbb{R}^3$ space passing through $\hat{n}$ and of parameters (l, m, n):

$$\begin{cases} n_1 = \hat{n}_1 + kt \\ n_2 = \hat{n}_2 + lt \\ n_3 = \hat{n}_3 + mt \end{cases}$$

let's express now:

$$\begin{aligned} n_1 &= \frac{n_3 - \hat{n}_3}{m}k + \hat{n}_1 \\ n_2 &= \frac{n_3 - \hat{n}_3}{m}l + \hat{n}_2 \end{aligned}$$

that we substitute in the equation of the sphere $n_1^2 + n_2^2 + n_3^2 = 1$. We obtain the two solutions of the second order equation whose coefficients are:

$$\begin{aligned} a^* &= \left(\frac{k}{m}\right)^2 + \left(\frac{l}{m}\right)^2 + 1 \\ b^* &= 2\left(\frac{k}{m}\hat{n}_1 - \left(\frac{k}{m}\right)^2\hat{n}_3 + \frac{l}{m}\hat{n}_2 - \left(\frac{l}{m}\right)^2\hat{n}_3\right) \\ c^* &= \hat{n}_1^2 - 2\frac{k}{m}\hat{n}_3\hat{n}_1 + \left(\frac{k\hat{n}_3}{m}\right)^2 + \hat{n}_2^2 - \\ &\quad 2\frac{l}{m}\hat{n}_3\hat{n}_2 + \left(\frac{l\hat{n}_3}{m}\right)^2 - 1 \end{aligned} \tag{3.18}$$

From this two solutions we consider the one such that $n_3 > 0$.

Remark 3.3 *In order to decrease the bad conditioning relative to the calculus of these points it is possible to express all in the variable n_1 or in n_2 by dividing through (respectively) k or l in the event that m is too small.*

Remark 3.4 *The point $\hat{n}$ represents itself one solution of the previous problem. The fact that $\hat{n}_3 = \bar{n}_3 < 0$ and that the straight line r passes through the origin, implies necessary the existence of an unique point $\hat{\hat{n}}$.*

The final passage has the aim to consider, for each point $\hat{\hat{n}}$, the correspondent couple of values in the gray scale values:

$$\begin{aligned} \widetilde{I}_1 &= \omega_1'\hat{\hat{n}}_1 + \omega_2'\hat{\hat{n}}_2 + \omega_3'\hat{\hat{n}}_3 \\ \widetilde{I}_2 &= \omega_1''\hat{\hat{n}}_1 + \omega_2''\hat{\hat{n}}_2 + \omega_3''\hat{\hat{n}}_3 \end{aligned} \tag{3.19}$$

and check if, for each pixel (i, j) exists the couple of values in gray scale $I_1(i, j)$ e $I_2(i, j)$ such that:

$$\begin{cases} |I_1(i,j) - \widetilde{I}_1| < \varepsilon \\ |I_2(i,j) - \widetilde{I}_2| < \varepsilon \end{cases} \tag{3.20}$$

with ε fixed small (0.001).

Definition 3.5 *Given a couple of images I_1 and I_2, we call as Σ_G^I the corresponding set of coordinates $(x_i, y_j) \in \Omega$ on the images (determined as explained before) respect to Σ_G.*

As we will see in the numerical test section, the set Σ_G^I depending on the shape of the surface, can be made from different disjoint parts, that is $\Sigma_G^I = \Sigma_G^I(1) \cup \ldots \cup \Sigma_G^I(g_k)$.

3.1.2 Uniqueness of the normal obtained by coincidence (Σ_R)

Differently from the first set, this second way to describe the uniqueness of the solution for the system (3.10) becomes considering the case wherein the two normal vectors are coincident in the part of the sphere that defines all the possible normals to the surface pictured. This set is determined by all the points on the sphere tangent to the straight line of parameters directors (k, l, m) between the two light planes π' and π''. First we determine the two extreme points of the geodesic ($\hat{P}_1$ and

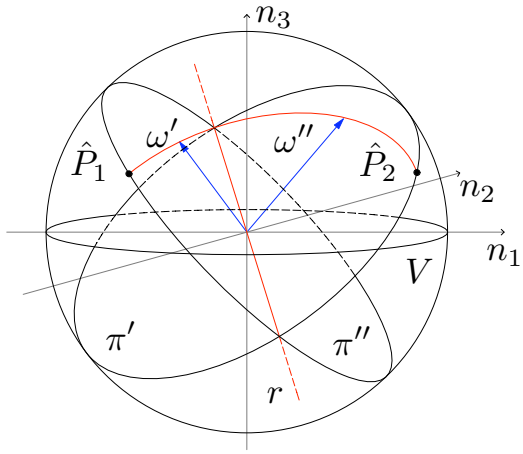

Figure 3.4. The geodesic in red is a part of the intersection of the sphere with the plane supported by ω' and ω''. Each normal $\hat{n}$ pointing to this line is known without ambiguity, since both normals coincide in this case.

$\hat{P}_2$) in order to apply a linear transformation for the parametrization of this curve through the angle included between the light vectors. Such points are determined from the intersection among the sphere, the plane orthogonal to the straight line r (passing through the origin) and the respective light plane (π' for $\hat{P}_1$ and π'' for $\hat{P}_2$). Let us solve therefore the next system considered now in a generalized form, as

follows:

$$\begin{cases} kn_1 + ln_2 + mn_3 = 0 \\ n_1^2 + n_2^2 + n_3^2 = 1 \\ \omega_1 n_1 + \omega_2 n_2 + \omega_3 n_3 = 0 \end{cases} \tag{3.21}$$

and that gives the solutions ($\hat{P}_1$ and $\hat{P}_2$) relative to ω' and ω''. The tangency is given by the first equation, that is the equation of the plane orthogonal to the straight line r and passing through the origin. For both cases (that is for each light plane) the number of solutions of (3.21) is two. The sought solution is easily identifiable considering the one with the third component positive.

Expressing, for example, n_2 and n_3 respectively from the first and the third equation of (3.21), it is possible to arrive to the following solutions:

$$\begin{aligned} n_1 &= \pm\left(\sqrt{1 + \frac{k^2}{l^2} + \frac{(m\widetilde{c}_3)^2}{l^2} + \frac{2km\widetilde{c}_3}{l^2} + \widetilde{c}_3^2}\right)^{-1} \\ n_2 &= \frac{-k - m\widetilde{c}_3}{l} n_1 \\ n_3 &= \widetilde{c}_3 n_1 \end{aligned} \tag{3.22}$$

Remark 3.6 *Also in this case, in order to avoid numeric instability effects, it is necessary to diversify the previous calculus with respect to the others variables depending on which of the three directors parameters (k, l, m) is bigger in absolute value.*

Once we determine these points, it is possible also to consider the angle included between them. Both these points belonging to the unitary radius sphere, the angle included is then $\theta = \arccos(\hat{P}_1 \cdot \hat{P}_2)$.

Next step consists in determining the affine application that allows us to represent the geodesic on the sphere like a part of the circumference on the plane (n_1, n_2) (see Fig.4.3). This step permits then a better discretization of this curve, taking into consideration, like parameter that discretize this curve, the angle which identifies these points. This application A must be such that:

$$\begin{aligned} A(1,0,0)^T &= \hat{P}_1 \\ A(\cos\theta, \sin\theta, 0)^T &= \hat{P}_2 \\ A(0,0,1)^T &= q \end{aligned} \tag{3.23}$$

We call q the unitary vector orthogonal to the plane on which lie the vectors $\hat{P}_1$ and $\hat{P}_2$ and opportunely oriented (that is with the direction towards the visible side of the sphere, $q_3 > 0$). That is, we consider the normalization of the vector (k, l, m) as possible q relatively to the sign of m. If it results $m < 0$ then we will take the opposite direction to this normalization. Now, considering the conditions imposed from (3.23) it is possible to determine the parameters of the application:

$$A = \begin{pmatrix} (\hat{P}_1)_1 & \frac{(\hat{P}_2)_1 - (\hat{P}_1)_1 \cos\theta}{\sin\theta} & q_1 \\ (\hat{P}_1)_2 & \frac{(\hat{P}_2)_2 - (\hat{P}_1)_2 \cos\theta}{\sin\theta} & q_2 \\ (\hat{P}_1)_3 & \frac{(\hat{P}_2)_3 - (\hat{P}_1)_3 \cos\theta}{\sin\theta} & q_3 \end{pmatrix} \tag{3.24}$$

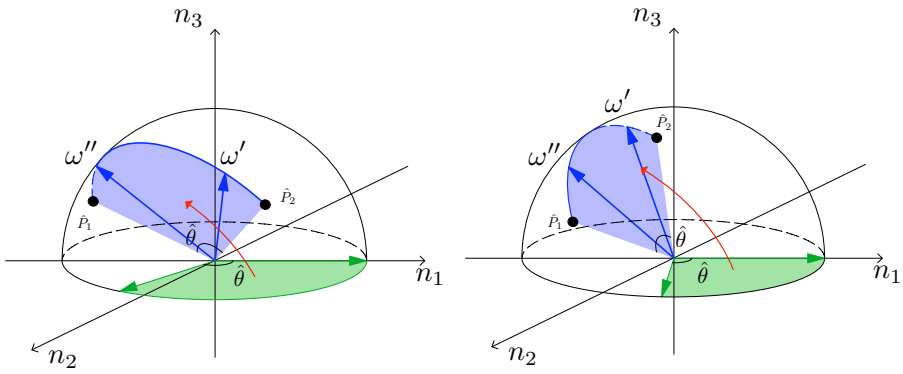

Figure 3.5. Two examples of applications A between the area defined by the arc of the circumference (in green) and the one relatives to the geodesic (in blue)

Now, considering an angle $\widetilde{\theta}$ such that $0 < \widetilde{\theta} < \theta$, it is possible to determine the point $\hat{\hat{n}}$ on the geodesic considering the previous application, that is:

$$A(\cos\widetilde{\theta}, \sin\widetilde{\theta}, 0)^T = \hat{\hat{n}} \tag{3.25}$$

Exactly like before it is possible to determine, on the image, all the elements of this set going to check them point to point one time calculated $\widetilde{I}_1$ and $\widetilde{I}_2$ like in (3.19) and check always the distance (3.20).

In the same way of Σ_G we can define the respective set for Σ_R in the images:

Definition 3.7 *Let Σ_R^I be the corresponding set of coordinates $(x_i, y_j) \in \Omega$ on the images (determined with the previous algorithm) respect to Σ_R.*

Also in this case we can define Σ_R^I as the union of connected sets, i.e. $\Sigma_R^I = \Sigma_R^I(1) \cup \ldots \cup \Sigma_R^I(r_k)$.

3.2 Preliminary advantages: predictable number of solutions and approximation of boundary condition

The reasoning explained in the previous section permits us to take some important preliminary advantages for the study of the SfS-PS problem with both differential and normal field approach. For the first method we are able, depending on the position of the sets Σ_R^I and Σ_G^I (on the image domain Ω), to approximate the boundary condition that permits to the differential approach to be primed.

3.2.1 Approximation of the boundary condition

A interesting advantages one can take from the study of the Σ_R and Σ_G sets is related to the combination of this study with the PDE approach (2.8). In fact let us suppose that the boundary points $(x_i, y_j) \in \partial\Omega$ don't belong to Σ_R. This means that we can approximate the height of the surface with at most two values (continuing to use the differentiability of the surface on the boundary). This implies that there are two different values for ∇u for each point. In general, once we fix the image

domain in the vertex points $(\widetilde{x}_i, \widetilde{y}_j)$ for $i, j = 0, 1$ (see Fig. 2.8), we can consider a parametrization of $\partial\Omega$ like a closed piecewise regular curve $\gamma : [0, 4] \to \partial\Omega$ as follow:

$$\gamma(t) = \begin{cases} (t\widetilde{x}_0 + (1-t)\widetilde{x}_1, \widetilde{y}_0), & 0 \leq t < 1; \\ (\widetilde{x}_1, (2-t)\widetilde{y}_0 + (t-1)\widetilde{y}_1), & 1 \leq t < 2; \\ ((t-2)\widetilde{x}_0 + (3-t)\widetilde{x}_1, \widetilde{y}_1), & 2 \leq t < 3; \\ (\widetilde{x}_0, (t-3)\widetilde{y}_0 + (4-t)\widetilde{y}_1), & 3 \leq t \leq 4; \end{cases} \tag{3.26}$$

Than we can obtain two boundary conditions considering:

$$g_1(\gamma(t)) = \int_0^t \nabla u_1(\gamma(s))\gamma'(s)ds + g_1(\gamma(0)) \tag{3.27}$$

and

$$g_2(\gamma(t)) = \int_0^t \nabla u_2(\gamma(s))\gamma'(s)ds + g_2(\gamma(0)) \tag{3.28}$$

That is, once we fix a common value for g_1 and g_2 in the vertex $(\widetilde{x}_0, \widetilde{y}_0)$ we can calculate them without ambiguity. Let us then fix $g_1(\widetilde{x}_0, \widetilde{y}_0) = g_2(\widetilde{x}_0, \widetilde{y}_0) = 0$.

We obtain than two different boundary conditions, let us call them $g_1(x_i, y_j)$ and $g_2(x_i, y_j)$ for every $(x_i, y_j) \in \partial\Omega_d$. We can now start solving the two differential problems that differ only for the boundary condition. Independently from the presence points inside the domain Ω belonging to Σ_R or Σ_g, we can approximate only one solution for each differential problem than, globally we have only two solutions. In the next section we will give an explanation of this paradox considering the way of the PDE resolution works respect the other local method. It is clear that only one boundary condition is the one that permits us to converge to the real solution of the problem. We can distinguish the right boundary condition just take into account that

$$\oint_{\partial\Omega} \nabla u ds = 0 \tag{3.29}$$

that is

$$g(\gamma(4)) - g(\gamma(0)) = 0 \tag{3.30}$$

that is the key property of a irrotational field. This means that, once we have calculated the two solutions of the linear system (∇u_1 and ∇u_2), the right solution can be selected before considering the one that is irrotational.

As we will emphasize with the numerical tests, the differentiability of the surface permits to both the sets to keep the same topology. That is, Σ_G^I continue to be a compact set (or a disjointed union of compact sets), while Σ_R^I remains a curve (or a disjointed union of curves) also in the image domain. In the case of the red set we will see that the differentiability of the surface guarantees us also the closure closure of these curves.

3.2.2 Predictable number of solutions

The second advantage is related to the completion of the SfS-PS problem using the normal field approximation. In fact, if the surface in differentiable everywhere (that is, if the normal field varies with continuity), we can count how many globally solutions this method permits to find. For example, if the Σ_R^I is empty while Σ_G^I is not empty than we have the uniqueness of solution. This analysis of the problem

permits to have a priori number of globally solutions for the local normal approach. The differentiability of the surface allows us to attach the parts obtaining different solution without ambiguity.

3.2.3 Ambiguity for the local normal vector field approach, no ambiguity for the differential approach: paradox explanation

Let us now explain why the differential problem, starting with the knowledge of the boundary condition, has not any ambiguities with respect to the local one and succeeds in the approximation of the surface.

With the aim to show how the vector field $b(x, y)$ of the problem (2.8) is placed respect the two solutions of the linear local problem (3.8), we start the example supposing to know the surface. Let us take a simple function that describe the surface as the follows:

$$u(x, y) = x \tag{3.31}$$

with gradient and normal field both constants

$$\nabla u(x, y) = (1, 0), \quad n(x, y) = \Big(-\frac{1}{\sqrt{2}}, 0, \frac{1}{\sqrt{2}} \Big). \tag{3.32}$$

Let us choose two light sources vectors that permits to have a constant characteristic field $b(x, y)$. This can succeed if one of the two light sources is chosen vertical, than:

$$\omega' = (0, 0, 1), \quad \omega'' = \left(\frac{1}{2}, \frac{1}{2}, \frac{\sqrt{2}}{2} \right)$$

where ω'' has its spherical coordinates equals to $\varphi_2 = \frac{\pi}{4}$ and $\theta_2 = \frac{\pi}{4}$. This permits to have the following two image functions constant, that is:

$$I_1(x, y) = \frac{1}{\sqrt{2}}, \quad I_2(x, y) = \frac{\sqrt{2} - 1}{2\sqrt{2}}.$$

With these kinds of data, the system (3.8) becomes:

$$\begin{cases} n_3(x_i, y_j) = \dfrac{1}{\sqrt{2}} \\ \dfrac{1}{2} n_1(x_i, y_j) + \dfrac{1}{2} n_2(x_i, y_j) + \dfrac{\sqrt{2}}{2} n_3(x_i, y_j) = \dfrac{\sqrt{2} - 1}{2\sqrt{2}} \end{cases} \tag{3.33}$$

that admits infinite solutions dependents by a parameter

$$\begin{pmatrix} n_1 \\ n_2 \\ n_3 \end{pmatrix} = \begin{pmatrix} -\frac{1}{\sqrt{2}} \\ 0 \\ \frac{1}{\sqrt{2}} \end{pmatrix} + t \begin{pmatrix} -1 \\ 1 \\ 0 \end{pmatrix}.$$

We can calculate the two solutions considering that both belong to the unitary sphere. That is, solving the equation $n_1^2 + n_2^2 + n_3^2 = 1$ we obtain the following two solutions:

$$n_{sol}^1 = \Big(-\frac{1}{\sqrt{2}}, 0, \frac{1}{\sqrt{2}} \Big), \quad n_{sol}^2 = \Big(0, -\frac{1}{\sqrt{2}}, \frac{1}{\sqrt{2}} \Big). \tag{3.34}$$

If we calculate the characteristic vector field using its definition we obtain:

$$b_1(x,y) = I_2\omega_1' - I_1\omega_1'' = -\frac{1}{2\sqrt{2}}, \quad b_2(x,y) = I_2\omega_2' - I_1\omega_2'' = -\frac{1}{2\sqrt{2}}.$$

With the aim to understand the relation between the vector field b and the two normal solutions. we consider the projection of the two vectors on the xy plane (P_{xy}), making the dot product with the constant vector field b, that is:

$$P_{xy}(n^1_{sol}) \cdot b = \left(-\frac{1}{\sqrt{2}}, 0\right) \cdot \left(-\frac{1}{2\sqrt{2}}, -\frac{1}{2\sqrt{2}}\right) = \\ = \left(0, -\frac{1}{\sqrt{2}}\right) \cdot \left(-\frac{1}{2\sqrt{2}}, -\frac{1}{2\sqrt{2}}\right) = P_{xy}(n^2_{sol}) \cdot b \quad (3.35)$$

Let us call as θ_1 and θ_2 the two angles between the vector b and, respectively, the vectors n^1_{sol} and n^2_{sol}. The equality between the previous two dot product implies that these two angles are equal. This means that the characteristic field crosses all the domain Ω passing in the middle of the two normal vectors (see Fig. 3.6). So, the characteristic field does not follow the same direction imposed by the correct normal vector solution. In fact, the vector field $b(x,y)$, that gives the direction where the characteristics have to take the information for the construction of the surface in the differential problem, permits to take the common information given from the two normal vector n^1_{sol} and n^2_{sol}.

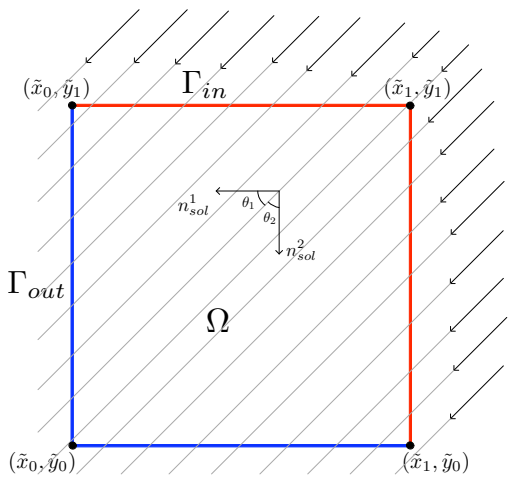

Figure 3.6. An example of the distribution of the Γ_{in} and Γ_{out} sets considering a constant characteristic field (represented by the arrows). In this picture are visible also the solution of the normal field problem.

3.3 Numerical tests

Here the results of the previous theory applied, for first on synthetic images. We report now some results obtained through the implementation of the previous algorithm. The images taken into consideration are relative to two surfaces showed in Fig. 4.4.

Figure 3.7. Set of surfaces used for the numerical tests

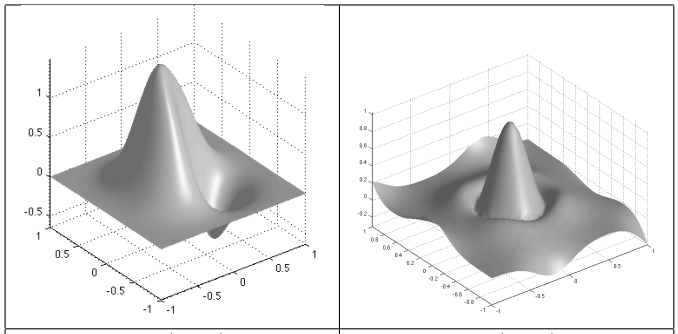

They have particular features. For example, v_{reg} has a very big slope between the maximum point and the minimum point with a flat boundary. Instead, the main feature of v_{lip} is its irregularity. In fact it has a smooth boundary, but in Ω it is not differentiable because of its structure. For both the surface we know from the beginning their analytical formula that we will call $v_{reg}(x,y)$ and $v_{lip}(x,y)$.

In all the tests the closed set that defines the domain is $\overline{\Omega} \equiv [-1,1] \times [-1,1] = \partial\Omega \cup \Omega$ and then $\Omega \equiv (-1,1) \times (-1,1)$. Working with digital image we call the discrete set of point where the images are defined as $\overline{\Omega}_d \equiv \partial\Omega_d \cup \Omega_d$ calling (x_i, y_j) the position of a generic pixel. That is, once we fix a step (namely Δ) like a distance from one pixel to the adjacent one, we can simply define the coordinates of the point $(x_i, y_j) \in \overline{\Omega}_d$ as $x_i = -1 + i\Delta$ and $y_j = -1 + j\Delta$ (for $i, j = 1, \ldots, r$, where r is the resolution of the square image of $r \times r$ pixels).

3.3.1 Counting the solutions

We start the presentation of the numerical part explaining in the practice how is possible to count the solutions considering the Σ_G^I and Σ_R^I disposition. Let us remind that we are able to do that only if the surface is smooth (i.e. it must be differentiable inside the image domain). In order to do that we consider the surface v_{reg}.

A first example of this study can be introduced by two images of Fig. 3.8 where the surface v_{reg} is lighted up (on the left) from the first light ω' (I_1) and (on the right) from second light vector ω'' (I_2). These light vectors are expressed in spherical coordinates ($\omega = (\sin\varphi\cos\theta, \sin\theta\sin\varphi, \cos\varphi)$) and the angles that define them are marked below each image of Fig. 3.8.

In this case the sets Σ_G^I and Σ_R^I can be seen in Fig. 3.9 where it is possible to see I_1 in the left side where is spotlighted Σ_G^I in green, whereas in the right one there is I_2 where we can note Σ_R^I in red. This kind of representation (of the sets Σ_G^I and Σ_R^I respectively on I_1 and I_2) is completely arbitrary and comes useful for an awareness in the domain Ω with respect to the surface.

First of all let us observe (from Fig. 3.9) the structure of these sets that draw the same topology on the sphere, that is , Σ_G^I is a convex set, while $\Sigma_R^I(1)$ and $\Sigma_R^I(2)$ are closed curves.

Just for understand how we can count the solutions, let us introduce the sets Σ_U and Σ_D. They are the subsets of the unitary sphere (of all the admissible normal vectors), respectively, upon and below the geodesic (Σ_R), see Fig. 3.10.

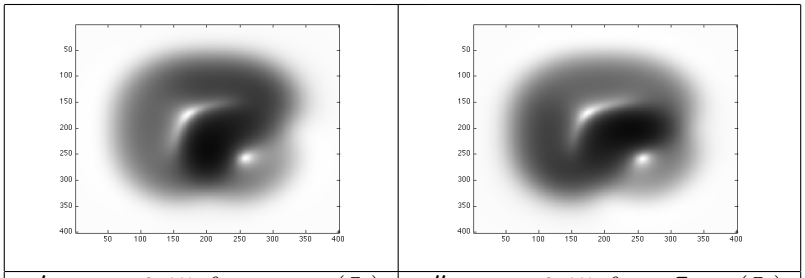

Figure 3.8. Synthetic images of the v_{reg} surface (400×400 pixels) used for count the number of solutions for the local normal field method.

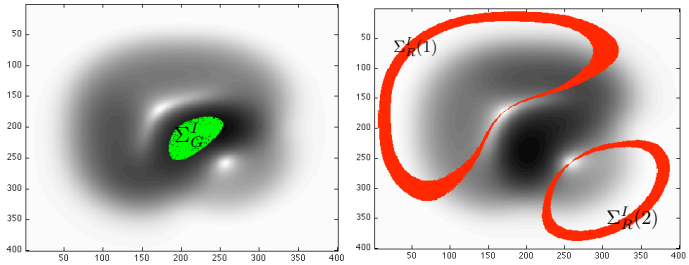

Figure 3.9. On the left the previous image I_1 with drown the set Σ_G^I. On the right the image I_2 with, in red, the two sets $\Sigma_R^I(1)$ and $\Sigma_R^I(2)$ which union gives Σ_R^I.

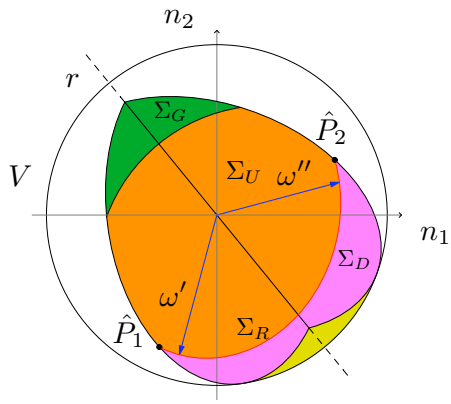

Figure 3.10. Vertical view of the sphere where Σ_U is the set colored in orange and in violet the set Σ_D.

Now, taking into account that these sets can be mapped in the image domain Ω (namely $\Sigma_U^I = \Sigma_U^I(1), \ldots, \Sigma_U^I(h)$ and $\Sigma_D^I = \Sigma_D^I(1), \ldots, \Sigma_D^I(q)$), we show in Fig. 3.11 the four solutions in term of the sets previously describe.

3.3.2 Uniqueness using normal field approximation

In this section we give an example that explain the analysis that can be made using the research of the Σ_G^I and Σ_R^I on the image domain. First of all we have to underline

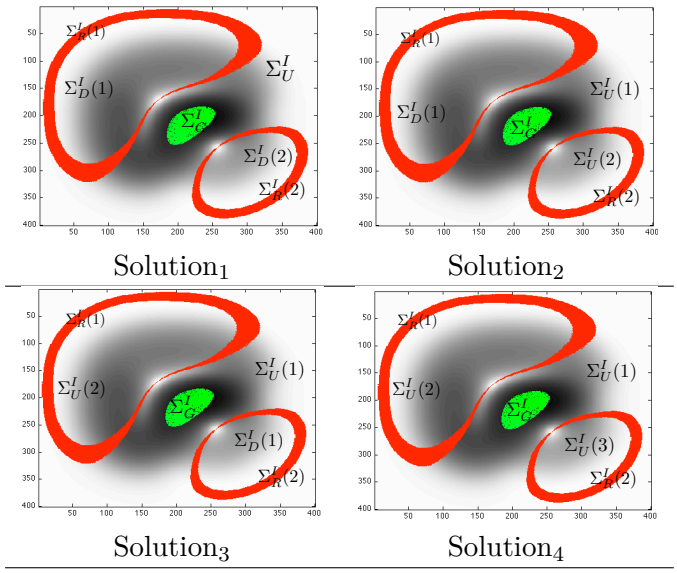

Figure 3.11. All the possible combinations that permits us to count the solutions obtainable with the normal approach.

the difficulties that we can find with this kind of analysis, in particular with respect to the resolution of the images. In fact the mathematical analysis of these two sets on Ω is exact inside a domain where the images functions $I_1(x, y)$ and $I_2(x, y)$ are know for every $(x, y) \in \overline{\Omega}$ (that is in the continuous domain). In particular, for the correct approximation of the boundary condition we should know these images functions all over $\partial\Omega$ and not only a discrete set of its points $\partial\Omega_d$.

Let us introduce the numerical test giving all the information relatively to the starting data (that is the images and the respective light sources) summarized in Fig. 3.12. In these two images is also possible to see (in blue) the set of points where the surface is not differentiable. The problem that we have to avoid is the presence of Σ_R^I

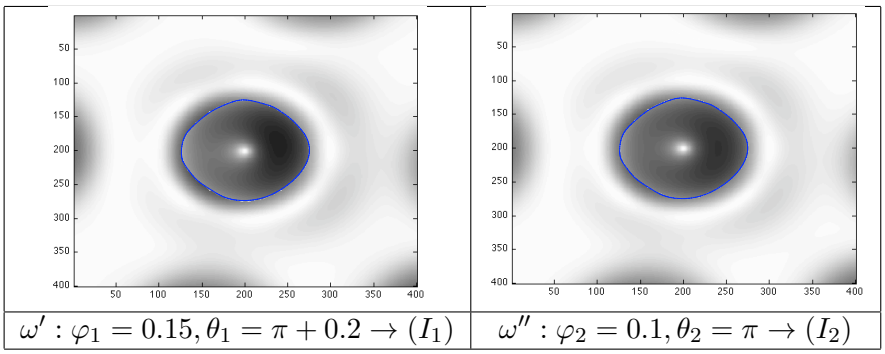

Figure 3.12. Two synthetic images (400×400 pixels) of v_{lip} used for the approximation of the boundary condition. In blue is emphasize the set of point where the surface is not differentiable.

on the boundary (that is $\Sigma_R^I \cap \partial\Omega_d = \emptyset$). As we have shown in the previous section, this sets make appear ambiguity. In fact, the normal can cross the geodesic passing

from Σ_D and Σ_U (or vice versa) or remain on the same set of provenance. With this aim we choose the light vectors very close to them with the purpose to have Σ_R and Σ_G small on the sphere and therefore to have a little possibility to find the respective sets on the image domain. Like in the previous section, if we have some points of $\partial\Omega_d$ belong to Σ_R^I we are able to count the different boundary conditions. In this case we obtain that $\Sigma_G^I \equiv \emptyset$ and, in particular, $\Sigma_G^I \equiv \emptyset$. This means that there are only two possible boundary conditions, but only one is admissible for a correct approximation of the surface.

Once we calculate the two normal field for every point of $\partial\Omega_d$ (n^+ and n^-), we approximate the boundary condition in a very simple way. That is, considering the definition of the normal vector depending from the gradient we can approximate the partial derivative (g_x^+, g_y^+ from n^+ and g_x^-, g_y^- from n^-) for every boundary point and then approximate the two values of u calling them $g^\pm$. Considering the boundary of the image like a rectangle where the cartesian reference system has the axis parallel to its sides, the order of approximation followed has been to start from a reference point (that is $(x_0, y_0) = (-1, -1)$) and continuing the integration of the gradient vector field simultaneously on the inferior and left sides. After that we continue the integration on the right and upper sides (Fig. 3.13).

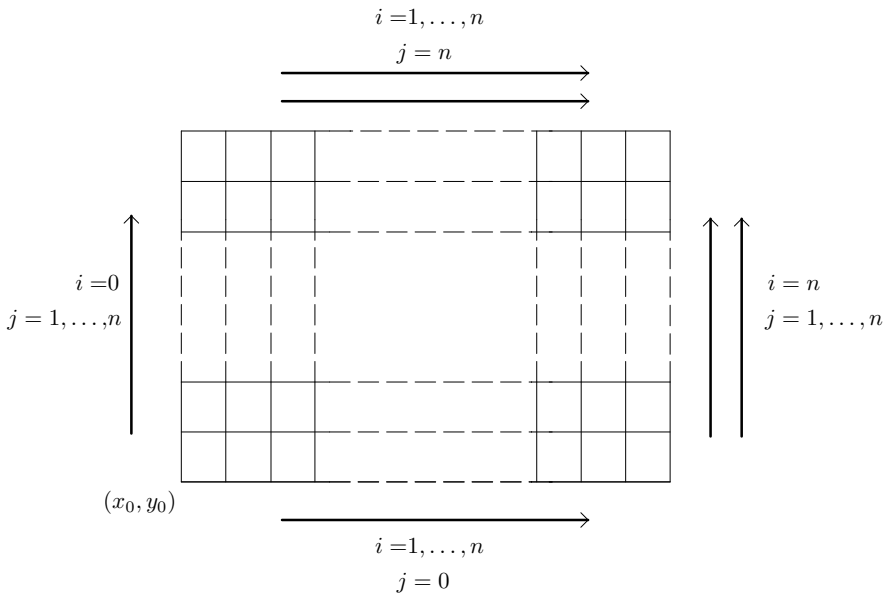

Figure 3.13. Order on integration for the approximation of the boundary data.

The integration of the gradient field starts by fixing a value for the reference point, that is $g^\pm(x_0, y_0) = v_{lip}(x_0, y_0)$ (just for estimate the error committed) and it continues using a backward integration scheme of the first order for the respective sides of the boundary, as follows:

- $g^\pm(x_i, y_j) = g^\pm(x_{i-1}, y_j) + u_x^\pm(x_i, y_j)\Delta$ per $i = 2, \ldots, r$, $j = 1$;
- $g^\pm(x_i, y_j) = g^\pm(x_i, y_{j-1}) + u_y^\pm(x_i, y_j)\Delta$ per $i = 1$, $j = 2, \ldots, r$;
- $g^\pm(x_i, y_j) = g^\pm(x_i, y_{j-1}) + u_y^\pm(x_i, y_j)\Delta$ per $i = r$, $j = 2, \ldots, r$;

- $g^{\pm}(x_i, y_j) = g^{\pm}(x_{i-1}, y_j) + u_x^{\pm}(x_i, y_j)\Delta$ per $i = 2, \ldots, r$, $j = r$.

The way we use to reconstruct the surface using the knowledge of its gradient value in the boundary is very simple. Others different ways to reconstruct the height of u starting from the same data can be find [90].

Let us call the right boundary condition as $\overline{g}$. In Tab. 3.1 is possible to find the error relative to the boundary conditions approximation in $L^{\infty}(\partial\Omega_d)$, that is:

$$||\overline{g} - v||_{L^{\infty}(\partial\Omega_d)} = \max_{(x_i,y_j)\in\partial\Omega_d} |\overline{g}(x_i, y_j) - v(x_i, y_j)|.$$

Following the same steps we repeat the approximation using the surface v_{reg} considering the images of Fig. 3.8. Underline one more time that also in this case we have not intersection between Σ_R^I and $\partial\Omega_d$ (see Fig. 3.9) we obtain the two boundary conditions with the error of Tab. 3.1.

	$L^{\infty}(\partial\Omega_d)$
$\overline{g} - v_{reg}$	5.38×10^{-3}
$\overline{g} - v_{lip}$	3.325×10^{-2}

Table 3.1. Errors in $L^{\infty}(\partial\Omega_d)$ norm between the correct boundary condition approximation $\overline{g}$ and the exact surface v.

Another thing we can note is the possibility to find the right normal field a posteriori. That is, once we approximate the right solution u of the differential problem (2.8) (using the boundary conditions $g^{\pm}$) we can find the its right normal field (on Ω_d) a posteriori even if our surface is not differentiable.

Chapter 4

SfS-PS problem using three images and symmetry

In the previous chapters we have presented a new model for the study of the SfS-PS. This differential approach uses the following data for the resolution of the problem:

1. two functions (that is, the intensity of the grayscale images) I_1, $I_2 : \Omega \subset \mathbb{R}^2 \to (0, 1]$;

2. two normalized vectors ω' and $\omega'' \in \mathbb{R}^3$ (with $\omega_3 > 0$) for which we obtain (through the SfS orthographic model) the respective aforementioned images;

3. the boundary condition $g(x, y) = u(x, y)\ \forall (x, y) \in \partial\Omega$.

We have seen in the Chapter (3) how the boundary condition results to be of primary importance not only for the well-posedness of the differential problem, but also for its very difficult deduction in real applications. In order to ease the usage of this differential approach in real applications, we need to be able to eliminate the necessity of knowing the height of the surface on the image boundary, by increasing the information on the surface.

4.1 Uniqueness of solution without boundary conditions

We can consider like a natural extension of our disposal data the possibility to consider a further additional image. The idea behind this approach is to use the third image for the approximation of the boundary condition (that is $g(x, y)\ \forall (x, y) \in \partial\Omega$). This approximation is based on two steps: the first is relative to the determination of the gradient field on the entire boundary $\partial\Omega$ of the domain Ω; the second is the approximation of the hight u on the boundary using the gradient value previously calculated. We solve this first step in two different but equivalent ways. The first take inspiration by our new differential method while the second one is given by some existent results.

4.1.1 Gradient values from the new differential SfS-PS model

The first one is based on considering the third image like a function that, coupled with the other two image functions, permits us to write the following linear PDEs:

$$\begin{cases} b^{(1,2)}(x,y)\cdot\nabla u(x,y) = f^{(1,2)}(x,y), & \text{a.e. } (x,y)\in\Omega; \\ b^{(1,3)}(x,y)\cdot\nabla u(x,y) = f^{(1,3)}(x,y), & \text{a.e. } (x,y)\in\Omega; \\ b^{(2,3)}(x,y)\cdot\nabla u(x,y) = f^{(2,3)}(x,y), & \text{a.e. } (x,y)\in\Omega. \end{cases} \tag{4.1}$$

where $b^{(h,k)}(x,y) = (I_k(x,y)\omega_1^h - I_h(x,y)\omega_1^k, I_k(x,y)\omega_2^h - I_k(x,y)\omega_2^k)$ and $f(x,y)^{(h,k)} = I_k(x,y)\omega_3^h - I_h(x,y)\omega_3^k$ where (h,k) is the combination of two of the first three natural integer without repeating.

Let us see how it is possible, using for example the first and the second equation of (4.1), to determine the boundary condition $g(x,y)$. One consideration we have to do is relative to a different connotation that one should give to these two equations. Once we fix a point (x_i,y_j) on the boundary of the image, we consider, rather than a system of PDEs, the following linear system:

$$\begin{cases} b_1^{(1,2)}(x_i,y_j)\dfrac{\partial u}{\partial x}(x_i,y_j) + b_2^{(1,2)}(x_i,y_j)\dfrac{\partial u}{\partial y}(x_i,y_j) = f^{(1,2)}(x_i,y_j) \\ b_1^{(1,3)}(x_i,y_j)\dfrac{\partial u}{\partial x}(x_i,y_j) + b_2^{(1,3)}(x_i,y_j)\dfrac{\partial u}{\partial y}(x_i,y_j) = f^{(1,3)}(x_i,y_j) \end{cases} \tag{4.2}$$

where the unknowns are the values of the partial derivative of u in the point $(x_i,y_j)\in\partial\Omega_d$. Let us prove the next result relative to the uniqueness of solution of the previous linear system.

Proposition 4.1 *Let*

$$A = \begin{pmatrix} b_1^{(1,2)}(x_i,y_j) & b_2^{(1,2)}(x_i,y_j) \\ b_1^{(1,3)}(x_i,y_j) & b_2^{(1,3)}(x_i,y_j) \end{pmatrix} \tag{4.3}$$

then $det(A) = 0$ *if and only if* ω', ω'', ω''' *are coplanar.*

Proof.

($\Rightarrow$) Let us prove that: $det(A) = 0$ implies ω', ω'', ω''' coplanar.

We generalize the proof simplifying the notation, by not considering the dependence on a specific point (x_i,y_j). We explicit the relative functions that appear in the matrix A in terms of the images and of the light sources and we obtain:

$$\begin{aligned} \det(A) =& \omega_1'\omega_2' I_2 I_3 - \omega_1'\omega_2''' I_1 I_2 - \omega_1''\omega_2' I_1 I_3 + \omega_1''\omega_2''' (I_1)^2 + \\ & - [\omega_1'\omega_2' I_2 I_3 - \omega_1'''\omega_2' I_1 I_2 - \omega_1'\omega_2'' I_1 I_3 + \omega_1'''\omega_2'' (I_1)^2] \end{aligned} \tag{4.4}$$

Let us consider the physical case where the three images I_1, I_2 and I_3 are defined by the surface u and the respective light sources as follows:

$$\begin{aligned} I_1(x,y) &= \frac{-\omega_1'\frac{\partial u}{\partial x}(x,y) - \omega_2'\frac{\partial u}{\partial y}(x,y) + \omega_3'}{\sqrt{1+||\nabla u(x,y)||^2}}, \\ I_2(x,y) &= \frac{-\omega_1''\frac{\partial u}{\partial x}(x,y) - \omega_2''\frac{\partial u}{\partial y}(x,y) + \omega_3''}{\sqrt{1+||\nabla u(x,y)||^2}}, \\ I_3(x,y) &= \frac{-\omega_1'''\frac{\partial u}{\partial x}(x,y) - \omega_2'''\frac{\partial u}{\partial y}(x,y) + \omega_3'''}{\sqrt{1+||\nabla u(x,y)||^2}}. \end{aligned} \tag{4.5}$$

Replacing the previous equalities in (4.4) we have:

$$\begin{aligned}
\det(A) = \\
I_1\Big[&\frac{\partial u}{\partial x}(\omega_1'\omega_1''\omega_2''' - \omega_2'\omega_1''\omega_1''') + \frac{\partial u}{\partial y}(\omega_1'\omega_2''\omega_2''' - \omega_2'\omega_2''\omega_1''') - \omega_1'\omega_3''\omega_2''' + \omega_2'\omega_3''\omega_1''' + \\
&+\frac{\partial u}{\partial x}(\omega_2'\omega_1''\omega_1''' - \omega_1'\omega_2''\omega_1''') + \frac{\partial u}{\partial y}(\omega_2'\omega_1''\omega_2''' - \omega_1'\omega_2''\omega_2''') - \omega_2'\omega_1''\omega_3''' + \omega_1'\omega_2''\omega_3''' + \\
&+\frac{\partial u}{\partial x}(\omega_1'\omega_2''\omega_1''' - \omega_1'\omega_1''\omega_2''')\frac{\partial u}{\partial y}(\omega_2'\omega_2''\omega_1''' - \omega_2'\omega_1''\omega_2''') + -\omega_3'\omega_2''\omega_1''' + \omega_3'\omega_1''\omega_2'''\Big] = \\
=&\frac{\partial u}{\partial x}\Big[- \omega_1'(- \omega_1'\omega_3''\omega_2''' + \omega_2'\omega_3''\omega_1''' - \omega_2'\omega_1''\omega_3''' + \omega_1'\omega_2''\omega_3''' + \omega_3'\omega_1''\omega_2''' - \omega_3'\omega_2''\omega_1''')\Big] + \\
&\frac{\partial u}{\partial y}\Big[- \omega_2'(- \omega_1'\omega_3''\omega_2''' + \omega_2'\omega_3''\omega_1''' - \omega_2'\omega_1''\omega_3''' + \omega_1'\omega_2''\omega_3''' + \omega_3'\omega_1''\omega_2''' - \omega_3'\omega_2''\omega_1''')\Big] - \\
&- \omega_3'(\omega_1'\omega_3''\omega_2''' - \omega_2'\omega_3''\omega_1''' + \omega_2'\omega_1''\omega_3''' - \omega_1'\omega_2''\omega_3''' - \omega_3'\omega_1''\omega_2''' + \omega_3'\omega_2''\omega_1''').
\end{aligned} \tag{4.6}$$

With the aim to prove the coplanarity of ω''' with respect to ω' and ω'', we define the director parameters of the plane generated by these last two vectors, that is:

$$\begin{aligned}
k &= \omega_2'\omega_3'' - \omega_3'\omega_2'', \\
l &= \omega_3'\omega_1'' - \omega_1'\omega_3'', \\
m &= \omega_1'\omega_2'' - \omega_2'\omega_1''.
\end{aligned} \tag{4.7}$$

The director parameters (k, l, m) of a plane represent a vector orthogonal to it, thus, orthogonal to every vector $v = (v_1, v_2, v_3)$ belonging to the plane. Therefore:

$$kv_1 + lv_2 + mv_3 = 0. \tag{4.8}$$

Now, considering $det(A)(x, y)$ like a polynomial in the variables $\xi = \frac{\partial u}{\partial x}(x, y)$ and $\eta = \frac{\partial u}{\partial x}(x, y)$, we have:

$$\begin{aligned}
\det(A)(\xi, \eta) = \\
&\xi\Big[- \omega_1'\Big(\omega_1'''(\omega_2'\omega_3'' - \omega_3'\omega_2'') + \omega_2'''(\omega_3'\omega_1'' - \omega_1'\omega_3'') + \omega_3'''(\omega_1'\omega_2'' - \omega_2'\omega_1'')\Big)\Big] + \\
&\eta\Big[- \omega_2'\Big(\omega_1'''(\omega_2'\omega_3'' - \omega_3'\omega_2'') + \omega_2'''(\omega_3'\omega_1'' - \omega_1'\omega_3'') + \omega_3'''(\omega_1'\omega_2'' - \omega_2'\omega_1'')\Big)\Big] + \\
&+ \omega_3'\Big(\omega_1'''(\omega_2'\omega_3'' - \omega_3'\omega_2'') + \omega_2'''(\omega_3'\omega_1'' - \omega_1'\omega_3'') + \omega_3'''(\omega_1'\omega_2'' - \omega_2'\omega_1'')\Big)
\end{aligned} \tag{4.9}$$

If we suppose that $det(A) = 0\ \forall(\xi, \eta)$ than this means that all the coefficients are zero, that is:

$$\omega_1'''(\omega_2'\omega_3'' - \omega_3'\omega_2'') + \omega_2'''(\omega_3'\omega_1'' - \omega_1'\omega_3'') + \omega_3'''(\omega_1'\omega_2'' - \omega_2'\omega_1'') = 0 \tag{4.10}$$

which implies the coplanarity.

($\Leftarrow$) Let us prove now that: ω', ω'', ω''' coplanar implies $det(A) = 0$.

We start by replacing in (4.4) the coplanarity equality $\omega''' = \alpha\omega' + \beta\omega''$ and, in

consequence, I_3 with $\alpha I_1 + \beta I_2$. We obtain:

$$\begin{aligned}
&\det(L) = \\
&-\omega_1'(\alpha\omega_2' + \beta\omega_2'')I_1I_2 - \omega_1''\omega_2'I_1(\alpha I_1 + \beta I_2) + \omega_1''(\alpha\omega_2' + \beta\omega_2'')(I_1)^2 + \\
&+(\alpha\omega_1' + \beta\omega_1'')\omega_2'I_1I_2 + \omega_1'\omega_2''I_1(\alpha I_1 + \beta I_2) - (\alpha\omega_1' + \beta\omega_1'')\omega_2''(I_1)^2 = \\
&= -\alpha\omega_1'\omega_2'I_1I_2 - \beta\omega_1'\omega_2''I_1I_2 - \alpha\omega_1''\omega_2'(I_1)^2 - \beta\omega_1''\omega_2'I_1I_2 + \alpha\omega_1''\omega_2'(I_1)^2 + \beta\omega_1''\omega_2''(I_1)^2 + \\
&+\alpha\omega_1'\omega_2'I_1I_2 + \beta\omega_1''\omega_2'I_1I_2 + \alpha\omega_1'\omega_2''(I_1)^2 + \beta\omega_1'\omega_2''I_1I_2 - \alpha\omega_1'\omega_2''(I_1)^2 - \beta\omega_1''\omega_2''(I_1)^2 = 0.
\end{aligned}$$

□

Remark 4.2 *The modelization of the SfS orthographic problem permits us to define the linear dependence of the images through their associated light vectors. In fact the way we consider the vector ω''' coplanar with the other two permits us to define, in the same way, the concept of linear dependent image functions.*

Definition 4.3 *Three image functions I_1, I_2 and I_3 obtained from the SfS orthographic model, are linearly independent if they are generated by three non coplanar light vectors.*

Instead, if we consider two images I_1 and I_2 obtained by the light vectors ω' and ω'' it is possible to get all the images obtainable with a light vector that is coplanar to the first two ($\omega''' = \alpha\omega' + \beta\omega''$), i.e.: $I_3 = \alpha I_1 + \beta I_2$ as α e β change.

Let us see how, once we choose $\omega''' = \alpha\omega' + \beta\omega''$, it results that $I_3 = \alpha I_1 + \beta I_2$.

Starting from the image definition of the SfS model we can write:

$$\begin{aligned}
I_3 &= \frac{-\frac{\partial u}{\partial x}\omega_1''' - \frac{\partial u}{\partial y}\omega_2''' + \omega_3'''}{\sqrt{1 + ||\nabla u||^2}} = \\
&= \frac{-\frac{\partial u}{\partial x}(\alpha\omega_1' + \beta\omega_1'') - \frac{\partial u}{\partial y}(\alpha\omega_2' + \beta\omega_2'') + (\alpha\omega_3' + \beta\omega_3'')}{\sqrt{1 + ||\nabla u||^2}} = \\
&= \alpha\frac{-\frac{\partial u}{\partial x}\omega_1' - \frac{\partial u}{\partial y}\omega_2' + \omega_3'}{\sqrt{1 + ||\nabla u||^2}} + \beta\frac{-\frac{\partial u}{\partial x}\omega_1'' - \frac{\partial u}{\partial y}\omega_2'' + \omega_3''}{\sqrt{1 + ||\nabla u||^2}} = \\
&= \alpha I_1 + \beta I_2.
\end{aligned} \tag{4.11}$$

The last proof, related to the singularity of the matrix A permits us to delineate a first strong hypothesis without which this procedure doesn't work: the non coplanarity of the light sources.

4.1.2 Gradient values from the Kozera method

For the second method of calculating the gradient of u on the $\partial\Omega_d$, we first recall the procedure used in [11] where, using the photometric stereo technique with three light sources, it succeeds to determine the value of the first partial derivatives of u all over the Ω domain through the following equality:

$$\begin{aligned}
\frac{\partial u}{\partial x}(x,y) &= \frac{(\omega_2''\omega_3''' - \omega_3''\omega_2''')I_1(x,y) + (\omega_3'\omega_2''' - \omega_2'\omega_3''')I_2(x,y) + (\omega_2'\omega_3'' - \omega_3'\omega_2'')I_3(x,y)}{(\omega_2''\omega_1''' - \omega_1''\omega_2''')I_1(x,y) + (\omega_1'\omega_2''' - \omega_2'\omega_1''')I_2(x,y) + (\omega_2'\omega_1'' - \omega_1'\omega_2'')I_3(x,y)} \\
\frac{\partial u}{\partial y}(x,y) &= \frac{(\omega_3''\omega_1''' - \omega_1''\omega_3''')I_1(x,y) + (\omega_1'\omega_3''' - \omega_3'\omega_1''')I_2(x,y) + (\omega_3'\omega_1'' - \omega_1'\omega_3'')I_3(x,y)}{(\omega_2''\omega_1''' - \omega_1''\omega_2''')I_1(x,y) + (\omega_1'\omega_2''' - \omega_2'\omega_1''')I_2(x,y) + (\omega_2'\omega_1'' - \omega_1'\omega_2'')I_3(x,y)}
\end{aligned} \tag{4.12}$$

4.1.3 Approximation of the boundary condition

After the calculus of the gradient for all the points of $\partial\Omega_d$, we can approximate the value of u based on the shape of the image domain. In this case the procedure we have followed, especially for the numerical tests, is been the same of the Chapter (3).

4.2 Reduction of the number of the images

Supposing that we are able to determine univocally the surface $u(x, y)$ of the SfS-PS problem using three images obtained with three non coplanar light sources, we want to consider some classes of particular functions for which it is possible to resolve the SfS-PS problem using less than three images.

4.2.1 Symmetric surfaces

We will prove a theorem that gives us the possibility to produce an image (of a particular surface) by using another image of the same surface, obtained from a light source happily chosen. Let us start to define the type of surface we can use in order to apply that.

Definition 4.4 *Let $z = u(x, y)$ be a function defined in $\Omega \subset \mathbb{R}^2$. Let π_s (symmetry plane) be a plane passing through the z axis and let r_s (symmetry straight line) be its intersection with the xy plane. We say that u is symmetric with respect to the plane π_s if, for every point $(x_0, y_0) \in \Omega$, it results:*

$$u(x_0, y_0) = u(x_1, y_1) \tag{4.13}$$

where $(x_1, y_1) \in \Omega$ is the symmetric point of (x_0, y_0) with respect to the straight line r_s (Fig. 4.1).

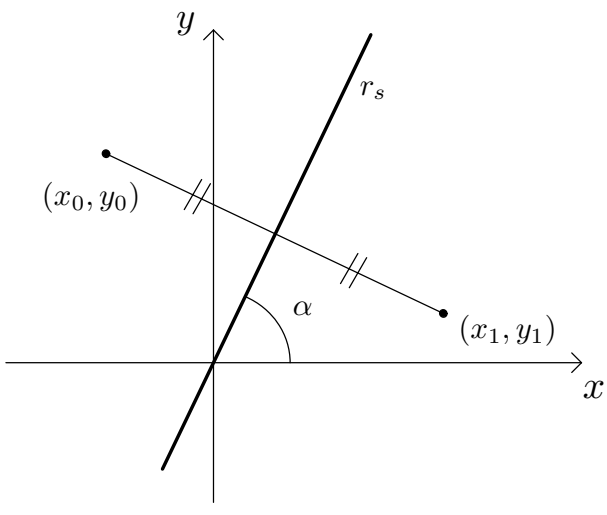

Figure 4.1. Orthogonal view of the plane (x, y): example of a positioning of the points (x_0, y_0) and (x_1, y_1) related to the symmetry straight line r_s.

With regard to the orthographic SfS problem, since the model has not a direct dependence on the value of the function u in a point, but only on its gradient, it

is indispensable to determine a symmetry relation with respect to the derivative for the point of the domain. We identify r_s like a particular straight line passing through the origin of the reference system xyz, that is

$$x \sin\alpha = y \cos\alpha, \text{ with } \alpha \in [0, \pi]. \tag{4.14}$$

We consider this straight line like a subspace generated by the vector $(\cos\alpha, \sin\alpha)$. It is possible to identify the perpendicular straight line to r_s from its base vector. Then, let

$$v = (\cos(\alpha + \frac{\pi}{2}), \sin(\alpha + \frac{\pi}{2})) = (-\sin\alpha, \cos\alpha) \tag{4.15}$$

be this perpendicular straight line. The main relation about the symmetry that we use in the SfS model is the following:

$$v \cdot \nabla u(x_0, y_0) = -v \cdot \nabla u(x_1, y_1) \tag{4.16}$$

4.2.2 Uniqueness theorem for the symmetric surfaces

We aim at obtaining further information relative to the symmetric surfaces by deducing the greyscale values of an image got from a particular light source whose position depends on the symmetry straight line r_s. These information, together with a third image, permit us to resolve the SfS-PS problem using three images linearly independent.

Theorem 4.5 *Let $u(x, y)$ be a symmetric surface with respect to any straight line. We suppose that the orthogonal projection of the camera point of view is a point belong to a considered straight line.*

Let $\omega' = (\widetilde{\omega}', \omega_3')$ and $\omega'' = (\widetilde{\omega}'', \omega_3'')$ be two light vectors such that:

1. *$\widetilde{\omega}'$ is perpendicular with respect to the symmetry straight line r_s;*
2. *$\widetilde{\omega}'' = -\widetilde{\omega}'$ (that is $\omega'' = (-\widetilde{\omega}', \omega_3')$ since the light vectors are constrained to be taken in the upper semi sphere)*

Then:

$$I_2(x_0, y_0) = I_1(x_1, y_1) \tag{4.17}$$

Proof:
Considering the image definition of the SfS problem, we have:

$$\begin{aligned} I_2(x_0, y_0) = \frac{-\widetilde{\omega}'' \cdot \nabla u(x_0, y_0) + \omega_3''}{\sqrt{1 + ||\nabla u(x_0, y_0)||^2}} =^{**} \frac{\widetilde{\omega}' \cdot \nabla u(x_0, y_0) + \omega_3'}{\sqrt{1 + ||\nabla u(x_0, y_0)||^2}} =^{*} \\ = \frac{-\widetilde{\omega}' \cdot \nabla u(x_1, y_1) + \omega_3'}{\sqrt{1 + ||\nabla u(x_0, y_0)||^2}} = \frac{-\widetilde{\omega}' \cdot \nabla u(x_1, y_1) + \omega_3'}{\sqrt{1 + ||\nabla u(x_1, y_1)||^2}} = I_1(x_1, y_1) \end{aligned} \tag{4.18}$$

where in ** we use the hypothesis *2*, whereas in * as the surface is symmetric, we consider furthermore that the normal vector in the point (x_0, y_0) has the same norm as in (x_1, y_1).

□

Once we choose $(x_0, y_0) \in \Omega$, the problem consists in determining the coordinates of the symmetric point (x_1, y_1) with respect to r_s. This point (x_1, y_1) belongs to the straight line $r_s^{\perp}$, perpendicular to r_s and passing through the point (x_0, y_0), whose equation is

$$(x - x_0)\cos\alpha = -(y - y_0)\sin\alpha. \tag{4.19}$$

Finally, observing that the symmetric straight line r_s passes through the origin, it results necessarily that the distances with respect to $(0, 0)$ of both points are the same. That is, both points belong to the same circumference centered in the origin of the axis. This formulation of the problem permits that the following non linear system

$$\begin{cases} (x - x_0)\cos\alpha = -(y - y_0)\sin\alpha \\ x^2 + y^2 = x_0^2 + y_0^2 \end{cases} \tag{4.20}$$

admits only two solutions, that is (x_0, y_0) and (x_1, y_1).

The procedure we use to solve the system (4.20) is relative to an algorithm that takes into account the numerical instability. To this purpose, some particularities appear.

A first difference in the calculus of the solutions of (4.20) is related to the angle α. In order to avoid numerical instability, we consider two possible sets to which this angle could belong:

$$A = \left[0, \frac{\pi}{4}\right] \cup \left[\frac{3\pi}{4}, \pi\right] \text{ and } B = \left(\frac{\pi}{4}, \frac{3\pi}{4}\right) \tag{4.21}$$

Let us suppose that $\alpha \in A$; we use the first equation of (4.20), and we write the first coordinate of the point (since the division by $\cos\alpha$ does not involve numerical instability). We have then:

$$x = (y_0 - y)\frac{\sin\alpha}{\cos\alpha} + x_0$$

which, replaced in the second equation of (4.20), gives a second order equation (in the general case written as $ay^2 + by + c = 0$) where the coefficients are:

$$\begin{aligned} a &= 1 + (\tan\alpha)^2 \\ b &= -2(y_0(\tan\alpha)^2 + x_0\tan\alpha) \\ c &= y_0^2(\tan\alpha)^2 + 2y_0x_0\tan\alpha - y_0^2. \end{aligned} \tag{4.22}$$

The two solutions of this equation are y_0 and y_1. It is possible to determine the exact solution since y_0 is known.

In the same way, if $\alpha \in B$ it is possible to divide by $\sin\alpha$. We write then the second coordinate of the point:

$$y = (x_0 - x)\frac{\cos\alpha}{\sin\alpha} + y_0$$

and, by substitution, we solve the second order equation in the x variable with the following coefficients:

$$\begin{aligned} a &= 1 + (\cot\alpha)^2 \\ b &= -2(x_0(\cot\alpha)^2 + y_0\cot\alpha) \\ c &= x_0^2(\cot\alpha)^2 + 2x_0y_0\cot\alpha - x_0^2. \end{aligned} \tag{4.23}$$

The choice of the right solution can be done exactly like explained before, that is excluding the value x_0 already known.

In the end, if we consider an image I_1 obtained with a light that respects the hypotheses of the theorem (4.5), it is possible to deduce another image I_2 in the way we explained before.

Corollary 4.6 *Let $u(x,y)$ be a symmetric surface with respect to a straight line passing through the orthogonal projection of the view point of the SfS model. Let*

1. *I_1 be an image obtained with a light vector $\omega' = (\widetilde{\omega}', \omega'_3)$ such that $\widetilde{\omega}'$ is perpendicular to the symmetry straight line of $u(x,y)$,*
2. *I_3 be an image obtained with a light source $\omega''' = (\widetilde{\omega}''', \omega'''_3)$ such that $\widetilde{\omega}' \cdot \widetilde{\omega}''' \neq \pm||\widetilde{\omega}'||||\widetilde{\omega}'''||$ (that is $\widetilde{\omega}'$ and $\widetilde{\omega}'''$ have not the same direction).*

Than it is possible to univocally determine the surface $u(x,y)$ using the SfS-PS model.

The use of the image I_2 defined in the theorem (4.5) is necessary to the application of the reconstruction technique using three images obtained with non coplanar light vectors.

Other simplifications in the calculus of the point (x_1, y_1) are possible when the surface $u(x,y)$ has a particular kind of symmetry. As a first particular case we consider now a symmetry relative to the orthogonal straight line. Let r'_s and r''_s be two symmetry straight lines of u orthogonal between them. Thus we have the relation

$$\nabla u(x_0, y_0) = -\nabla u(-x_0, -y_0) \tag{4.24}$$

for which we note the facility of calculus in the point previously called $(x_1, y_1) = (-x_0, -y_0)$.

Remark 4.7 *As the link between the points (x,y) and $(-x-y)$ is relative to a rotation of π radiant, i.e.:*

$$\begin{pmatrix} \cos(\pi) & -\sin(\pi) \\ \sin(\pi) & \cos(\pi) \end{pmatrix} \begin{pmatrix} x \\ y \end{pmatrix} = \begin{pmatrix} -x \\ -y \end{pmatrix} \tag{4.25}$$

the image I_2 results to be a rotation of π radiants of I_1.

A very interesting particular case is related to the surfaces with four symmetry straight lines. In relation to these surfaces, in fact, it is possible to solve the classical SfS problem considering only one image generated from any light source. For this case the constraint concerning the light sources direction vanishes. As before, we follow the procedure of reconstructing the missing information (that is the three linear independent images). In this case, because of the particular surface geometry, we are able to obtain the necessary three images only from one. That is we can reconstruct the two missing images (generated with non coplanar light vectors) starting from only one image of the surface lighted up by any light source.

Let us consider the image I_1 and let ω' be its relative light source. The other two images can be calculated in the following way:

$$\begin{aligned} I_2(x,y) &= I_1(-x,-y) \text{ with } \omega'' = (-\widetilde{\omega}', \omega'_3) \\ I_3(x,y) &= I_1(-y,x) \text{ with } \omega''' = (\omega'_2, -\omega'_1, \omega'_3) \end{aligned} \tag{4.26}$$

Relative to the third image, we use $(v_1, v_2) \cdot \nabla u(x, y) = -(v_2, -v_1) \cdot \nabla u(-y, x)$, where (v_1, v_2) is any vector of the plane (x, y). The choice of the light placing, together with the way to determine the images, is not unique. The aim of this construction is to obtain linearly independent reconstructed images for which the uniqueness of solution for the SfS problem stands.

Theorem 4.8 *Let $I(x, y)$ be an image of the surface $u(x, y) \in W^{1,\infty}(\overline{\Omega})$, with four straight lines of symmetry obtained by the SfS model such that $0 < I(x, y) \leq 1$ $\forall (x, y) \in \overline{\Omega}$ with the light source ω. Then it is possible to determine this surface univocally solving the SfS classic problem.*

The procedure followed until now is a constructive prove of the previous theorem and permits to solve, for a particular class of surfaces, the classical SfS problem passing through the SfS-PS one. Furthermore, our analysis of the problem permits us to give also a numerical method for the approximation of this unique weak solution.

Remark 4.9 *Following this procedure it is possible to prove the uniqueness of a weak solution of the classic SfS problem also if the surface is radial.*

4.3 Applications: linear dependent image reconstruction

An interesting application regarding the orthographic SfS model is related to the possibility of generating the images of an object making vary the light source between two points ω' and ω'' for which we already have the relative images. That is, supposing we have two images I_1 and I_2 obtained with two light sources ω' and ω'' respectively, it is possible to deduce all the linearly dependent images. In the geometrical sense, if we consider these two light vectors like points of the upper hemi-sphere $B((0, 0, 0), 1)$, then it is possible to calculate all the images obtainable with a light source in the geodesic identified by ω' and ω''.

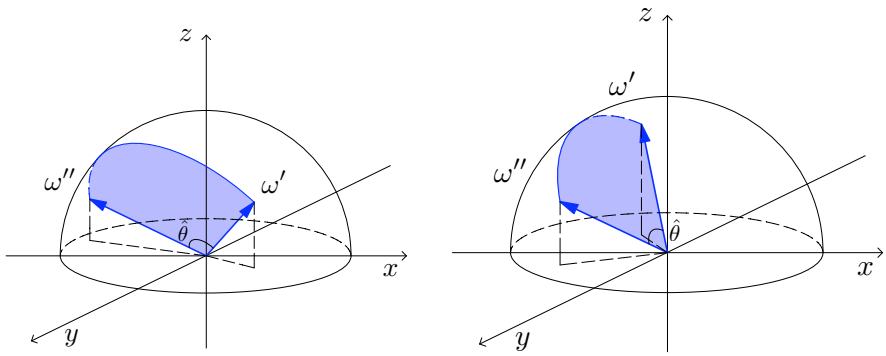

Figure 4.2. Examples of geodesics (in blue) on the unitary sphere between ω' and ω''

The main idea is the same of the previous chapter related to the approximation of the points of a geodesic defined between the two light sources vector on the unitary sphere. We briefly repeat some passages only to make coherent the notation with the next step of the algorithm.

The method we use to calculate the vector defined from the geodesic is based on the Remark (4.2). In fact, once we fix the extremal points, the main idea is to discretize the geodesic through an affine application that permits us to see this curve as an arc of a circumference on the xy plane. Let us start by observing that the angle between the two unitary light vectors $\hat{\theta}$ is computable using the dot product between them. In fact:

$$\hat{\theta} = \arccos(\omega' \cdot \omega'') \tag{4.27}$$

Now, we determine the affine application repeating the same procedure as in the previous chapter. This function permits the use of one angular parameter for the discretization of all the curve. Let us define then the linear application T such that:

$$\begin{aligned} T(1,0,0)^T &= \omega' \\ T(\cos\hat{\theta}, \sin\hat{\theta}, 0)^T &= \omega'' \\ T(0,0,1)^T &= q. \end{aligned} \tag{4.28}$$

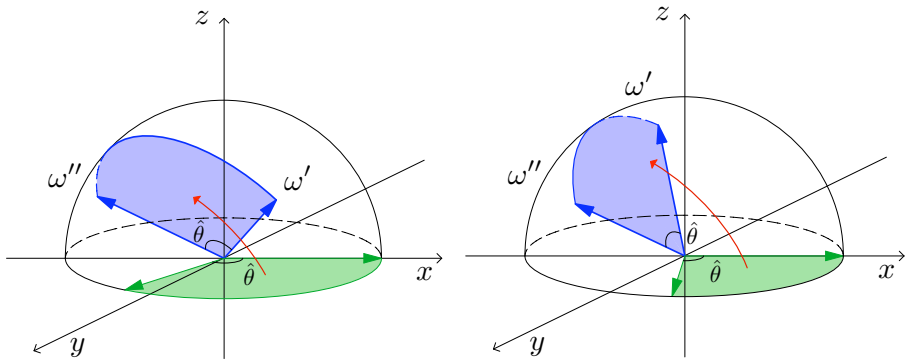

Figure 4.3. Examples of affine applications T between the area defined by the arc of the circumference (in green) and the one relative to the geodesic (in blue)

We note as q the unitary vector (opportunely oriented) orthogonal to the plane where lie the vectors ω' and ω'' (such that they are outgoing from the plane, i.e. $q_3 > 0$). We consider the plane generated by the vectors ω' and ω'' which has the following director parameters:

$$\begin{aligned} k &= \omega'_2\omega''_3 - \omega'_3\omega''_2 \\ l &= \omega'_3\omega''_1 - \omega'_1\omega''_3 \\ m &= \omega'_1\omega''_2 - \omega'_2\omega''_1 \end{aligned} \tag{4.29}$$

We consider the normalization of the vector (k, l, m) like a possible vector q depending on the sign of m. If $m < 0$ we take the opposite direction to the normalization.

Let us explicit the condition imposed by (4.28) by writing the coefficients of the matrix that represents the application:

$$T = \begin{pmatrix} \omega'_1 & \frac{\omega''_1 - \omega'_1\cos\hat{\theta}}{\sin\hat{\theta}} & q_1 \\ \omega'_2 & \frac{\omega''_2 - \omega'_2\cos\hat{\theta}}{\sin\hat{\theta}} & q_2 \\ \omega'_3 & \frac{\omega''_3 - \omega'_3\cos\hat{\theta}}{\sin\hat{\theta}} & q_3 \end{pmatrix} \tag{4.30}$$

If we consider an angle θ such that $0 < \theta < \hat{\theta}$, we obtain a third light $\bar{\omega}$ using just the previous application, that is:

$$T(\cos\theta, \sin\theta, 0)^T = \bar{\omega} \tag{4.31}$$

Now, we have built $\bar{\omega}$ coplanar to the previous two light vectors, then we have $\bar{\omega} = \alpha\omega' + \beta\omega''$. Next step is to determine the coefficients $\alpha, \beta \in \mathbb{R}$. We write the previous equality and we obtain:

$$\begin{cases} \bar{\omega}_1 = \alpha\omega'_1 + \beta\omega''_1 \\ \bar{\omega}_2 = \alpha\omega'_2 + \beta\omega''_2 \\ \bar{\omega}_3 = \alpha\omega'_3 + \beta\omega''_3 \end{cases} \tag{4.32}$$

With the aim to calculate the coefficients that determine the third light source, we solve the following linear system of two equations in two unknowns:

$$C \begin{pmatrix} \alpha \\ \beta \end{pmatrix} = b \tag{4.33}$$

The matrix C and the vector (α, β) vary depending on the first two light vectors $\omega' = (\cos(\theta_1)\sin(\varphi_1), \sin(\theta_1)\sin(\varphi_1), \cos(\varphi_1))$ and $\omega'' = (\cos(\theta_2)\sin(\varphi_2), \sin(\theta_2)\sin(\varphi_2), \cos(\varphi_2))$ (with $\theta_1, \theta_2 \in [0, 2\pi]$). In fact, if we consider the following set:

$$\bar{A} = \left[0, \frac{\pi}{4}\right] \cup \left[\frac{3\pi}{4}, \frac{5\pi}{4}\right] \cup \left[\frac{7\pi}{4}, 2\pi\right] \tag{4.34}$$

we take

$$\begin{pmatrix} \omega'_2 & \omega''_2 \\ \omega'_3 & \omega''_3 \end{pmatrix} \begin{pmatrix} \alpha \\ \beta \end{pmatrix} = \begin{pmatrix} \bar{\omega}_2 \\ \bar{\omega}_3 \end{pmatrix} \quad \text{if} \quad \theta_1, \theta_2 \in \bar{A} \tag{4.35}$$

while

$$\begin{pmatrix} \omega'_1 & \omega''_1 \\ \omega'_3 & \omega''_3 \end{pmatrix} \begin{pmatrix} \alpha \\ \beta \end{pmatrix} = \begin{pmatrix} \bar{\omega}_1 \\ \bar{\omega}_3 \end{pmatrix} \quad \text{otherwise.} \tag{4.36}$$

Once we determine the coefficient α, β, we can compute the linear dependent image as follows:

$$\bar{I} = \alpha I_1 + \beta I_2 \tag{4.37}$$

4.4 Numerical Tests

In this section we present the numerical tests that explain, as well as the theoretical part relatives to the Chapter (4), also the one relative to the Chapter (2). Indeed the semi- lagrangian (SL) schemes used for the approximation on the next surfaces is the same introduced previously.

4.4.1 Synthetic surfaces (3,2,1 image/s)

Let us start the numerical tests studying several surfaces. Every single one is of a typology that permits us to apply each variant of the previuos results explained.

We consider also surfaces with symmetric characteristics that permit to study all the different way to approximate and deduce the others images in all the previous

Figure 4.4. Set of surfaces used for the numerical tests

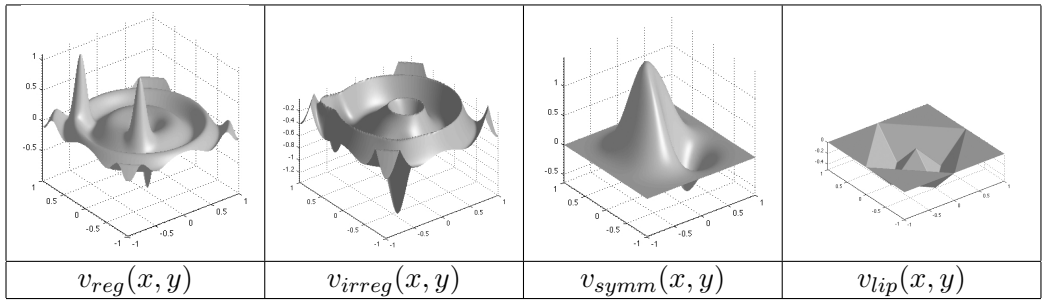

$v_{reg}(x,y)$	$v_{irreg}(x,y)$	$v_{symm}(x,y)$	$v_{lip}(x,y)$

cases explained before. These surfaces have symmetries that permits us to apply all the previous techniques that solve the SfS-PS problem.

The different typologies of the four surfaces represented in Fig. 4.4 is such that their geometrical characteristics differentiate the number of necessary images for their tridimensional reconstruction, in fact:

- $v_{reg}(x,y)$ is a non symmetric surface. For its tridimensional reconstruction, then, we need of three its linear independents images;
- $v_{irreg}(x,y)$ is still a non symmetric surface, but it is also non smooth. In fact it is the weakest case we present like test;
- $v_{simm}(x,y)$ is a surface with a symmetry axes (the straight line $y+x=0$) for which we need of two images;
- $v_{lip}(x,y)$ instead is a surface used (in a very similar vesion) also in the previous numerical test. It has four axis of symmetry (that is $y=\pm x$, $y=0$, $x=0$). For its reconstruction we need of only one image. We note that it is also a Lipschitz surface.

For these starting data, summarized in Fig. 4.5 we made different tests modifying the size of the grid Δ, uniform for all the domain Ω. About the discretization step h of the directional derivative we have taken it equal to Δ for every test in order to reach the best consistence order.

All the numerical tests have been made using a computer with Intel Core 2 Duo processor of 2.13 GHz and 2GB of RAM.

The numerical approximation was carried out with both the semi-Lagrangian schemes, forward (SL-F) and backward (SL-B), and the implicit finite difference scheme (IFD U^5). We calculated the errors in $L^\infty(\Omega_d)$ norm by varying the uniform discretization step following the same procedure of the previous numerical tests. The results relative to v_{reg} are presented in Tab. 4.1. Here and in the almost all the previous tables (relative to the other surfaces) is possible to see the order estimation approximatively close to one. We have used the same angles for v_{irreg} (see Tab. 4.2) for compare the difference with v_{reg} when the size of the grid decreases. We note that the irregularity of the surface appears in the different approximation order. In fact, the one of v_{irreg} is much more far from one than the order relative to v_{reg} and the difference becomes bigger when Δ decreases.

In Tab. 4.3 and Tab. 4.4 we have tested the same surface v_{sym} using two different dispositions of light sources in order to show that there is no difference (in

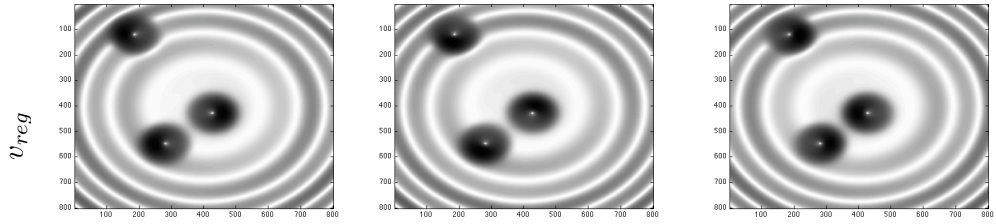

$\omega' : \varphi_1 = 0.1, \theta_1 = 0 \to (I_1)$ $\omega'' : \varphi_2 = 0.1, \theta_2 = \frac{7}{18}\pi \to (I_2)$ $\omega''' : \varphi_3 = 0.1, \theta_3 = \pi \to (I_3)$

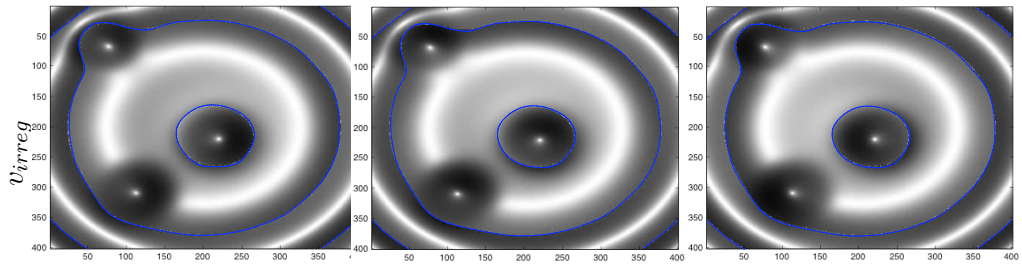

$\omega' : \varphi_1 = 0.1, \theta_1 = 0 \to (I_1)$ $\omega'' : \varphi_2 = 0.1, \theta_2 = \frac{7}{18}\pi \to (I_2)$ $\omega''' : \varphi_3 = 0.1, \theta_3 = \pi \to (I_3)$

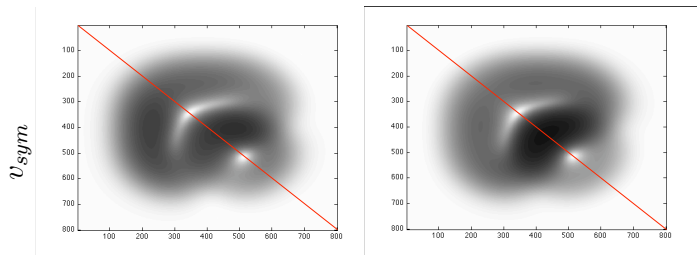

$\omega' : \varphi_1 = 0.1, \theta_1 = \frac{\pi}{4} \to (I_1)$ $\omega'' : \varphi_2 = 0.1, \theta_2 = \frac{3}{4}\pi \to (I_2)$

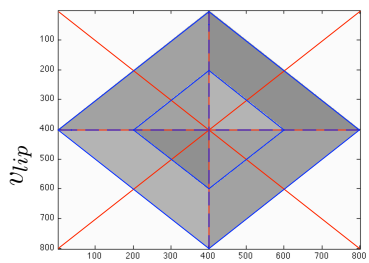

$\omega' : \varphi_1 = 0.1, \theta_1 = \frac{\pi}{4} \to (I_1)$

Figure 4.5. Set of images used with the respective light sources described by their spherical coordinates. For each surface is possible to see the straight line of symmetry (in red) and the curve where the surface is not differentiable (in blue).

the error and in the order) using one of the two angles that give the perpendicularity with respect the symmetry straight line. In fact, in Tab. 4.3 we deduce the supplementary image starting from an angle $\theta_1 = \frac{\pi}{4}$ and in Tab. 4.4 from $\theta_1 = \frac{5}{4}\pi$ (both perpendicular to the straight line $y + x = 0$).

The computer used for computing the CPU time has an Intel Core 2 Duo processor of 2.66 GHz and 4GB of RAM. Relatively to this, the computing time for

Δ	SL-F error	SL-F order	SL-B error	SL-B order	IFD U^5 error
0.02	2.085×10^{-1}	0.8993	1.7434×10^{-1}	0.9762	3.6446×10^{-1}
0.01	1.1179×10^{-1}	0.9358	8.862×10^{-2}	0.9886	2.1028×10^{-1}
0.005	5.844×10^{-2}	0.9654	4.466×10^{-2}	0.9936	1.692×10^{-1}
0.0025	2.993×10^{-2}		2.243×10^{-2}		1.652×10^{-1}

Table 4.1. Error in $L^\infty(\Omega_d)$ norm and order of convergence relative to v_{reg} with angles: $\theta_1 = 0$, $\theta_2 = \frac{7}{18}\pi$ and $\theta_3 = \pi$; $\varphi_1 = \varphi_2 = \varphi_3 = 0.1$.

Δ	SL-F error	SL-F order	SL-B error	SL-B order
0.02	1.6475×10^{-1}	0.7091	1.8247×10^{-1}	1.0098
0.01	1.0078×10^{-1}	0.5543	9.062×10^{-2}	0.8870
0.005	6.863×10^{-2}	0.8582	4.900×10^{-2}	0.6973
0.0025	3.786×10^{-2}		3.022×10^{-2}	

Table 4.2. Error in $L^\infty(\Omega_d)$ norm and order of convergence relative to v_{irreg} with angles: $\theta_1 = 0$, $\theta_2 = \frac{7}{18}\pi$ and $\theta_3 = \pi$; $\varphi_1 = \varphi_2 = \varphi_3 = 0.1$.

Δ	SL-F error	SL-F order	SL-B error	SL-B order
0.02	5.254×10^{-2}	1.0050	6.856×10^{-2}	1
0.01	2.618×10^{-2}	1.0022	3.428×10^{-2}	1.0088
0.005	1.307×10^{-2}	1.3025	1.713×10^{-2}	0.9992
0.0025	5.299×10^{-3}		8.570×10^{-3}	

Table 4.3. Error in $L^\infty(\Omega_d)$ norm and order of convergence relative to v_{sym} with angles: $\theta_1 = \frac{\pi}{4}$ and $\theta_2 = \frac{3}{4}\pi$; $\varphi_1 = \varphi_2 = 0.1$.

Δ	SL-F error	SL-F order	SL-B error	SL-B order
0.02	1.600×10^{-4}	1	1.016×10^{-2}	0.9039
0.01	8.000×10^{-5}	1	5.430×10^{-3}	0.9351
0.005	4.000×10^{-5}	1	2.840×10^{-3}	0.8188
0.0025	2.000×10^{-5}		1.610×10^{-3}	

Table 4.4. Error in $L^\infty(\Omega_d)$ norm and order of convergence relative to v_{sym} with angles: $\theta_1 = \frac{5}{4}\pi$ and $\theta_2 = \frac{7}{4}\pi$; $\varphi_1 = \varphi_2 = 0.1$.

the tests of Tab. 4.5 goes from 0.86 seconds for the SL forward scheme and 0.832 seconds for the backward one with $\Delta = 0.02$ (that is with images of size 100×100 pixels). It arrives till 451.037 seconds (about 7 minutes and 30 seconds) for the SL forward scheme and 452.832 seconds (about 7 minutes and 32 seconds) for the backward one with the size grid of 0.0025 (i.e. using images of size 800×800). Instead, since the implicit finite difference scheme is a direct method, it needs at the maximum of only few tenths of a second. On the other side it is possible to note that in the cases of Tab. 4.2, 4.3 and 4.4 the direction of the vector field b does not permit the correct convergence of the scheme. In fact in these cases $b_2(x, y)$ (i.e. the

second component of b) that compares in the denominator of all the non-diagonal coefficients of the discretization matrix is very close to zero for all the points of the domain. Another particular case is the one of Tab. 4.1 where the convergence is not guaranteed always because of the "bad" disposition of the vector field b.

Δ	SL-F error	SL-F order	SL-B error	SL-B order	IFD U^5 error
0.02	2.731×10^{-2}	0.8975	2.731×10^{-2}	0.8975	1.327×10^{-2}
0.01	1.466×10^{-2}	0.8630	1.466×10^{-2}	0.8630	6.73×10^{-3}
0.005	8.060×10^{-3}	0.9165	8.060×10^{-3}	0.9165	3.35×10^{-3}
0.0025	4.270×10^{-3}		4.270×10^{-3}		1.68×10^{-3}

Table 4.5. Error in $L^\infty(\Omega_d)$ norm and order of convergence relative to v_{lip} with angles: $\theta_1 = \frac{\pi}{4}$ and $\varphi_1 = 0.1$.

From Tab. 4.5 and Tab. 4.6 is possible to note also that the way we use the images permits to obtain the same errors (for the SL forward and backward schemes). That is the images we generate are such that the integration of the differential problem (2.35) does not depends from the direction we want to use (i.e. if we want to start from Γ_{in} or from Γ_{out}).

A very interesting result is relative to the Tab. 4.6. In fact, we can see that the order is not close to one at all, but it is almost 0.5. This depends from the vector field $b(x, y)$, in fact from the Fig. 4.6 is possible to see that some curves where the surface is not differentiable coincide exactly with the projection of the characteristic.

Δ	SL-F error	SL-F order	SL-B error	SL-B order	IFD U^5 error
0.02	6.221×10^{-2}	0.5131	6.221×10^{-2}	0.5131	2.619×10^{-2}
0.01	4.359×10^{-2}	0.5067	4.359×10^{-2}	0.5067	1.316×10^{-2}
0.005	3.068×10^{-2}	0.5036	3.068×10^{-2}	0.5036	6.56×10^{-3}
0.0025	2.164×10^{-2}		2.164×10^{-2}		3.28×10^{-3}

Table 4.6. Error in $L^\infty(\Omega_d)$ norm and order of convergence relative to v_{lip} with angles: $\theta_1 = \pi$ and $\varphi_1 = 0.1$.

4.4.2 Real case (Beethoven 3 images)

In this section we want to solve the SfS-PS problem on real application using three linear independent images taken from the web. We apply it for the pictures of a Beethoven bust shown in Fig. 4.7. The size of the images is 77×210 pixels and this rectangular structure is due to the fact that the complete bust has not a simple structure of the boundary. As we will see in the next section (where the complete pictures are used) the boundary of the statue with respect the background is not rectangular. This does not permit us to approximate the boundary condition using the procedure explained in Section (4.1.3).

The spherical coordinates of the light sources used for these picture are, respectively:

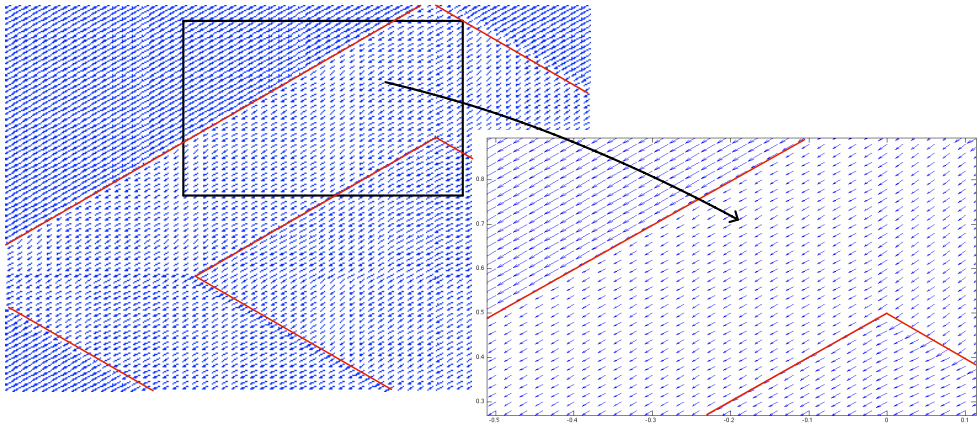

Figure 4.6. In these overlapping images are emphasize in red the point where the surface is note differentiable. We can also note that the the vector field $b(x, y)$ (in blue) has the same direction of one of these curves.

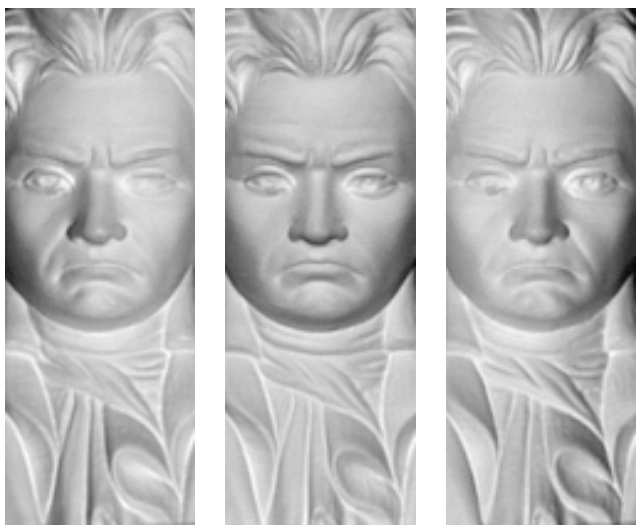

I_1^{real} I_2^{real} I_3^{real}

Figure 4.7. Beethoven bust: real images.

$$\varphi_1 = 0.263,\ \theta_1 = -0.305 \text{ for } I_1^{real};$$
$$\varphi_2 = 0.2,\ \theta_2 = 3.226 \text{ for } I_2^{real};$$
$$\varphi_3 = 0.281,\ \theta_3 = 3.502 \text{ for } I_3^{real}.$$

The reasons for which we use three pictures are essentially two. The first is that, as we can see from the pictures, the surface is not symmetric because of some details (like the hair and the foulard). The second problem is relative to the light sources direction. In fact, in order to apply the reduction of the images necessary to the reconstruction we need of a light source such that $\widetilde{\omega}$ is perpendicular to the symmetry straight line. This is the way, even if we cut the images around the face of Beethoven (that is around the part of the statue that seems to be symmetric with respect a vertical axes), we can not apply the reduction method.

The computing times relative to the SL forward and backward scheme have been, respectively, of 2.033 and 2.13 seconds. The surfaces approximated with both schemes are shown in Fig. 4.8.

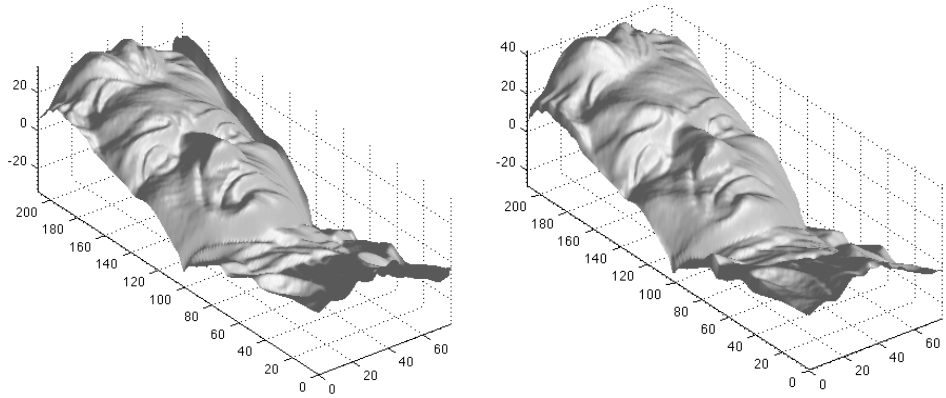

Figure 4.8. Approximated surface of the Beethoven bust using the SL forward scheme (on the left) and the SL backward scheme (on the right).

Observing the reconstructed surface we note, especially for the SL forward scheme, that the boundary condition is not respected very well on the right side. In fact the surface on that side does not match with the boundary value precalculated. This depends on the direction of the vector field $b(x, y)$ that determines the direction of the approximation of the surface. Indeed, the propagation of the information, oriented by $b(x, y)$, starts from the left side with respect to the SL forward arriving on the right side with a substantial accumulate error. Relatively to the SL backward scheme, even if the information propagation starts from right, the compensation of the errors during the iterations balances much more better the matching with the left boundary.

The noise and the approximation of the spherical coordinates of the light sources can be also seen like a loss of consistence of the boundary condition (see Section (2.2) of the second chapter). This means that the surfaces of Fig. 4.8 are different because they start with incongruous boundary conditions respect the grayscale value of the images altered by the noise and the rough spherical coordinates.

4.4.3 Linear Independent Images

The tests on the linear independent images concept were carried out both on synthetic and real surfaces.

For the synthetic case we consider like test surface the one in Fig. 4.9.

Like starting images we consider the first and the last one of the right column of Fig. 4.10. Once we choose the respective angle θ ($\theta_1 = 0$ and $\theta_2 = \pi$), we calculate the optimal angle φ (respectively $\varphi_1 = 0.26$ and $\varphi_2 = 0.19$) in order to have the biggest angle $\hat{\theta}$ (4.27) avoiding the black shadows. In Fig. 4.10 are represented the three intermediate images obtained with three light vectors coplanar to the first two ω' e ω''.

For the real case, we focus our attention on the first and last image of the left column of Fig. 4.10 already used in the previous section (namely I_1^{real} and I_3^{real}).

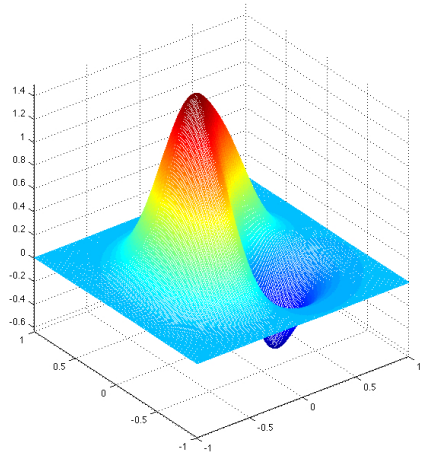

Figure 4.9. Test surface for the calculus of the linear independent in the synthetic case.

In Fig. 4.10 the three intermediate images are obtained from our method as linear combinations of the given ones (pictures 1 and 5).

$\omega'_{real} : \varphi_1 = 0.263, \theta_1 = -0.305 \rightarrow (I_1^{real})$

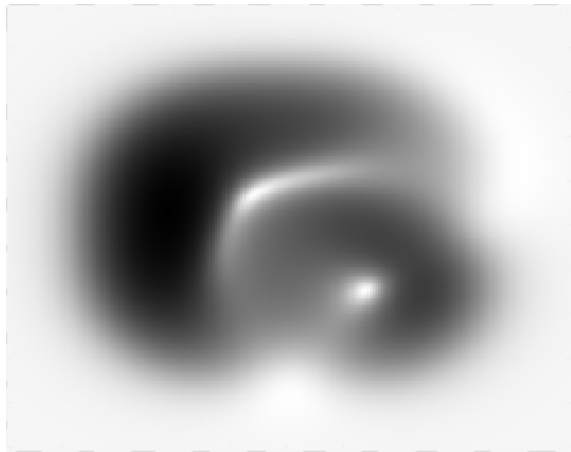

$\omega' : \varphi_1 = 0.26, \theta_1 = 0.0 \rightarrow (I_1)$

$\omega'''_{real} : \varphi_3 = 0.281, \theta_3 = 3.502 \rightarrow (I_3^{real})$

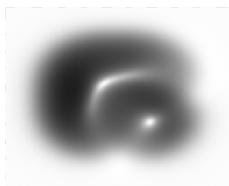

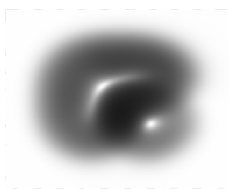

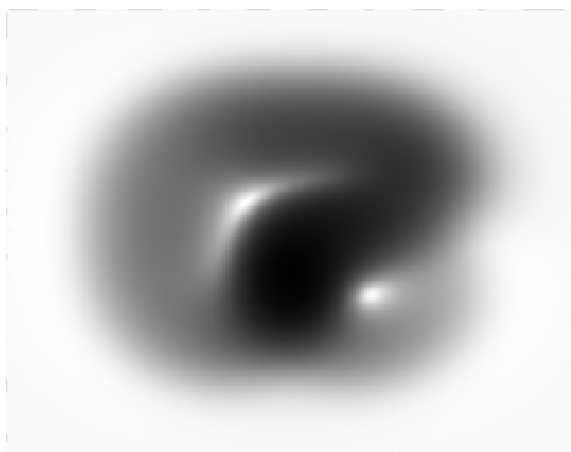

$\omega'' : \varphi_2 = 0.19, \theta_3 = \pi \rightarrow (I_2)$

Figure 4.10. Results of the simulation of linear dependent images.

List of publications

[1] S. Larnier, R. Mecca, *Fractional-Order Anisotropic Diffusion for Image Reconstruction*, in preparation.

Abstract:

The paper presents new applications of fractional partial differential equations in the image processing field, particularly in the inpainting problem. The algorithm presented in this work combines two previous notions: the fractional derivative implementation from [93] and the edge detection by topological gradient from [94]. The purpose of the paper is to extend some existing results in denoising problem with fractional order anisotropic diffusion equations and presents new results in inpainting, coupled or not with denoising. The results emphasize the importance of particular fractional-orders.

[2] R. Mecca, *Shape from Shading Using Photometric Stereo Techniques*, Proceedings of IEEE International Conference on Image Processing (ICIP), 2011.

[3] R. Mecca and J. D. Durou, *Unambiguous Photometric Stereo Using Two Images*, Proceedings of the International Conference on Image Analysis and Processing (ICIAP), 2011.

[4] R. Mecca and S. Tozza, *Uniqueness of symmetric solutions for the orthographic Shape from Shading via Photometric Stereo*, Proceedings of the conference Innovations for Shape Analysis: Models and Algorithms, 2011.

[5] R. Mecca and J. D. Durou, *Unambiguous Photometric Stereo using two Images*, in preparation;

[6] R. Mecca and M. Falcone, *Photometric Shape from Shading a new analytic and numerical approach*, in preparation;

Bibliography

[1] B. K. P. Horn and M. J. Brooks, *Shape from Shading*, The MIT Press, 1989.

[2] J.D. Durou, M. Falcone, and M. Sagona, "Numerical methods for shape from shading: a new survey with benchmarks computer vision and image understanding," *Elsevier*, vol. 109, no. 1, pp. 22–43, 2008.

[3] B. K. P. Horn, "Obtaining shape from shading information," *The Psychology of Computer Vision, Winston, P. H. (Ed.)*, pp. 115–155, 1975.

[4] J. Van Diggelen, "A photometric investigation of the slopes and heights of the ranges of hills in the maria of the moon.," *Bulletin of the Astronomical Institute of the Netherlands*, vol. 11, no. 423, pp. 283–290, 1951.

[5] B. W. Hapke, "A theoretical photometric function for the lunar surface," *Journal of Geophysical Research*, vol. 68, no. 15, pp. 4571–4586, 1963.

[6] T. Rindfleisch, "Photometric method for lunar topography," *Photometric Engineering*, vol. 32, no. 2, pp. 262–277, 1966.

[7] B. K. P. Horn, *Shape from Shading: a Method for Obtaining the Shape of a Smooth Opaque Object from One View.*, Ph.D. thesis, Department of Electrical Engieerining and Computer Science, Massachusetts Institute of Technology, 1970.

[8] E. Rouy, *Approximation numérique des solutions de viscosité des équatios d'Hamilton-Jacobi et example*, Ph.D. thesis, Univeristé Paris IX Dauphine, Paris, France, 1988.

[9] P. L. Lions, E. Rouy, and A. Tourin, "Shape-from-shading, viscosity solutions and edges," *Numerische Mathematik*, vol. 64, no. 3, pp. 323–353, 1993.

[10] A. Chambolle, "A uniqueness result in the theory of stereo vision: coupling shape from shading and binocular information allows unambiguous depth reconstruction," *Annales de l'Institute Henri Poincaré*, vol. 11, no. 1, pp. 1–16, 1994.

[11] R. Kozera, "Existence and uniqueness in photometric stereo," *Applied Mathematics and Computation*, vol. 44, no. 1, pp. 103, 1991.

[12] R. J. Woodham, "Photometric method for determining surface orientation from multiple images," *Optical Engineering*, vol. 19, no. 1, pp. 134–144, 1980.

[13] B. K. P. Horn, "Height and gradient from shading," *The International Journal of Computer Vision, Winston*, vol. 5, pp. 37–75, 1990.

[14] K. Ikeuchi and B. K. P. Horn, "Numeical shape from shading and occluding boundaries," *Artificial Intelligence Journal*, vol. 17, pp. 181–184, 1981.

[15] A. R. Bruss, "The eikonal equation: Some results appliable to computer vision," *Journal of Mathematical Physics*, vol. 23, no. 5, pp. 890–896, 1982.

[16] M. J. Brooks, W. Chojnacki, and R. Kozera, "Shading without shape," *Quarterly of Applied Mathematics*, vol. L, no. 1, pp. 27–38, 1992.

[17] B. K. P. Horn, R. S. Szeliski, and A. L. Yuille, "Impossible shaded images," *IEEE Transactions on Pattern Analysis and Machine Intelligence*, vol. 15, no. 2, pp. 166–169, 1993.

[18] J. D. Durou and H. Maitre, "On convergence in the methods of strat and smith for shape from shading," *The International Journal of Computer Vision*, vol. 17, no. 3, pp. 273–289, 1996.

[19] J. D. Durou and D. Piau, "Ambiguous shape from shading with critical points," *Journal of Mathematical Imaging and Vision*, vol. 12, pp. 99–108, 2000.

[20] P. Dupuis and J. Oliensis, "An optimal control formulation and related numerical methods for a problem in shape reconstruction," *The Annals of Applied Probability*, vol. 4, no. 2, pp. 287–346, 1994.

[21] E. Rouy and A. Tourin, "A viscosity solutions approach to shape-from-shading," *SIAM Journal of Numerical Analysis*, vol. 29, no. 3, pp. 867–884, 1992.

[22] W. Chojnacki, M. J. Brooks, and D. Gibbins, "Pentland's estimator of light source direction," *Journal of Optical Society of America - Part A: Optics, ImageScience, and Vision*, vol. 11, no. 1, pp. 118–124, 1994.

[23] M. S. Drew, "Direct solution of orientation-form-color problem using a modification of pentland's light source direction estimator," *Computer Vision and Image Understanding*, vol. 64, no. 2, pp. 286–299, 1996.

[24] P. N. Belhumer, D. J. Kriegman, and A. L. Yuille, "The bas-relief ambiguity," *International Journal of Computer Vision*, vol. 35, no. 1, pp. 33–44, 1999.

[25] M. Oren and S. K. Nayar, "Generalization of the lambertian model and implications for machine vision," *International Journal of Computer Vision*, vol. 14, no. 3, pp. 227–251, 1995.

[26] S. M. Bakshi and Y. H. Yang, "Shape from shading for non-lambertian surfaces," *IEEE International Conference on Image Processing*, vol. II, 1994.

[27] K. M. Lee and C. C. J. Kuo, "Shape from shading with a generalized reflectance map model," *Computer Vision and Image Understanding*, vol. 67, no. 2, pp. 143–160, 1997.

[28] H. Ragheb and E. R. Hancock, "A probabilistic framework for specular shape-from-shading," *Pattern Recognition*, vol. 36, no. 2, pp. 407–427, 2003.

[29] A. J. Stewart and M. S. Langer, "Toward accurate recovery of shape from shading under diffuse lighting," *IEEE Transactions on Pattern Analysis and Machine Intelligence*, vol. 19, no. 9, pp. 1020–1025, 1997.

[30] Y. Wang and D. Samaras, "Estimation of multiple illuminants from a single image of arbitrary known geometry," vol. III, 2002.

[31] S. K. Nayar, K. Ikeuchi, and T. Kanade, "Shape from interreflections," *International Journal of Computer Vision*, vol. 6, no. 3, pp. 173–195, 1991.

[32] D. A. Forsyth and A. Zisserman, "Reflaction on shading," *IEEE Transactions on Pattern Analysis and Machine Intelligence*, vol. 13, no. 7, pp. 671–679, 1991.

[33] M. A. Penna, "A shape from shading analysis for a single perspective image of a polyhedron," *IEEE Transactions on Pattern Analysis and Machine Intelligence*, vol. 11, no. 6, pp. 545–554, 1989.

[34] K. M. Lee and C. C. J. Kuo, "Shape from shading with perspective projection, computer vision, grapichs, and image processing," *Image Understanding*, vol. 59, no. 2, pp. 202–212, 1994.

[35] J. k. Hasegawa and C. L. Tozzi, "Shape from shading with perspective projection and camera calibration," *Computers and Graphics*, vol. 20, no. 3, pp. 351–364, 1996.

[36] T. Okatani and K. Deguchi, "Shape reconstruction from an endoscope image by shape from shading technique for a point light source at the projection center," *Computer Vision and Image Understanding*, vol. 66, no. 2, pp. 119–131, 1997.

[37] D. Samaras and D. N. Metaxas, "Coupled lightining direction and shape estimation from single images," *IEEE International Conference on Computer Vision*, vol. II, pp. 868–874, 1999.

[38] M. G. Crandall, "Viscosity solutions of hamilton-jacobi equations. in nonlinear problems: Present and future," vol. 61, pp. 117–125, 1982.

[39] M. G. Crandall, H. Ishii, and P.L. Lions, "User's guide to viscosity solutions of second order partial differential equations," *Bulletin of the American Society*, vol. 27, pp. 1–67, 1992.

[40] M. G. Crandall and P. L. Lions, "Viscosity solutions of hamilton-jacobi equations," *Transaction of American Mathematical Society*, vol. 277, pp. 1–13, 1983.

[41] P. L. Lions, "Generalized solutions of hamilton-jacobi equations," *Number 69 in Research Notes in Mathematics*, 1982.

[42] M. Bardi and I. Capuzzo Dolcetta, *Optimal control and viscosity solutions of Hamilton-Jacobi-Bellman equations*, Birkhäuser, 1997.

[43] G. Barles, *Solutions de Viscosité des Equations de Hamilton-Jacobi*, Springer-Verlag, 1994.

[44] A. Ishii, "A simple, direct proof of uniqueness for solutions of the hamilton-jacobi equations of eikonal type," *Proceedings of the American Mathematical Society*, pp. 247–251, 1987.

[45] E. Prados, O. Faugeras, and E. Rouy, "Shape from shading and viscosity solutions," *Rapport de Recherche INRIA*, , no. 4638, 2002.

[46] J. Oliensis and P. Dupuis, "A global algorithm for shape from shading," pp. 692–701, 1993.

[47] H. Ishii and M. Ramaswamy, "Uniqueness results for a class of hamilton-jacobi equations with singular coefficients," *Communications in Partial Differential Equations*, vol. 20, pp. 2187–2213, 1995.

[48] F. Camilli and M. Falcone, "An approximation scheme for the maximal solution of the shape-from-shading model," pp. 49–52, 1996.

[49] F. Camilli and A. Siconolfi, "Maximal subsolutions of a class of degenerate hamilton-jacobi problems," *Indiana University Mathematics Journal*, vol. 48, no. 3, pp. 1111–1131, 1999.

[50] M. Falcone and M. Sagona, "An algorithm for the global solutions of the shape-from-shading model," vol. I, 1997.

[51] M. Sagona, *Numerical methods for degenerate Eikonal type equations and applications*, Ph.D. thesis, Dipartimento di Matematica dell'Università di Napoli "Federico II", 2001.

[52] J. Kain and D. N. Ostrov, "Numerical shape-from-shading for discontinuous photographic images," *International Journal of Computer Vision*, vol. 44, no. 3, pp. 163–173, 2001.

[53] E. Prados and O. Faugeras, "A mathematical and algorithmic study of the lambertian sfs problem for orthographic and pinhole cameras," Tech. Rep., Institut National de Recherche an Informatique et an Automatique, 2003.

[54] J. Oliensis, "Uniqueness in shape from shading," *International Journal of Computer Vision*, vol. 6, no. 2, pp. 75–104, 1991.

[55] J. Oliensis, "Shape from shading as a partially well-constrained problem," *Computer Vision, Graphic, and Image Processing: Image Understanding*, vol. 54, no. 2, pp. 163–183, 1991.

[56] M. J. Brooks, W. Chojnacki, and R. Kozera, "Impossible and ambiguous shading patterns," *International Journal of Computer Vision*, vol. 7, no. 2, pp. 119–126, 1992.

[57] R. Kozera, "Uniqueness in shape from shading revisited," *Journal of Mathematical Imaging and Vision*, vol. 7, no. 2, pp. 123–128, 1997.

[58] L. C. Evans, *Partial differential equations*, American Mathematical Society, 2004.

[59] A. M. Bruckstein, "On shape from shading," *Computer Vision, Graphic, and Image Processing*, vol. 44, no. 2, pp. 139–154, 1988.

[60] A. M. Bruckstein and R. Kimmel, "Global shape from shading," *Computer Vision and Image Understanding*, vol. 62, no. 3, pp. 360–369, 1995.

[61] A. M. Bruckstein and R. Kimmel, "Tracking level sets by level sets: A method for solving the shape from shading problem," *Computer Vision and Image Understanding*, vol. 62, no. 1, pp. 47–58, 1995.

[62] E. Prados, F. Camilli, and O. Faugeras, "A viscosity solution method for shape-from-shading without image boundary data," *ESAIM: Mathematical Modelling and Numerical Analysis*, vol. 40, no. 2, pp. 393–412, 2006.

[63] B. K. P. Horn and M. J. Brooks, "The variational approach to shape from shading," *Computer Vision, Graphic, and Image Processing*, vol. 33, no. 2, pp. 174–208, 1986.

[64] Y. G. Leclerc and A. F. Bobick, "The direct computation of height from shading," *IEEE International Conference on Computer Vision and Pattern*, pp. 552–558, 1991.

[65] P. Daniel and J. D. Durou, "From deterministic to stochastic methods for shape from shading," *4th Asian Conference on Computer Vision*, pp. 187–192, 2000.

[66] T. M. Strat, "A numerical method for shape-from-shading from a single image," M.S. thesis, Department of Electrical Engineering and Computer Science, 1979.

[67] R. T. Frankot and Chellappa, "A method for enforcing integrability in shape from shading algorithms," *IEEE Transactions on Pattern Analysis and Machine Intelligence*, vol. 10, no. 4, pp. 439–451, 1988.

[68] R. S. Szeliski, "Fast shape from shading," *Computer Vision, Graphic, and Image Processing: Image Understanding*, vol. 53, no. 2, pp. 129–153, 1991.

[69] D. Lee, "A provably convergent algorithm for shape from shading," *DARPA Image Understanding Workshop*, pp. 489–496, 1985.

[70] M. J. Brooks and B. K. P. Horn, "Shape and source from shading," *9th International Joint Conference on Artificial Intelligence*, pp. 932–936, 1985.

[71] P. L. Worthington and E. R. Hancock, "New constraints on data-closeness and needle map consistency for shape-from-shading," *IEEE Transactions on Pattern Analysis and Machine Intelligence*, vol. 21, no. 12, pp. 1250–1267, 1999.

[72] T. C. Pong, R. M. Haralick, and L. G. Shapiro, "Shape from shading using the facet model," *Pattern Recognition*, vol. 22, no. 6, pp. 683–695, 1989.

[73] K. M. Lee and C. C. J. Kuo, "Shape from shading with a linear triangular element surface model," *IEEE Transactions on Pattern Analysis and Machine Intelligence*, vol. 15, no. 8, pp. 815–822, 1993.

[74] D. Samaras and D. N. Metaxas, "Incorporating illumination constraints in deformable models," *IEEE Conference on Computer Vision and Pattern Recognition*, pp. 322–329, 1998.

[75] F. Courteille, J. D. Durou, and G. Morin, "A global solution to the sfs problem using b-spline surface and simulated annealing," *18th International Conference on Pattern Recognition*, pp. 332–335, 2006.

[76] Q. Zheng and R. Chellappa, "Estimation of illuminant direction, albedo, and shape from shading," *IEEE Transactions on Pattern Analysis and Machine Intelligence*, vol. 13, no. 7, pp. 680–702, 1991.

[77] P. L. Worthington and E. R. Hancock, "Needle map recovery using robust regularized," *Image and Vision Computing*, vol. 17, no. 8, pp. 545–557, 1999.

[78] A. Crouzil, X. Decombes, and J. D. Durou, "A multiresolution approach for shape from shading coupling deterministic and stochastic optimization," *IEEE Transactions on Pattern Analysis and Machine Intelligence*, vol. 25, no. 11, pp. 1416–1421, 2003.

[79] H. Saito and N. Tsunashima, "Estimation of 3-d parametric models from shading image using genetic algorithms," *12th International Conference on Pattern Recognition*, pp. 668–670, 1994.

[80] F. Courteille, A. Crouzil, J. D. Durou, and P. Gurdjos, "Towards shape from shading under realistic photographic conditions," *17th International Conference on Parttern Recognition*, pp. 277–280, 2004.

[81] R. Onn and A. M. Bruckstein, "Integrability disambiguates surface recovery in two-image photometric stereo," *International Journal of Computer Vision*, vol. 5, no. 1, pp. 105–113, 1990.

[82] H. Rademacher, "Über partielle und totale differenzierbarkeit von funktionen mehrerer variabeln und über die transformation der doppelintegrale," *Math. Ann.*, vol. 79, no. 4, pp. 340–359, 1919.

[83] T. Wei and R. Klette, "Finite difference methods for linear shape from shading," *Communication and Information Technology Research Technical Report*, vol. 110, 2001.

[84] T. Wei and R. Klette, "Theoretical analysis of finite difference algorithms for linear shape from shading," *Computer Analysis of Images and Patterns*, pp. 632–645, 2001.

[85] G. Ulich, "Provably convergent methods for the linear and nonlinear shape from shading problem," *Journal of Mathematical Imaging and Vision*, vol. 9, pp. 69–82, 1998.

[86] J. Strikwerda, "Finite schemes and partial differential equations," *Wodsworth and Brooks*, 1989.

[87] S. Ishikawa, "Fixed points and iteration of a nonexpansive mapping in a banach space," *American Mathematical Society*, vol. 59, no. 1, pp. 65–71, 1976.

[88] J. D. Durou and F. Courteille, "Integration of a normal field without boundary condition," *Proceedings of the First International Workshop on Photometric Analysis For Computer Vision*, 2007.

[89] J. D. Durou, J. F. Aujol, and F. Courteille, "Integrating the normal field of a surface in the presence of discontinuities," 2009.

[90] T. Wei and R. Klette, "A new algorithm for gradient field integration," Tech. Rep., Communication and Information Technology Research Technical Report 103, 2001.

[91] J. Bai and X. C. Feng, "Fractional-order anisotropic diffusion for image denoising," *IEEE Transactions on Image Processing*, vol. 16, no. 10, pp. 2492–2502, 2007.

[92] L. J. Belaid, M. Jaoua, Masmoudi, and Siala, "Image restoration and edge detection by topological asymptotic expansion," *Comptes Rendus Mathematique*, vol. 342, no. 5, pp. 313–318, 2006.